On the characterization of generalized quantum thermodynamic machines

Diplomarbeit von
Georg Michael Reuther

08. Mai 2007

Hauptberichter: Prof. Dr. G. Mahler
Mitberichter: Prof. Dr. U. Seifert

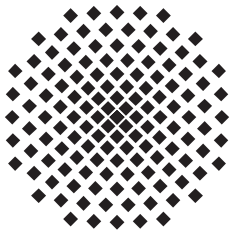

1. Institut für Theoretische Physik
Universität Stuttgart
Pfaffenwaldring 57, 70550 Stuttgart

Ehrenwörtliche Erklärung

Ich erkläre, daß ich diese Arbeit selbständig verfaßt und keine anderen als die angegebenen Quellen und Hilfsmittel benutzt habe.

Stuttgart, 08. Mai 2007 *Georg Michael Reuther*

Contents

List of Figures

List of Tables

1. Introduction

Since modern applications in the realm of physics shrink more and more towards quantum scales, the question of how classical thermodynamics could be understood on the basis of quantum mechanics has grown in importance. It has recently been shown that entanglement between a small quantum system and its large environment leads to a local equilibrium state and thus to thermodynamic behavior, without any further assumptions to be invoked [1, 2]. This has not been the case so far for previous descriptions of statistical mechanics introduced by Boltzmann [3], describing the emergence of classic macroscopic behavior out of few microscopic properties. For example, the widely accepted Gibbsian ensemble theory does not get along without ergodicity [4], being plausible but incapable of proof.

The present work deals with thermodynamic machines on the quantum level. An adequate description of corresponding machine cycles first requires mapping of the established classical thermodynamic variables to quantum mechanical analogs, which is done by exploiting typical properties of quantum systems such as energetic discreetness. For example, work and heat may be linked to the temporal change of the spectrum and the occupation probabilities, respectively. Also the definition of a temperature in quantum systems is feasible if correlations such as entanglement are small [5].

Like in the classical case, two basic conditions precedent to a quantum machine cycle are the presence of asymmetry, following the Curie principle [6], and agreement with the second law of thermodynamics. Thus, on the one hand, a quantum system running a thermodynamic cycle needs to be coupled to two environments of different temperatures to exchange heat with. Moreover, internal asymmetry is required in order that work is released or consumed by the system during interaction with a work reservoir. On the other hand, it is generally claimed that the celebrated Carnot efficiency can never be exceeded by a quantum machine either.

An early investigation of a quantum thermodynamic cycle is given in [7]. More recent approaches are found in [8] and [9, 10, 11], where externally driven discrete quantum systems interacting with environmental baths are analyzed. Further on, discussions of quantum thermodynamic machines are provided in [12, 13]. Eventually, [14] deals with a study on an autonomous machine model.

In the frame of this work a previously investigated model of an inhomogeneously split Heisenberg spin chain locally coupled to two heat baths with different temperatures [15, 16] is used. The baths are modeled by a master equation under Born-Markov approximation featuring a non-equilibrium state as stationary solution [17, 18]. Depending on the global temperature gradient and the local Zeeman splittings the system runs as a heat pump or heat engine if a part of the chain is periodically modulated by an external field. The driven spin is in a thermal state due to the decohering bath influence

and thus has a local temperature and thermal entropy. If it comes into resonance with the bath contact spins a heat current between the system and the baths occurs. This thermodynamic cycle on the quantum level is identified as Quantum Otto cycle. The thermodynamic variables heat and work are controlled by the temporal change of the spectrum and the occupation probabilities, respectively.

After an overview of pertinent theoretical concepts in chapter 2, the quantum thermodynamic machine model described above is introduced in 3 with respect to the ideal Quantum Otto cycle, assuming perfectly controlled cycle steps. In the following, extensions to the three-spin model are numerically investigated and compared to each other with respect to essential thermodynamic properties such as efficiency and heat transport capability. Hence chapter 4 deals with quantum machines connected in parallel whereas chapter 5 points at serial circuits.

Further on, chapter 6 gives a short outlook of more complex quantum machine circuits of which some examples are treated. Finally, the models presented in chapter 5 are mapped on a scenario of a thermal Brownian motor [19] in chapter 7.

2. Theoretical Basics

2.1. Classical Thermodynamics

2.1.1. Gibbsian Fundamental Form

The intrinsic energy U of a thermodynamic system is generally described by the Gibbsian fundamental form

$$\mathrm{d}U = đQ + đA = T\mathrm{d}S + \sum_i \xi_i \mathrm{d}X_i \tag{2.1}$$

where the entropy S and the generalized volumes X_i are energetic extensive variables defined in phase space. The conjugated energetic intensive variables are temperature T and the generalized pressures ξ_i:

$$T = \frac{\partial U}{\partial S} \qquad \xi_i = \frac{\partial U}{\partial X_i} \,. \tag{2.2}$$

For any closed path in phase space energy is conserved: $\oint \mathrm{d}U = 0$. A periodic process therefore returns to the initial state after one performed cycle [20].

2.1.2. The Second Law of Thermodynamics

The second law can be expressed in multiple ways. For example, it is impossible to construct a periodically working machine which simply converts heat from a single reservoir into mechanical work. Another way of explanation is to say that heat never spontaneously flows from a colder to a hotter reservoir. In terms of entropy this is expressed as

$$\mathrm{d}S \geq 0 \,. \tag{2.3}$$

The equal sign holds for reversible processes where no entropy is produced and the described thermodynamic system remains in a global stationary equilibrium state. Otherwise an irreversible process is on hand which does not autonomously run backwards, rather entropy has to be produced somewhere else in the world in order to reverse it.

From a macroscopic point of view this behavior is intuitively clear as it corresponds to everyday experience. From a microscopic point of view, however, one would not initially expect that a system should evolve irreversibly into a stationary state since the classical microscopic Hamilton equations as well as Hamiltonians are invariant under time inversion and therefore should yield reversible dynamics.

Thus, further assumptions are needed in order to derive the second law from the microscopical equations of motion, the more so as those cannot be calculated for each

single particle. One approach is given by Boltzmann's postulate, linking entropy to the number of accessible microstates under given macroscopic constraints. Further, the Gibbsian ensemble approach introduces a statistical ensemble in which each accessible microstate is virtually represented by a point in phase space Γ. For big systems the discrete ensemble of points passes into the density of states, giving the probability to find the system in a certain space element of Γ. Since the concept of quasi-ergodicity claims the system trajectory to come arbitrarily close to every possible point of Γ within its evolution in time, the temporal system average is replaced by an ensemble average over all microstates for infinite timescales. However, these assumptions cannot be generally proved. In addition, irreversibility has to be introduced rather artificially by the concept of "coarse graining".

These deficiencies are overcome by the theory of quantum thermodynamics, being a recent approach based on quantum mechanics where the evolution of a small quantum system weakly coupled to a bigger environmental system is investigated. It turns out that the derivation of the second law out of Schrödinger dynamics is possible without further assumptions such as ergodicity or coarse-graining. More detailed descriptions may be found in [21, 2, 1].

2.1.3. Carnot Cycle

In the frame of this thesis about quantum thermodynamic machines their classical equivalents shall be briefly described first. See also [20].

A Carnot cycle is a periodic thermodynamic process where energy in the form of heat and work is transferred between two heat reservoirs of different temperatures T_h and T_c, referred to as the hot and the cold bath, respectively, and a reversible work reservoir such as a piston. The latter always features constant entropy since it exchanges no heat with the working gas, and neither do the heat reservoirs exert any work. In order to fulfill these conditions the cycle has to run in the quasistatic limit, that is, infinitesimally slow.

Furthermore, an auxiliary system is needed which must not count for the overall energetic balance. Thus, it necessarily has to be restored to its initial state after each cycle. It represents the virtual physical machine and is realized by an ideal working gas in most instances.

If heat is about to be transferred into mechanical work, the system works as heat engine. If otherwise mechanical work is applied in order to transport heat from the cold to the hot reservoir, the system works as heat pump or refrigerator.

The Carnot cycle runs in four steps:

1. Isothermal expansion: The working gas, initially at temperature T_h, is coupled to the hot bath and to the piston at the same time. Then a heat flux ΔQ_h emerges from the hot bath to the working gas. The latter therefore expands and transfers an amount of work ΔW_1 to the piston.

2. Adiabatic expansion: The working gas is decoupled from the hot bath and undergoes an isentropic expansion until its temperature equals that of the cold bath, T_c.

A further amount of work ΔW_2 is transferred to the piston.

3. Isothermal compression: The working gas gets coupled to the cold bath into which it ejects a heat quantity ΔQ_c while receiving the work ΔW_3 from the piston.

4. Adiabatic compression: After having been decoupled from the cold bath, the working gas undergoes an isentropic compression during which it receives the work ΔW_4 from the piston, until it reaches again the temperature T_h in order to return to its initial state.

The Gibbs relation for one completed cycle reads

$$\Delta U = \Delta W + \Delta Q \stackrel{!}{=} 0\,, \tag{2.4}$$

corresponding to a closed path in phase space. The entire amount of work exchange between the working gas and the piston then is

$$\Delta W = \Delta Q_\mathrm{h} + \Delta Q_\mathrm{c} = \Delta S(T_\mathrm{h} - T_\mathrm{c}) \tag{2.5}$$

which can be calculated with the help of the ST-diagram. Hereof the efficiency of the Carnot engine follows, indicating the minimum heat quantity to be taken from the hot bath in order to exert a given amount of work:

$$\eta_\mathrm{en}^\mathrm{Carnot} = \frac{\Delta W}{\Delta Q} = 1 - \frac{T_\mathrm{c}}{T_\mathrm{h}}\,. \tag{2.6}$$

In analogy to this, the Carnot heat pump efficiency is defined as

$$\eta_\mathrm{p}^\mathrm{Carnot} = \frac{\Delta Q}{\Delta W} = \frac{1}{1 - \frac{T_\mathrm{c}}{T_\mathrm{h}}} = 1/\eta_\mathrm{en}^\mathrm{Carnot}\,, \tag{2.7}$$

indicating the minimum amount of work to be carried out in order to pump a certain heat quantity from the cold to the hot bath. According to the second law the entropy balance reads

$$-\frac{Q_\mathrm{h}}{T_\mathrm{h}} + \frac{Q_\mathrm{c}}{T_\mathrm{c}} = S_\mathrm{prod} \geq 0 \tag{2.8}$$

where S_prod denotes the entropy production per cycle [22]. For the ideal (reversible) Carnot cycle equality holds. For this reason $\eta_\mathrm{en}^\mathrm{Carnot}$ is the fundamental limit of a thermodynamic engine efficiency which cannot be exceeded.

In practice, thermodynamic cycles neither run quasistatically nor ideally why, after (2.8) entropy is produced due to dissipation. This results in the engine efficiency

$$\eta = \eta_\mathrm{en}^\mathrm{Carnot} - \frac{T_\mathrm{c} S_\mathrm{prod}}{Q_\mathrm{h}}\,. \tag{2.9}$$

Carnot Engine Efficiency at Maximum Power Output

The ideal Carnot machine runs infinitesimally slow and therefore has zero power output. In [23] the efficiency for a heat engine with maximum power output running on finite timescales was derived,

$$\eta_{\mathrm{Pmax}} = 1 - \sqrt{\frac{T_\mathrm{c}}{T_\mathrm{h}}}\,. \tag{2.10}$$

Since the bath contact times during the isothermal steps are limited, a finite heat conductance within the supplies between the working gas and the baths is assumed. This leads to entropy production, causing the cycle to be irreversible. The working gas itself still performs an ideal Carnot cycle but only "sees" effective bath temperatures.

2.1.4. Otto Cycle

The Otto cycle consists of two adiabatic and two isochoric steps. On the isochores the position of the piston, i. e. the volume of the ideal working gas remains constant whereas its temperature changes. Thus, work is carried out only on the adiabats. The efficiency of the Otto cycle is given as

$$\eta_\mathrm{en}^\mathrm{Otto} = 1 - \left(\frac{V_2}{V_1}\right)^{\left(\frac{c_\mathrm{p}}{c_\mathrm{v}}-1\right)} \tag{2.11}$$

where $V_2 < V_1$ denote the volumes the working gas takes up on the isochores, and c_p and c_v are the specific heats at constant pressure and volume, respectively.

At the beginning of an isochoric step there is a finite temperature gradient between the working gas and the respective bath it is exchanging heat with. Since reversible operation requires a quasi-statical heat flux between the gas and the reservoir, an ideal isochore cannot simply be equivalent to one single bath contact but rather to a series of contacts with multiple baths at different temperatures. For this reason the maximally achievable classical Otto cycle efficiency is always smaller than the Carnot efficiency, $\eta^\mathrm{Otto} < \eta^\mathrm{Carnot}$ since, in order to achieve maximum efficiency, a reversible machine process must not run between more than two reservoirs at given temperatures. This, in turn, is exactly the case for the Carnot cycle. See also [24, 20].

2.1.5. Serial Circuits of Thermodynamic Machines

In order to obtain an expression for the efficiency of a serial circuit of thermodynamic machines, we consider a chain of N coupled machines of same type, say Carnot or Otto machines, between two heat baths without any additional infinite heat sinks or sources in between. Each subunit may either run as heat engine or heat pump. If the entire circuit works as heat engine, its total efficiency $\eta_\mathrm{en}^\mathrm{tot}$ can then be calculated out of the local subunit efficiencies $\eta_\mathrm{en}^i = W_i/Q_i$ with the following expression [25]:

$$\eta_\mathrm{en}^\mathrm{tot} = \frac{1}{Q_\mathrm{h}}\sum_{i=1}^{N} W_i = \frac{1}{Q_\mathrm{h}}\sum_{i=1}^{N-1} Q_i - Q_{i+1} = 1 - \frac{Q_N}{Q_\mathrm{h}} = 1 - \prod_{i=1}^{N}\left(1-\eta_\mathrm{en}^i\right) \tag{2.12}$$

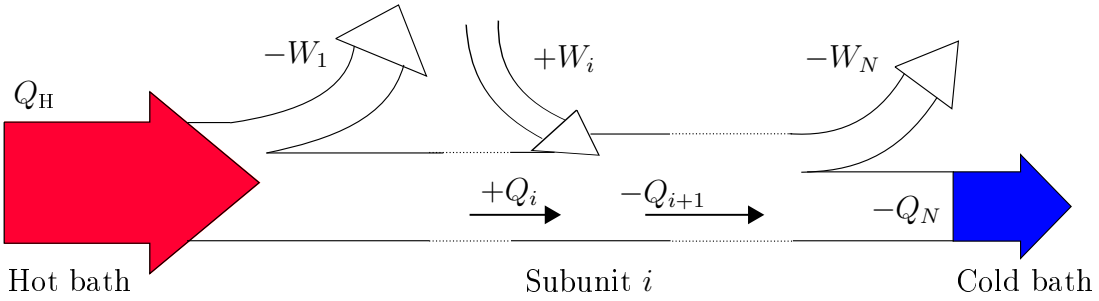

Figure 2.1.: Illustration of a serial thermodynamic circuit

where Q_h, Q_i and Q_N stand for the amounts of heat taken from the hot bath, flowing into subsystem i and ejected into the cold bath, respectively. This is illustrated in Fig. 2.1. Each subunit carries out or consumes an amount of work W_i with $W = \sum_i^N W_i < 0$. The local efficiencies η_i of the subunits can be positive or negative, depending on the local mode of operation. If $W > 0$, the entire system works as heat pump with a total efficiency $\eta_\mathrm{p}^\mathrm{tot} = 1/\eta_\mathrm{en}^\mathrm{tot}$.

In general, for one subunit the local mode of operation as heat pump or engine is determined by those of the adjacent ones. If Carnot machine units are connected in series, the local modes of operation must be chosen such that the working gases of adjacent subunits exhibit identical temperatures if being in contact. Contrarily, in the case of a chain of mutually coupled Otto machines the strokes of subsequent machine units have to match.

2.2. Basic principles of quantum mechanics

2.2.1. Schrödinger Equation

The dynamic evolution of a quantum mechanical system in a time-dependent state $|\psi(t)\rangle$ is governed by the Schrödinger equation

$$\hat{H}(t)\,|\psi(t)\rangle = \mathrm{i}\hbar\frac{\partial}{\partial t}\,|\psi(t)\rangle \tag{2.13}$$

where $\hat{H}(t)$ denotes the system Hamiltonian and $|\psi(t)\rangle$ the system state at time t. The latter is a vector in a N-dimensional Hilbert space $\mathcal{H}$ and can be developed into a complete orthonormal basis $|n\rangle$ spanning $\mathcal{H}$:

$$|\psi(t)\rangle = \sum_{n=1}^{N} c_n(t)\,|n\rangle \qquad \text{with} \quad \sum_n |n\rangle\langle n| = \hat{1} \tag{2.14}$$

where $c_n(t) = \langle n|\psi(t)\rangle$ are time-dependent coefficients. Following the statistical interpretation of quantum mechanics, a state has the meaning of a probability amplitude,

thus its absolute square represents a probability density. For normalized states $|\psi\rangle$ with

$$\langle\psi|\psi\rangle = \sum_{m,n} c_m^* c_n \langle m|n\rangle = \sum_{m,n} c_m^* c_n \delta_{mn} = \sum_n |c_n|^2 \stackrel{!}{=} 1 \tag{2.15}$$

the coefficient squares $|c_n|^2$ denote the probabilities to find the system in the respective states $|n\rangle$. In this basis the Hamiltonian can be written as a matrix with the elements

$$H_{mn} = \langle m|\,\hat{H}\,|n\rangle\,. \tag{2.16}$$

For a time-independent Hamiltonian $\hat{H}(t) \equiv \hat{H}$ the formal solution of (2.13) is

$$|\psi(t)\rangle = \mathrm{e}^{-\mathrm{i}(t-t_0)\hat{H}/\hbar}\,|\psi(t_0)\rangle \equiv \hat{U}(t,t_0)\,|\psi(t_0)\rangle\ . \tag{2.17}$$

Here $\hat{U}(t,t_0)$ is the unitary time-evolution operator with

$$\hat{U}^\dagger\hat{U} = \hat{U}\hat{U}^\dagger = \hat{1}\,. \tag{2.18}$$

According to the Ehrenfest theorem, the projector $\hat{P} = |n\rangle\langle n|$ to an energy eigenstate $|n\rangle$ of $\hat{H}$ obeys the relation

$$\left[\hat{P},\hat{H}\right] = 0 \quad\Longrightarrow\quad \langle\hat{P}\rangle = \langle|n\rangle\langle n|\rangle = \langle\psi|n\rangle\,\langle n|\psi\rangle = |c_n|^2 = \mathrm{const}\,, \tag{2.19}$$

why the energy distribution is conserved.

2.2.2. Density Operator

A quantum mechanical state can most generally expressed by the density operator $\hat{\varrho}$. Some elementary properties of $\hat{\varrho}$ are:

- Normalization:
$$\mathrm{Tr}\{\hat{\varrho}\} = 1 \tag{2.20}$$
where $\mathrm{Tr}\{\ldots\}$ is the trace operator.
- Hermiticity: $\hat{\varrho} = \hat{\varrho}^\dagger$.
- The expectation value of an arbitrary operator $\hat{B}$ is
$$\langle\hat{B}\rangle = \mathrm{Tr}\Big\{\hat{\varrho}\hat{B}\Big\}\,. \tag{2.21}$$
- Purity: $P = \mathrm{Tr}\{\hat{\varrho}^2\} \leq 1$

Here the equal sign only holds for a pure state $\hat{\varrho} = |\psi\rangle\langle\psi|$ which is exactly known. Otherwise the state is called non-pure or mixed, that is, maximal information about it is not available. In the case of a discrete spectrum the spectral representation of a mixed state reads

$$\hat{\varrho} = \sum_i p_i\,|\psi_i\rangle\langle\psi_i|\ . \tag{2.22}$$

Due to the conditions given above, $\hat{\varrho}$ is positively definite. The eigenvalues p_i are real positive numbers and their sum equals unity:

$$\sum_i p_i = 1 \qquad p_i = p_i^* \qquad 0 \leq p_i \leq 1\,. \tag{2.23}$$

They can thus be interpreted as probabilities of the system to be in one certain state out of the mixture of pure states $|\psi_i\rangle$.

2.2.3. von-Neumann equation

For the density operator, the equivalent to the Schrödinger equation (2.13) is the von-Neumann equation

$$\frac{\mathrm{d}}{\mathrm{d}t}\hat{\varrho}(t) = -\frac{\mathrm{i}}{\hbar}\Big[\hat{H}(t), \hat{\varrho}(t)\Big] \equiv \hat{\mathcal{L}}(\hat{\varrho}(t)) \tag{2.24}$$

which describes the system evolution under Schrödinger dynamics. The super-operator $\hat{\mathcal{L}}$ is defined in Liouville space and acts on the density operator $\hat{\varrho}$ defined in Hilbert space. In general, a Liouville super-operator transforms one Hilbert space operator into another.

Interaction Picture

If the system Hamiltonian is given as the sum of a constant and a time-dependent part,

$$\hat{H}(t) = \hat{H}_0 + \hat{V}(t)\,, \tag{2.25}$$

the von-Neumann equation can be written as

$$\frac{\mathrm{d}}{\mathrm{d}t}\hat{\varrho}_I(t) = -\frac{\mathrm{i}}{\hbar}\Big[\hat{V}_I(t), \hat{\varrho}_I(t)\Big] \tag{2.26}$$

with

$$\hat{\varrho}_I(t) = \mathrm{e}^{\mathrm{i}\hat{H}_0(t-t_0)/\hbar}\,\hat{\varrho}(t)\,\mathrm{e}^{-\mathrm{i}\hat{H}_0(t-t_0)/\hbar} \equiv \hat{U}_0^\dagger(t,t_0)\hat{\varrho}(t)\hat{U}_0(t,t_0) \tag{2.27}$$

and

$$\hat{V}_I(t) = \hat{U}_0^\dagger(t,t_0)\hat{V}(t)\hat{U}_0(t,t_0) \tag{2.28}$$

with the unitary time evolution operator $\hat{U}^\dagger(t,t_0)$ (see e. g. [26]). Passing to the interaction picture, the time dependence of the density matrix is partially transferred to the Hilbert space $\mathcal{H}$. The case of $\hat{V}(t) = 0$ marks the Heisenberg picture, if $\hat{H}_0 = 0$ we are again in the Schrödinger picture.

2.2.4. Von-Neumann Entropy

For a state $\hat{\varrho}$ the von-Neumann entropy $S(\hat{\varrho})$ is defined as

$$S(\hat{\varrho}) = -k_\mathrm{B}\,\mathrm{Tr}\{\hat{\varrho}\ln\hat{\varrho}\} \tag{2.29}$$

where k_B is the Boltzmann factor. The von-Neumann entropy is invariant under unitary evolution,

$$S\left(\hat{U}^\dagger(t,t_0)\hat{\varrho}(t_0)\hat{U}(t,t_0)\right) = S(\hat{\varrho}(t_0))\,. \tag{2.30}$$

Likewise the purity defined above, the entropy is a measure for the pureness of states. A pure state has zero entropy, a maximally mixed state with $\varrho_{ij} = \frac{1}{n}\delta_{ij}$ has maximal entropy $S_\mathrm{max} = k_\mathrm{B} \ln n$ and minimal purity $P_\mathrm{min} = 1/n$, where n is the dimension of the Hilbert space $\mathcal{H}$. See also [27, 2].

2.2.5. Composite Quantum Systems

A Hilbert space $\mathcal{H}$ consisting of two or more subspaces $\mathcal{H}_1, \mathcal{H}_2, \ldots, \mathcal{H}_N$ can be written as the tensor product of these subspaces. For a bipartite system, e. g.,

$$\mathcal{H} = \mathcal{H}_1 \otimes \mathcal{H}_2\,. \tag{2.31}$$

The dimension n of $\mathcal{H}$ is a product of the subspace dimensions n_i, here

$$n = n_1 n_2\,. \tag{2.32}$$

In general, the Theorem of Araki and Lieb applies for the local and global entropy:

$$|S(\hat{\varrho}_1) - S(\hat{\varrho}_2)| \leq S(\hat{\varrho}) \leq |S(\hat{\varrho}_1) + S(\hat{\varrho}_2)|\,. \tag{2.33}$$

The right equality sign only holds if the subsystems are uncorrelated. In this case the local entropies $S(\hat{\varrho}_1)$ and $S(\hat{\varrho}_2)$ add up to the global entropy $S(\hat{\varrho})$, and the entire state $\hat{\varrho}(t)$ can be written as a product state out of its substates [2]. Otherwise, if the product form is non-applicable, this is due to correlations between both partial states (see below).

If one is interested in only one partial subspace, e. g. $\mathcal{H}_1$, the respective state $\hat{\varrho}_1(t)$ can be obtained by tracing out the degrees of freedom of the other subspace,

$$\hat{\varrho}_1(t) = \mathrm{Tr}_2\{\hat{\varrho}(t)\} \tag{2.34}$$

where $\mathrm{Tr}_i\{\ldots\}$ denotes the partial trace over subspace $\mathcal{H}_i$ [27].

2.2.6. Entropy, Correlations and Entanglement

If a composite system state is non-separable, i. e. cannot be written as a tensor product out of its partial states, this is caused by correlations such as entanglement originating from the interaction between different subsystems. Non-separability of partial states also reflects in that the respective local entropies are non-additive (see Eq. (2.33)). Thus, entropy gives an appropriate measure of correlations.

Tracing out a substate after Eq. (2.34) leads to a loss of information about correlations between partial states, and due to (2.33) local entropies generally increase in time during the system evolution. This also applies for the case a small quantum system interacts with an environment [28]. In contrast, global entropy is constant in time due to (2.30).

An adequate distance measure for two states $\hat{\varrho}$ and $\hat{\varrho}'$ is given by the Bures metric [2],

$$D^2_{\hat{\varrho}\hat{\varrho}'} = \mathrm{Tr}\{(\hat{\varrho} - \hat{\varrho}')^2\}\,. \tag{2.35}$$

If $\hat{\varrho}$ is the actual composite state and $\hat{\varrho}'$ some product form, $D^2_{\hat{\varrho}\hat{\varrho}'}$ can be used as a measure for correlations.

Entanglement is a purely quantum mechanical phenomena. A standard example for a maximally entangled quantum state is the Einstein-Podolsky-Rosen (EPR) state [29]

$$|\psi\rangle = \frac{1}{\sqrt{2}}\left(|1\rangle\,|0\rangle - |0\rangle\,|1\rangle\right) \tag{2.36}$$

describing two interacting spins, where $|0\rangle$ and $|1\rangle$ stand for "spin up" and "spin down", respectively. If, in a measurement, the first spin is found to be in "up" state, the second spin will automatically be in "down" state. This holds without the need for a further measurement, even if both spins are outside the range of interaction. Hence the entangled state only contains collective information on both subsystems. This principal non-locality is an essential ingredient of entanglement. See also [30].

2.3. Open Quantum Systems and Master Equation

2.3.1. Derivation of the Quantum Master Equation

A convenient method to describe the interaction of a small quantum system with a large environment (heat bath) is by means of a quantum master equation (QME). Since usually the degrees of freedom of the environment are too numerous for further investigation, they are traced out and disregarded ab initio. This leads to an effective equation of motion for the dissipative dynamics the reduced density matrix $\hat{\varrho}_\mathrm{S}$ of the considered open quantum system is subject to.

Several different approaches to open quantum systems exist, see e. g. [26, 31, 32]. The master equation used in this work is described in [17]. A recent description and comparison to other models can be found in [18] and also in [16] in the context of quantum thermodynamic machines.

The compound of the system of interest S and its environmental bath B is described by the Hamiltonian

$$\hat{H} = \hat{H}_S + \hat{H}_B + \hat{H}_\mathrm{int} \tag{2.37}$$

where the bath is modeled by an infinite number of uncoupled harmonic oscillators

$$\hat{H}_B = \sum_{k=1}^{\infty} \omega_k \hat{b}_k^\dagger \hat{b}_k \tag{2.38}$$

with the bosonic creation and annihilation operators $\hat{b}_k^\dagger$ and $\hat{b}_k$. The interaction Hamiltonian $\hat{H}_\mathrm{int}$ is specified as

$$\hat{H}_\mathrm{int} = \sum_\alpha \hat{A}_\alpha \otimes \hat{B}_\alpha \tag{2.39}$$

where $\hat{A}_k$ and $\hat{B}_k$, respectively, are hermitian system and bath operators to be ascertained below. The time evolution of the whole system's density operator $\hat{\varrho}$ is governed by the von-Neumann Eq. (2.24), written in the interaction picture ($\hbar \equiv 1$):

$$\frac{\mathrm{d}\hat{\varrho}(t)}{\mathrm{d}t} = -\mathrm{i}\Big[\hat{H}_{\mathrm{int}}(t), \hat{\varrho}(t)\Big] \,. \tag{2.40}$$

The formal solution hereof is

$$\hat{\varrho}(t) = \hat{\varrho}(0) - \mathrm{i}\int_0^t \Big[\hat{H}_{\mathrm{int}}(s), \hat{\varrho}(s)\Big]\mathrm{d}s \tag{2.41}$$

The density operator of the subsystem of interest is then obtained by

$$\hat{\varrho}_S = \mathrm{Tr}_B\{\hat{\varrho}(t)\} \,. \tag{2.42}$$

Inserting (2.41) into (2.40) and applying (2.42) yields

$$\frac{\mathrm{d}\hat{\varrho}_S(t)}{\mathrm{d}t} = -\int_0^t \mathrm{Tr}_B\Big\{\Big[\hat{H}_{\mathrm{int}}(t), \Big[\hat{H}_{\mathrm{int}}(s), \hat{\varrho}(s)\Big]\Big]\Big\} \tag{2.43}$$

where it is assumed that

$$\mathrm{Tr}_B\Big\{\Big[\hat{H}_{\mathrm{int}}, \hat{\varrho}(0)\Big]\Big\} = 0 \tag{2.44}$$

Now one performs the Born approximation, claiming the coupling between system and bath to be weak enough so that the back-action of the system on the bath is negligible. Hence the state of the entire system may be approximated by a tensor product:

$$\hat{\varrho}(t) \approx \hat{\varrho}_S(t) \otimes \hat{\varrho}_B \,. \tag{2.45}$$

The bath state is assumed to be canonical,

$$\hat{\varrho}_B = \frac{\mathrm{e}^{-\beta\hat{H}_B}}{\mathrm{Tr}_B\{\mathrm{e}^{-\beta\hat{H}_B}\}} \tag{2.46}$$

with $\beta = 1/T$ being the inverse temperature and $k_\mathrm{B} \equiv 1$.

A further simplification is introduced by the Markov approximation, assuming coarse grained time scales. This means the excitations in the baths are not resolved as they happen on much smaller time scales τ_B than those on which the system evolves (τ_S). Furthermore, the same is assumed to apply for the decay of the bath correlation functions or memory effects. Thus, in Eq. (2.45) we replace $\hat{\varrho}(s)$ by $\hat{\varrho}(t)$, and s is substituted by $t - s$ while the upper bound of the integral is set to $t \to \infty$. This makes the integrand vanish rapidly enough for $s \gg \tau_B$. Then,

$$\frac{\mathrm{d}\hat{\varrho}_S(t)}{\mathrm{d}t} = -\int_0^\infty \mathrm{d}s\, \mathrm{Tr}_B\Big\{\Big[\hat{H}_{\mathrm{int}}(t), \Big[\hat{H}_{\mathrm{int}}(t-s), \hat{\varrho}(t) \otimes \hat{\varrho}_B\Big]\Big]\Big\} \,. \tag{2.47}$$

Skipping some lengthy calculations, the QME becomes, again in the Schrödinger picture,

$$\begin{aligned}\frac{\mathrm{d}\hat{\varrho}_S(t)}{\mathrm{d}t} = &-\mathrm{i}\Big[\hat{H}_S, \hat{\varrho}_S(t)\Big] - \int_0^\infty \mathrm{d}s \int_{-\infty}^\infty \mathrm{d}\omega \mathrm{e}^{\mathrm{i}\omega s} \times \\ &\sum_{\alpha,\gamma}\Big(\Gamma_{\alpha\gamma}(\omega)\Big[\hat{A}_\gamma(-s)\hat{\varrho}_S(t), \hat{A}_\alpha\Big] + \Gamma_{\gamma\alpha}(-\omega)\Big[\hat{A}_\alpha, \hat{A}_\gamma(-s)\hat{\varrho}_S(t)\Big]\Big)\end{aligned} \tag{2.48}$$

with

$$\hat{A}_\gamma(-s) = \mathrm{e}^{-\mathrm{i}\hat{H}_S s}\hat{A}_\gamma \mathrm{e}^{\mathrm{i}\hat{H}_S s}\,. \tag{2.49}$$

Here the bath correlation functions

$$\Gamma_{\alpha\gamma}(s,\beta) = \Big\langle \hat{B}_\alpha(s)\hat{B}_\gamma(0)\Big\rangle_B \equiv \mathrm{Tr}_B\Big\{\hat{B}_\alpha(s)\hat{B}_\gamma(0)\hat{\varrho}_B\Big\} \tag{2.50}$$

with $\hat{\varrho}_B$ given by (2.46) have been introduced. Their Fourier transformations, representing transition rates, lead to the bath correlation tensor

$$\Gamma_{\alpha\gamma}(\omega,\beta) = \int_{-\infty}^\infty \mathrm{d}s \mathrm{e}^{\mathrm{i}\omega s}\,\Gamma_{\alpha\gamma}(s,\beta)\,. \tag{2.51}$$

For terms of $\Gamma(-\omega)$ the Kubo-Martin-Schwinger (KMS) condition gives

$$\Gamma_{\alpha\gamma}(\omega) = \mathrm{e}^{-\beta\omega}\Gamma_{\gamma\alpha}(-\omega)\,. \tag{2.52}$$

The first term of Eq. (2.48) describes the coherent unitary dynamics of the system while the second term, the dissipator $\hat{\mathcal{D}}(\hat{\varrho}_S(t))$, defined in Liouville space, represents the decohering and damping environmental influence. The Liouville-von Neumann equation describing the reduced dynamics of the system is thus rewritten as

$$\frac{\mathrm{d}\hat{\varrho}_S(t)}{\mathrm{d}t} = -\mathrm{i}\Big[\hat{H}_S, \hat{\varrho}_S(t)\Big] + \hat{\mathcal{D}}(\hat{\varrho}_S(t)) \equiv \hat{\mathcal{L}}(\hat{\varrho}_S(t))\,. \tag{2.53}$$

where $\hat{\mathcal{L}}$ is the corresponding Liouville super-operator acting on $\hat{\varrho}_S(t)$.

Now, in the frame of this thesis only local coupling of a spin chain to a heat bath via the outermost spin will be considered. Hence the system part of the interaction Hamiltonian (2.39) is chosen as:

$$\hat{A}_1 = \hat{\sigma}_x^{(1)} \otimes \hat{1}^{(2)} \otimes \ldots \otimes \hat{1}^{(n)}\,, \tag{2.54}$$

and there remains but one pair of interaction operators ($\alpha = \gamma = 1$), therefore these indices are omitted in the following.
The bath operator $\hat{B}$ is set to be linear in the oscillator amplitudes (cf. (2.38)),

$$\hat{B} = \sum_{l=1}^\infty c_l \hat{b}_l^\dagger + c_l^* \hat{b}_l \tag{2.55}$$

where the c_k are coupling constants. Inserting (2.55) into (2.50) and applying the Fourier transformation (2.51), the bath correlation tensor can be written in terms of the spectral density $J(\omega)$,

$$\Gamma(\omega,\beta) = \kappa \frac{J(\omega) - J(-\omega)}{\mathrm{e}^{\beta\omega} - 1}\,, \tag{2.56}$$

introducing the system-bath coupling parameter κ. A usual form of $J(\omega)$ is that of an Ohmic bath,

$$J(\omega) = \omega\Theta(\omega)\,, \tag{2.57}$$

where $\Theta(\omega)$ is the Heaviside step function,

$$\Theta(\omega) = \begin{cases} 1 & \omega > 0 \\ 0 & \omega \leq 0\,. \end{cases} \tag{2.58}$$

The expression for the dissipator $\hat{\mathcal{D}}(\hat{\varrho}_S(t))$ derived so far is not yet convenient for numerical purpose. Therefore $\hat{\mathcal{D}}(\hat{\varrho}_S(t))$ is now expressed in terms of the energy eigenstates of the system via the projectors $|i\rangle$. As an example this is done here for the first term of (2.48):

$$\langle k|\,\hat{\mathcal{D}}(\hat{\varrho}_S(t))\,|n\rangle = \sum_{l,m} \int_0^\infty \mathrm{d}s \int_{-\infty}^\infty \mathrm{d}\omega \mathrm{e}^{\mathrm{i}\omega s} \Big(\Gamma(\omega) \underbrace{\langle k|\,\hat{A}(-s)\,|l\rangle}_{(*)} \langle l|\,\hat{\varrho}_S(t)\,|m\rangle \langle m|\,\hat{A}\,|n\rangle + \dots \,. \tag{2.59}$$

The term labeled $(*)$ becomes

$$\begin{aligned} \langle k|\,\hat{A}(-s)\,|l\rangle &= \langle k|\,\mathrm{e}^{-\mathrm{i}s\hat{H}_S}\hat{A}\mathrm{e}^{\mathrm{i}s\hat{H}_S}\,|l\rangle = \langle k|\,\mathrm{e}^{-\mathrm{i}E_k s}\hat{A}\mathrm{e}^{\mathrm{i}E_l s}\,|l\rangle \\ &= \mathrm{e}^{-\mathrm{i}(E_k - E_l)s}\,\langle k|\,\hat{A}\,|l\rangle = \mathrm{e}^{-\mathrm{i}\omega_{kl}s}\,\langle k|\,\hat{A}\,|l\rangle\,. \end{aligned} \tag{2.60}$$

where E_i are system eigenvalues belonging to the eigenstates $|i\rangle$ of $\hat{H}_S$, and $\omega_{kl} = E_k - E_l$. The integrals can then be dissolved with the help of the formula

$$\int_0^\infty \mathrm{d}s\, \mathrm{e}^{\mathrm{i}(\omega-\omega_{kl})s} = \delta(\omega - \omega_{kl}) + \mathcal{P}\frac{\mathrm{i}}{\omega - \omega_{kl}}\,, \tag{2.61}$$

neglecting the Cauchy principal value $\mathcal{P}$. Now the traceless transition operator $\hat{R}$ is introduced whose matrix elements are

$$\langle l|\,\hat{R}\,|m\rangle = \langle l|\,\hat{A}\,|m\rangle\,\Gamma(\omega_{lm}) \tag{2.62}$$

where, by insertion of (2.56)-(2.58), and with regard to (2.52) the bath correlation tensor writes

$$\Gamma(\omega_{lm}) = \Gamma(E_l - E_m) = \kappa\left(\frac{\theta(\omega_{lm})}{\mathrm{e}^{\omega_{lm}\beta} - 1} + \frac{\theta(\omega_{ml})\mathrm{e}^{\omega_{ml}\beta}}{\mathrm{e}^{\omega_{ml}\beta} - 1}\right)\,, \tag{2.63}$$

with $\Gamma(\omega_{ll} \equiv 0) = 0$.

The transition rates introduced in (2.51) obviously depend on both the temperature $T = 1/\beta$ and the system-environment coupling strength κ, which must be small to justify the Born approximation (2.45). Finally the dissipator is compactly written as

$$\hat{\mathcal{D}}(\hat{\varrho}_S(t)) = \Big[\hat{A}, \hat{R}\hat{\varrho}_S(t)\Big] + \Big[\hat{A}, \hat{R}\hat{\varrho}_S(t)\Big]^\dagger \tag{2.64}$$

It is easily shown that the stationary solution of (2.53), $\dot{\hat{\varrho}}_S(t) = 0$, is the canonical equilibrium state with the Boltzmann distribution

$$\hat{\varrho}_S^{\mathrm{stat}} = \frac{\mathrm{e}^{-\beta\hat{H}_S}}{\mathrm{Tr}_S\{\mathrm{e}^{-\beta\hat{H}_S}\}}\,, \tag{2.65}$$

being the eigenstate of the Liouvillian $\hat{\mathcal{L}}$ to the eigenvalue zero. Independently on initial conditions, a system locally coupled to only one heat reservoir is expected to end up in a state of canonical equilibrium due to the decohering bath influence represented by the transition operator $\hat{R}$.

2.3.2. Open Quantum Systems in Thermal Non-Equilibrium

As in the further proceeding a non-equilibrium scenario of a spin chain between two heat baths will be investigated, a second dissipator representing the additional reservoir is added to (2.53),

$$\frac{\mathrm{d}\hat{\varrho}_S(t)}{\mathrm{d}t} = -\mathrm{i}\Big[\hat{H}_S, \hat{\varrho}_S(t)\Big] + \hat{\mathcal{D}}_h(\hat{\varrho}_S(t)) + \hat{\mathcal{D}}_c(\hat{\varrho}_S(t)) \equiv \hat{\mathcal{L}}(\hat{\varrho}_S(t)) \tag{2.66}$$

where h and c denote the hot and cold heat reservoir, respectively. The stationary solution of Eq. (2.66) is a non-equilibrium state since, in the eigenrepresentation of the system Hamiltonian $\hat{H}_S$, it exhibits non-vanishing off-diagonal elements describing correlations between the different system eigenstates.

At the same time a finite stationary heat current through the system emerges, running from the hot to the cold reservoir (see Sec. 2.5.2) and obviously linked to the remaining correlations in the system [33].

Although there is no global equilibrium established, single subunits of the system may nevertheless be found in a local equilibrium state (cf. Sec. 2.4.1) since it turns out that, locally, correlations are damped out by the baths.

2.4. Thermal Properties of Spin Systems

2.4.1. Two-Level Systems in Thermal Equilibrium

In Pauli $\hat{\sigma}_z$-representation, the Hamiltonian of a two-level system (TLS) such as a spin-1/2 particle ("spin") reads

$$\hat{H}_{\mathrm{TLS}} = \frac{1}{2}\,\Delta E \hat{\sigma}_z \tag{2.67}$$

where ΔE is the local energy splitting. The ground and excited states are $-\frac{1}{2}\,\Delta E$ and $+\frac{1}{2}\,\Delta E$, located symmetrically around the zero energy level. If the TLS density matrix is diagonal in this basis, i. e.

$$\hat{\varrho} = \begin{pmatrix} \varrho_{00} & 0 \\ 0 & \varrho_{11} \end{pmatrix} \tag{2.68}$$

with ϱ_{00} and ϱ_{11} being the occupation probabilities of the lower and upper energy state, respectively, the TLS is always in a canonical equilibrium state [34],

$$\hat{\varrho}_{\mathrm{eq}} = \frac{\mathrm{e}^{-\beta \hat{H}_{\mathrm{TLS}}}}{\mathrm{Tr}\{\mathrm{e}^{-\beta \hat{H}_{\mathrm{TLS}}}\}}\,. \tag{2.69}$$

The von-Neumann entropy of the same system,

$$S = -\,\mathrm{Tr}\{\hat{\varrho}\ln\hat{\varrho}\} = -(\varrho_{00}\ln\varrho_{00} + \varrho_{11}\ln\varrho_{11}) \tag{2.70}$$

can then be interpreted as the thermal entropy [2].

For a TLS or spin in a canonical state it is also possible to define a local temperature $T = 1/\beta$ ($k_{\mathrm{B}} \equiv 1$),

$$\frac{\varrho_{11}}{\varrho_{00}} = \mathrm{e}^{-\beta\Delta E} \tag{2.71}$$

The spin energy expectation value $\langle E\rangle$, considered as intrinsic energy U of the TLS, writes [2]

$$U \equiv \langle E\rangle = \mathrm{Tr}\{\hat{\varrho}\hat{H}_{\mathrm{TLS}}\} = -\frac{\Delta E}{2}(\varrho_{00} - \varrho_{11}) = -\frac{\Delta E}{2}\tanh\left(\frac{\Delta E}{2T}\right) \tag{2.72}$$

Recalling the standard thermodynamic temperature definition $T = \frac{\partial U}{\partial S}$ one finds, in agreement with (2.71),

$$T = -\frac{\Delta E}{\ln(\varrho_{11}/\varrho_{00})} \tag{2.73}$$

Generalizations to multi-level systems are possible, see [5, 35, 36].

2.4.2. Global versus Local Temperature

In general, it is a possible condition for the existence of temperature on nanoscales that the corresponding system has to be in a canonical state. In [36, 5, 37] it was shown

that this holds for a subgroup of spins or a single spin within a coupled spin system if correlations between the respective subgroups are small.

This was validated in [38, 35] by means of a Heisenberg spin chain of a few subunits which, in terms of (2.54), is locally coupled to a bath modeled after (2.64). The chain as a whole is found to relax into a stationary canonical state, exhibiting the same global temperature as the bath, independently of the internal spin-spin coupling strength λ. However the local spin temperatures do depend on λ and are only descriptive if the internal coupling strength is weak enough compared to the local spin energy splittings ΔE_i. In this case, as a good approximation, the system energy is extensive in the number of spins and temperature is intensive since global and local temperatures coincide.

Otherwise correlations between single spins and spin groups and thus the local entropy increase, making local temperatures deviate more and more from the global one with increasing λ. In this case the system energy is not extensive in the number of spins any longer since energy is increasingly stored in the interaction between single units.

2.5. Heat Transport in Spin Chains

This section shall give a brief overview of the theoretical framework of heat conduction in spin chains, according to [34, 38] and also to [39, 40].

2.5.1. Heisenberg Spin Chain

The Hamiltonian of a chain consisting of N spins with a nearest neighbor interaction reads

$$\hat{H} = \sum_{\mu=1}^{N} \hat{H}_{\mathrm{loc}}(\mu) + \lambda \sum_{\mu=1}^{N-1} \hat{H}_{\mathrm{int}}(\mu, \mu+1) \tag{2.74}$$

The local Hamiltonian $\hat{H}_{\mathrm{loc}}(\mu)$ of spin μ is given by (2.67), λ denotes the site-independent pair coupling strength and $\hat{H}_{\mathrm{int}}$ is the interaction Hamiltonian. In this work only the anti-ferromagnetic Heisenberg spin chain is used where $\lambda > 0$ and

$$\hat{H}_{\mathrm{int}}(\mu, \mu+1) = \sum_{i=x,y,z} \hat{\sigma}_i(\mu) \otimes \hat{\sigma}_i(\mu+1) \tag{2.75}$$

with a non-resonant coupling part $\hat{\sigma}_z \otimes \hat{\sigma}_z$. The operators $\hat{\sigma}_i$ are the Pauli matrices.

2.5.2. Heat Current

An analytical expression for the heat current through a system of several subunits, e. g. a spin chain, can be obtained after [34, 26]. Starting from the Liouville-von Neumann Eq. (2.53) for the reduced system dynamics

$$\dot{\hat{\varrho}}_S(t) = -\mathrm{i}\Big[\hat{H}_S, \hat{\varrho}_S(t)\Big] + \hat{\mathcal{D}}(\hat{\varrho}_S(t)) \tag{2.76}$$

multiplying this with the system Hamiltonian $\hat{H}_S$ and applying the trace yields

$$\mathrm{Tr}\Big\{\hat{H}_S\dot{\hat{\varrho}}_S\Big\} = -\mathrm{i}\frac{\partial}{\partial t}\,\mathrm{Tr}\Big\{\hat{H}_S\hat{\varrho}_S\Big\} = \mathrm{Tr}\Big\{\hat{H}_S\hat{\mathcal{D}}(\hat{\varrho}_S)\Big\} \tag{2.77}$$

where the trace over the system contribution $[\hat{H}_S,[\hat{H}_S,\hat{\varrho}_S]]$ vanishes. The left-hand side of this expression denotes for the total change of energy in the system,

$$\frac{\mathrm{d}}{\mathrm{d}t}\langle E\rangle = \frac{\mathrm{d}}{\mathrm{d}t}\,\mathrm{Tr}\{\hat{H}_S\hat{\varrho}_S\}\,,$$

and therefore may be identified with a heat current J between the system and the heat bath modeled by the dissipator $\hat{\mathcal{D}}$,

$$J = \mathrm{Tr}\{\hat{H}_S\hat{\mathcal{D}}(\hat{\varrho}_S)\}\,. \tag{2.78}$$

With regard to the the stationary solution $\dot{\hat{\varrho}}_S = 0$ of Eq. (2.66) in the non-equilibrium scenario described in Sec. 2.3.2, the overall energy change in the system must be equal to zero due to energy conservation. Thus, with (2.78),

$$\frac{\mathrm{d}}{\mathrm{d}t}\langle E\rangle = \mathrm{Tr}\Big\{\hat{H}_S\hat{\mathcal{D}}_h(\hat{\varrho}_S)\Big\} + \mathrm{Tr}\Big\{\hat{H}_S\hat{\mathcal{D}}_c(\hat{\varrho}_S)\Big\} \equiv J_h + J_c \stackrel{!}{=} 0\,. \tag{2.79}$$

Hence a stationary leakage current $J_h = -J_c$ through the system emerges, running from the hot (h) to the cold (c) reservoir. By convention a heat current floating into the system is signed positive.

2.5.3. Fourier's Law in Open Quantum Systems

A common way to describe heat transport through a material is a characteristic differential equation widely known as Fourier's law, linking the heat current J and an external temperature gradient $\nabla T(\boldsymbol{r},t)$ via the conductivity K,

$$J = -K\,\nabla T(\boldsymbol{r},t) \tag{2.80}$$

Fourier's law in an open quantum system can be investigated by realizing a stationary setup of a homogeneously split spin chain with a weak nearest neighbor Heisenberg interaction (see (2.75)) locally coupled to two heat baths via the outermost spins of the chain, accordingly to (2.66). This is possible since, after [34, 39], the heat current in a Heisenberg spin chain is not a conserved quantity, leading to a finite conductivity and therefore allowing for regular heat transport.

As mentioned in Sec. 2.3.2, the system as a whole is in a stationary thermal non-equilibrium state. However, the single spins may still be found in local equilibrium states due to the bath-induced damping and therefore exhibit local temperatures (see (2.73)) under the constraints noted in Sec. 2.4.2.

It turns out that the spin chain exhibits a linear temperature gradient ΔT with respect to the single units in the chain. This comes along with a stationary heat current running

through the system (cf. Sec. 2.5.2) and linearly depending on the temperature gradient ΔT imposed by the baths. Thus, Fourier's law is fulfilled for this kind of quantum systems, cf. [34, 38, 40].

Ref. [16] mentions the strong dependence of the heat currents $J_{h,c}$ on the local energy splittings. The currents are maximal at overall resonance, i. e. for a homogeneously split chain, and decrease to zero the more the energy splittings are detuned. This is equivalent to a decrease in heat conductivity and thus to an increase of the spin chain resistance [41].

It is therefore possible to decouple a part of the spin chain from one or both baths factually by simply detuning the local energy gaps of adjacent spins. As it will be discussed below, this aspect is fundamental for the concept of a quantum thermodynamic machine realized by an inhomogeneously split spin chain between two heat baths.

3. Quantum Thermodynamic Machines

3.1. Quantum Thermodynamic Variables

A description of thermodynamic processes requires adequate definitions of the variables heat and work. For a quantum system $\hat{H}$ with a discrete spectrum, being in a state described by the density operator $\hat{\varrho}$, we start from the energy expectation value

$$U = \langle E \rangle = \mathrm{Tr}\Big\{\hat{H}\,\hat{\varrho}\Big\} = \sum_i p_i E_i \tag{3.1}$$

where p_i are the occupation probabilities of the energetic levels belonging to the eigenvalues E_i. The total differential of Eq. (3.1) becomes

$$\mathrm{d}U = \frac{1}{2}\sum_i \underbrace{E_i \mathrm{d}p_i}_{đQ} + \underbrace{p_i \mathrm{d}E_i}_{đW} \tag{3.2}$$

Identifying this with the Gibbs relation (2.1), the heat Q and the work W are associated with the change of occupation probabilities and the spectral deformation, respectively. In analogy to classical thermodynamics, the spectrum is thus interpreted as a "volume" since an amount of mechanical work ΔW is always related to a change of volume ΔV.

A cyclic process requires, following (2.30),

$$\Delta U = \Delta Q + \Delta W \stackrel{!}{=} 0 \qquad \text{or} \quad \Delta W = -\Delta Q\,. \tag{3.3}$$

The work is calculated by integrating over the ST-diagram which is closed for a cyclic process:

$$\Delta W = -\oint T \mathrm{d}S\,. \tag{3.4}$$

The heat ΔQ results from integrating the respective heat currents J_α obtained with (2.78) over one period $\tau = 2\pi/\omega$ if the system is connected with the bath α,

$$\Delta Q_\alpha = \int_0^\tau J_\alpha \mathrm{d}t\,, \tag{3.5}$$

For a cyclic machine process where two heat baths are present, we arrive at

$$\Delta Q = \Delta Q_h + \Delta Q_c\,. \tag{3.6}$$

where ΔQ_h and ΔQ_h denote the heat transferred between the system and the hot ($\alpha = h$) and cold bath ($\alpha = c$). From Eqns. (3.4) and (3.5) the efficiencies for the heat engine (en) and heat pump (p) result as

$$\eta_{\mathrm{en}} = \Delta W / \Delta Q_h \qquad \eta_{\mathrm{p}} = \Delta Q_h / \Delta W \,. \tag{3.7}$$

For a TLS in a canonical state the further needed thermodynamic variables entropy and temperature are given by Eqns. (2.70) and (2.73).

3.2. Quantum Otto Cycle

3.2.1. The Three-Spin Quantum Machine

The elementary quantum thermodynamic machine model underlying all further models to be investigated in this thesis is depicted in figure 3.1 and has been widely discussed and treated numerically in [15, 16]. It consists of an inhomogeneously split chain of three spins locally coupled to a hot (h) and cold (c) heat bath via the outermost spins. The interaction between nearest neighbors is of Heisenberg type, cf. (2.75). The system Hamiltonian reads, in analogy to (2.74),

$$\hat{H} = \sum_{\mu=1}^{3} \left(\frac{1}{2} \Delta E_\mu \hat{\sigma}_z^\mu + \lambda \sum_{i=x,y,z} \hat{\sigma}_i^\mu \otimes \hat{\sigma}_i^{\mu+1} \right) \tag{3.8}$$

where ΔE_μ is the local energy splitting of spin μ and $\hat{\sigma}_i^\mu$ are the Pauli matrices. The bath contact spins 1 and 3 exhibit different constant local energy splittings, imposing an energy gradient on the system and thus spatial asymmetry. Following the Curie principle [6] this is one elementary requirement for any machine function. Furthermore, the presence of two heat baths satisfies the claim for thermal non-equilibrium, being the condition for any conversion of heat out of a thermal bath into work after the second law. In the approach of this work external control on the system is implemented via a semiclassical $\hat{\sigma}_z$-driver which only acts on spin 2 by periodically modulating its local energy gap ΔE_2. From a classical point of view the driven spin takes the role of a "working gas" running a cyclic process while the external driver may be interpreted as a "piston", controlling the work in the system.

In a possible experimental scenario the $\hat{\sigma}_z$-driver might be realized via an external magnetic field. However, this is not suitable as work reservoir since, lack of any retro-action on the driver, the work released by the driven spin cannot be picked off. For this reason the chosen driver is rather classical than quantum mechanical. Nevertheless this problem may be circumvented by coupling the gas spin to an autonomous driver such as a harmonic oscillator. This was investigated e. g. in [14].

At the same time the driver is also enabled to control heat transfer between the system and the reservoirs. This is accomplished by the resonance effect cited in Sec. 2.5.3, provided spin 2 is alternately driven into resonance with both bath contact spins. For

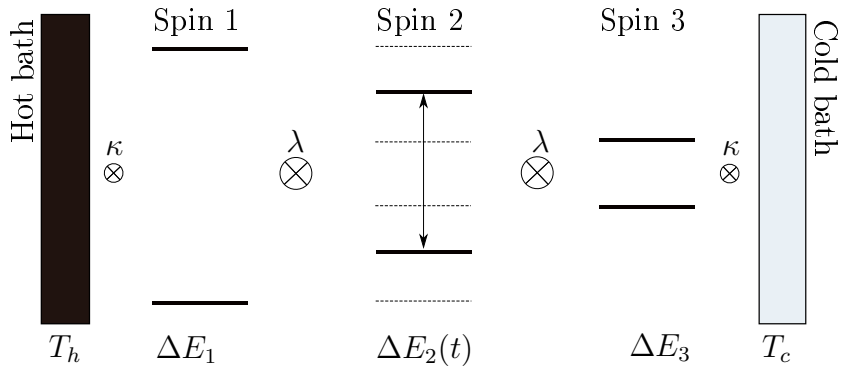

Figure 3.1.: Elementary quantum machine model of a three-spin chain between two heat baths. T_h and T_c are the bath temperatures, λ and κ are coupling constants and ΔE_μ are the local energy gaps of spins $\mu = 1, 2, 3$. ΔE_2 depends on time since the middle spin is driven.

this the resonance conditions

$$\Delta E_1 \geq \Delta E_2(t) \geq \Delta E_3 \tag{3.9}$$

must be fulfilled. Heat currents between the system and the baths only occur if the energy splitting of spin 2 equals one of the constant bounds, i. e. $\Delta E_1 = \Delta E_2$ or $\Delta E_3 = \Delta E_2$. In between, heat currents are negligible so that the occupation probabilities of spin 2 remain constant while its energy splitting is modulated.

Following Eq. (3.2), the first case is related to heat transport at constant spectrum whereas the second case is related to work at constant entropy. Since in Sec. 3.1 it was argued that a spectral deformation corresponds to a volume deformation in classical terms, this quantum thermodynamic cycle can be identified as the quantum analog to the classical Otto cycle, featuring isochoric steps with constant spectrum and adiabatic steps with constant entropy. Therefore it is referred to as the Quantum Otto cycle. With regard to the cycle steps, this analogy will be demonstrated in detail in the following section.

3.2.2. Cycle Steps

Similarly to a classical thermodynamic Otto cycle, the quantum Otto cycle runs in four steps.

1. Isochoric step: Spin 2 is in resonance with spin 3 and therefore coupled to the cold reservoir at temperature T_c. The heat current J_c between this bath and the system gets large, while J_h remains negligibly small. The occupation probabilities and thus the local temperatures of spins 2 and 3 approach as both evolve towards contact equilibrium.

2. Adiabatic step: Spin 2 is driven out of resonance with spin 3, leading to a decrease of J_c. The occupation probabilities, i. e. entropy remains almost unchanged, whereas work is applied or released due to the spectral deformation.

3. Isochoric step: Spin 2 is in resonance with spin 1. The heat current J_h gets large while J_c is negligible. As both spins equilibrate, local temperatures approach each other.

4. Adiabatic step: contrarily analog to step 2.

There are two possible working modes: either the system runs as heat engine, transporting heat from the hot to the cold bath and releasing work, or it runs as heat pump, acting the other way round and consuming work.

3.2.3. Numerical Implementation

In order to calculate the time-dependent system state $\hat{\varrho}_{\mathrm{S}}$, the master equation (2.66) is solved numerically since the super-operator $\hat{\mathcal{L}}$ is too high-dimensional for a closed analytical solution to be available. Independently of its initial state $\hat{\varrho}_S(0)$ the system is found to reach a stable time-dependent attractor state. This also applies for all numerical simulations presented further on and therefore will not be mentioned explicitly any more. For more details on numerical methods used in this work it is referred to Sec. A in the appendix.

Since numerical reasons require a smooth modulation function for $\Delta E_2(t)$, sinusoidal driving is considered in the frame of this work,

$$\Delta E_2(t) = \Delta E_2^0 + a \sin \omega t \tag{3.10}$$

where the offset $\Delta E_2^0 = \frac{1}{2}(\Delta E_1 + \Delta E_3)$ and the detuning parameter $a = \frac{1}{2}(\Delta E_1 - \Delta E_3)$ are chosen to agree with condition (3.9).

The driving frequency ω and the bath temperatures $T_h > T_c$ are given in units of the local spin energy splittings ΔE_i. The same holds for the coupling parameters λ and κ which, due to the Born approximation and Sec. 2.4.2, must stay in the weak coupling limit,

$$\kappa, \lambda \ll \Delta E_i \tag{3.11}$$

The Markov assumption enters by claiming the driving frequency ω to be small enough in order to sufficiently damp the system:

$$\omega \ll \Delta E_2 \tag{3.12}$$

Otherwise, energy transfer between the system and the heat reservoirs via spin resonance would not be possible any more, causing the machine function to break down. On the other hand, choosing a too small driving frequency, i. e. $\omega \ll \kappa$ would make the system run in the quasi-stationary limit where only leakage currents remain and the useful system work turns to zero [16].

This marks an essential difference to conventional classical thermodynamic machine cycles which are normally considered in the quasistatic limit, running infinitesimally slowly but producing a finite amount of work per cycle. In contrast, the Quantum Otto cycle described above must be run in finite time in order to yield a finite work output for the chosen manner of driving.

3.3. The Ideal Quantum Otto Cycle

For any kind of machine functionality crucially depends on the achievable degree of external control on the cycle steps. Obviously this control is limited in the case of time-dependent driving as discussed in the previous section, which will also be shown later on by means of numerical investigations.

In general, one is interested in idealized, fully manageable cycle steps in order to obtain an upper bound for the characteristics of arbitrary machine processes. Regarding the Quantum Otto cycle, a corresponding model shall be briefly reviewed, following [42, 11, 16]. Here, the spectrum and the occupation probabilities within the driven quantum system underlie total control, and so do the cycle steps described in Sec. 3.2.2. Consequently, in this ideal machine process heat is only exchanged during bath contacts and work is only performed on the adiabats. Furthermore, any kinds of losses are ruled out and perfect contact equilibrium is assumed between two spins coming into resonance.

It is now possible to obtain analytical expressions for the work, heat and efficiencies by simply taking into account the energy expectation values of the driven spin before and after each step.

After the driven spin has been in contact with contact spin at the cold bath, it is in the same canonical state:

$$\hat{\varrho}_2 = \frac{1}{Z}\begin{pmatrix} \mathrm{e}^{\Delta E_3/2T_c} & 0 \\ 0 & \mathrm{e}^{-\Delta E_3/2T_c} \end{pmatrix} \tag{3.13}$$

where the partition function reads

$$Z = \mathrm{e}^{\Delta E_3/2T_c} + \mathrm{e}^{-\Delta E_3/2T_c} = \cosh\left(\frac{\Delta E_3}{2T_c}\right) . \tag{3.14}$$

After the following adiabatic step it is $\Delta E_2 = \Delta E_1$ while $\hat{\varrho}_2$ remains unchanged. The work is given by the energetic difference before and after the step (see (2.72)):

$$W_{3\to 1} = \frac{1}{2}\left(\Delta E_3 - \Delta E_1\right)\tanh\frac{\Delta E_3}{2T_c} . \tag{3.15}$$

Together with the contracting adiabatic step the total work becomes

$$\Delta W_{\mathrm{tot}} = \frac{1}{2}\left(\Delta E_1 - \Delta E_3\right)\left(\tanh\frac{\Delta E_1}{2T_h} - \tanh\frac{\Delta E_3}{2T_c}\right) . \tag{3.16}$$

In analogy to this the heat transferred between spins 1 and 2 is

$$\Delta Q_h = \frac{1}{2}\Delta E_1\left(\tanh\frac{\Delta E_1}{2T_h} - \tanh\frac{\Delta E_3}{2T_c}\right) . \tag{3.17}$$

which corresponds to an entire swap of the states of both spins. Calculating Q_c analogously, the Gibbs relation (2.4) is easily verified. With (3.16) and (3.17) the heat engine and heat pump efficiencies for the ideal Quantum Otto cycle result as

$$\eta_{\mathrm{p}}^{\mathrm{Otto}} = \frac{\Delta Q_h}{\Delta W_{\mathrm{tot}}} = \frac{\Delta E_1}{\Delta E_1 - \Delta E_3} , \qquad \eta_{\mathrm{en}}^{\mathrm{Otto}} = \frac{\Delta W_{\mathrm{tot}}}{\Delta Q_h} = 1 - \frac{\Delta E_3}{\Delta E_1} . \tag{3.18}$$

These expressions remind of the classical Otto efficiency (2.11) as they only depend on the spectrum (the "volume") but not on the bath temperatures.

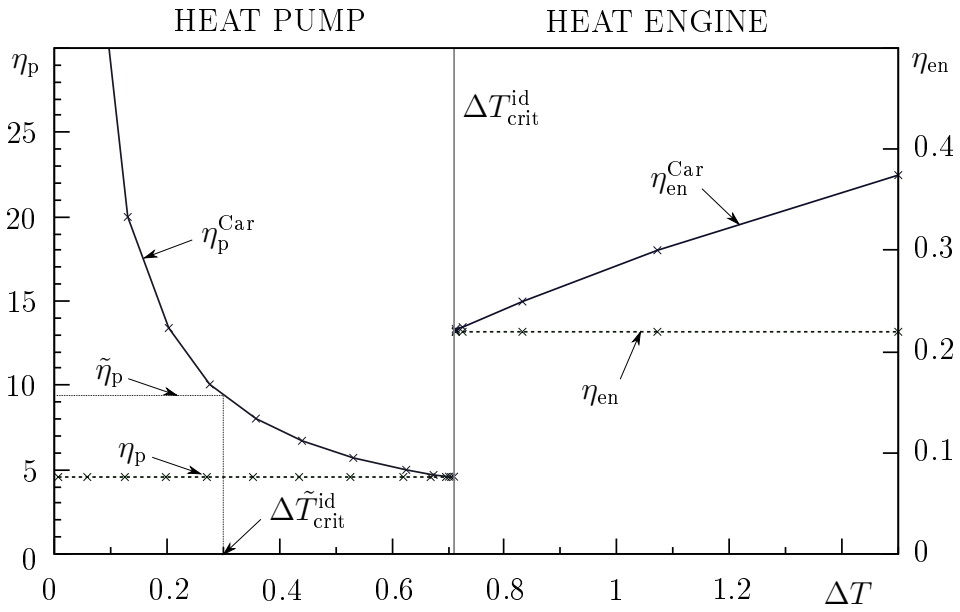

Figure 3.2.: Three-spin machine with decoupling: Efficiencies η_p of the heat pump and η_en heat engine and corresponding Carnot efficiencies $\eta^\mathrm{Car}_\mathrm{en/p}$ as functions of ΔT. Note the different scaling with regard to pump and engine efficiencies.

3.3.1. Three-Spin Machine with Artificial Decoupling

For numerical verification of the ideal Quantum Otto cycle introduced in Sec. 3.3 and particularly of Eq. (3.18), the present author performed numerical simulations of a dynamically driven three-spin machine including an artificial decoupling between adjacent spins in order to impose a high degree of control on the cycle steps and, in particular, to eliminate leakage currents being omnipresent for a permanent coupling (cf. Sec. 4.2). In practice, the Heisenberg couplings are "switched on" only within a given interval during which the driven spin and the respective bath spin are in resonance and set to zero else.

Although one may question whether this procedure is practicable in physical regard, it turns out to be an effective numerical tool to check the plausibility of (3.18) by simulating its premises.

The coupling parameter between the spin pair 1 and 2 is chosen as periodically continued smooth piecewise function $\lambda(t)$ which, over one period $\tau = 2\pi/\omega$, is defined as

$$\lambda_{12}(t) = \begin{cases} \lambda \sin^2\left[a\omega\left(t - b\frac{\pi}{\omega}\right)\right] & b\frac{\pi}{\omega} \leq t \leq (b+\frac{1}{a})\frac{\pi}{\omega} \\ 0 & \text{else} \end{cases} . \tag{3.19a}$$

Similarly, the coupling parameter for the second spin pair 2 and 3 gets

$$\lambda_{23}(t) = \begin{cases} \lambda \sin^2\left[a\omega\left(t - c\frac{\pi}{\omega}\right)\right] & c\frac{\pi}{\omega} \leq t \leq (c+\frac{1}{a})\frac{\pi}{\omega} \\ 0 & \text{else} \end{cases} . \tag{3.19b}$$

Here $\lambda = 0.01$ denotes the spin-spin coupling constant and $\omega = 2\pi/128 = 804.25$ is the driving frequency. The parameters a, b, c have to be selected appropriately such

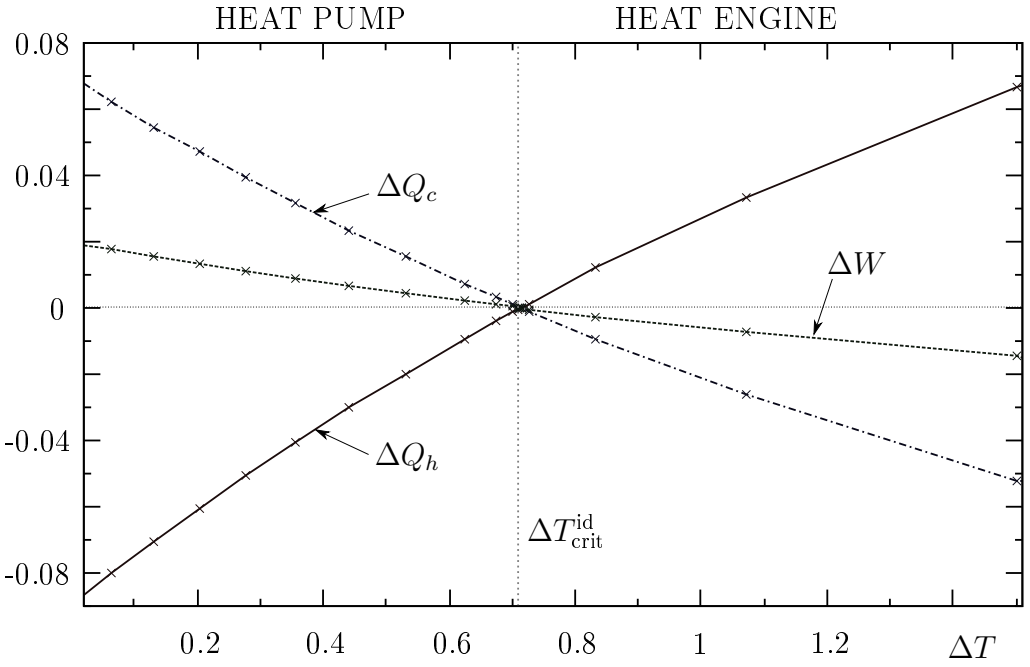

Figure 3.3.: Three-spin machine with decoupling: Work ΔW and heat ΔQ_h, ΔQ_c as functions of ΔT. The critical temperature gradient is $\Delta T^{\rm id}_{\rm crit} = 0.714$.

that interaction times between resonant spins are sufficiently long and, on the other hand, leakage currents are suppressed. An adequate set of parameters is $a = 2.5$, $b = \frac{\pi}{2}(1-\frac{1}{a}) = 0.3\pi$ and $c = 1+b = 1.3\pi$. The local energy splittings are $\Delta E_1 = 2.25$, $\Delta E_2 = 2.0 + 0.25 \sin \omega t$ and $\Delta E_3 = 1.75$. The cold bath temperature $T_c = 1/\beta_c = 2.5$ is kept constant while that of the hot bath, T_h, is varied. Since the additional deformation of the spectrum due to the time-dependent coupling $\lambda(t)$ is only of magnitude $10^{-2}\,[\Delta E]$ it may be neglected.

Further information on numerical treatment are found in Sec. 3.2.3 and Sec. A in the appendix.

Efficiencies, Heat and Work

For the three-spin quantum machine with artificial decoupling, the heat pump and heat engine efficiencies $\eta_{\rm p}$ and $\eta_{\rm en}$ are obtained via (3.7) and plotted in Fig. 3.2 as functions of the temperature gradient $\Delta T = T_h - T_c$, together with the respective Carnot efficiencies $\eta_{\rm p}^{\rm Car}$ and $\eta_{\rm en}^{\rm Car}$ (cf. (2.6) and (2.7)). Indeed the results agree with the predictions from Sec. 3.3. In particular, the efficiencies $\eta_{\rm en/p}$ coincide perfectly with the Quantum Otto efficiencies for the given local energy splittings. According to Eq. (3.18), these take the values $\eta_{\rm p}^{\rm Otto} = 4.5$ for the heat pump and $\eta_{\rm en}^{\rm Otto} = 0.22$ for the heat engine. They are independent of ΔT except at a critical external temperature gradient $\Delta T^{\rm id}_{\rm crit}$ where they reach their respective Carnot equivalents. This is however not a violation of the second law of thermodynamics. Fig. 3.3 shows the transferred heat ΔQ_h and ΔQ_c between the system and the hot and cold reservoir obtained with (3.5) as well as the work ΔW,

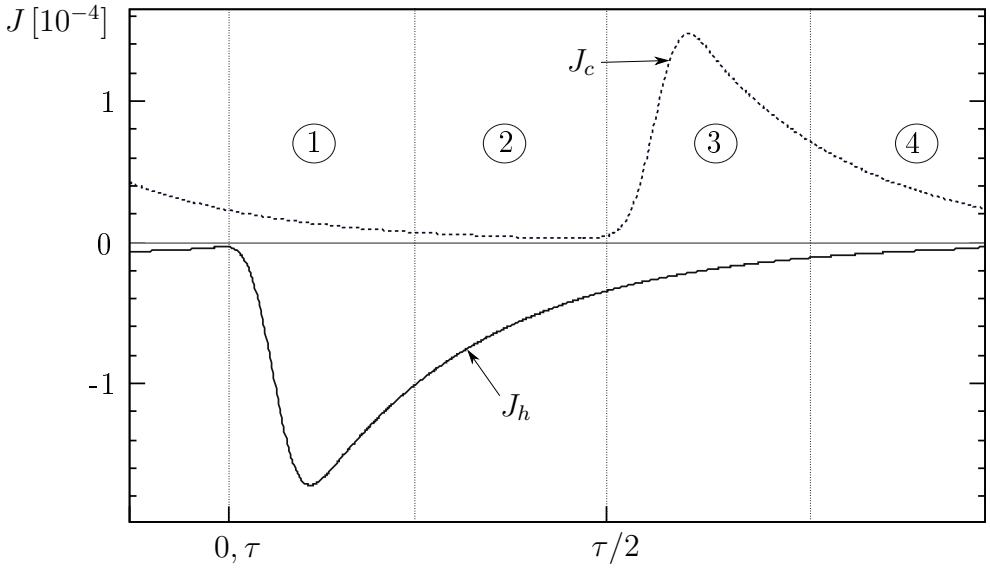

Figure 3.4.: Heat currents J_c and J_h over one period τ for the Quantum Otto machine with artificial decoupling, working as heat pump ($\Delta T = 0.13$).

calculated via (3.4), both as functions of ΔT. It follows that at $\Delta T_{\text{crit}}^{\text{id}}$ no work is carried out or exhausted, i. e. $\Delta W = 0$. On both sides the work as well as the heat functions change sign.

As a consequence, the mode of operation of the Quantum Otto machine switches between a heat pump and a heat engine at this point. This can be easily understood by comparing the canonical distributions of the bath spins which the driven spin exhibits alternately. In an ideal Quantum Otto cycle no heat should be transported if the canonical distributions of both bath spins are identical, so the work is also expected to vanish. By condition,

$$\frac{\varrho_1^{11}}{\varrho_1^{00}} = \frac{\varrho_3^{11}}{\varrho_3^{00}} \quad \Longrightarrow \quad \mathrm{e}^{-\Delta E_1/T_h} = \mathrm{e}^{-\Delta E_3/T_c} \tag{3.20}$$

or $\Delta E_1/\Delta E_3 = T_h/T_c$. Inserting this into (3.18) immediately leads to equality of the Quantum Otto and Carnot efficiencies at $\Delta T_{\text{crit}}^{\text{id}}$, in accordance with the numerics. Otherwise, $\eta^{\text{Otto}} < \eta^{\text{Car}}$ in agreement with the second law. If the "$<$" sign holds in (3.20) the system transports heat from the cold to the hot reservoir against the internal energy gradient. During the increase of its local energy gap ΔE_2 the driven spin carries the distribution $\mathrm{e}^{-\Delta E_3/T_c}$ and work is released since the energy of the higher occupied lower level is decreased. On the other hand, work has to be inserted to reduce ΔE_2 when spin 2 carries the distribution $\mathrm{e}^{-\Delta E_1/T_h}$ after heat transfer between the system and the hot bath, since now the energy of the lower level is increased again. Altogether a net amount of work $\Delta W > 0$ has to be inserted if the system runs as heat pump.

In the case the "$>$" sign holds in (3.20) the system works as heat engine why a net amount of work $\Delta W < 0$ is released.

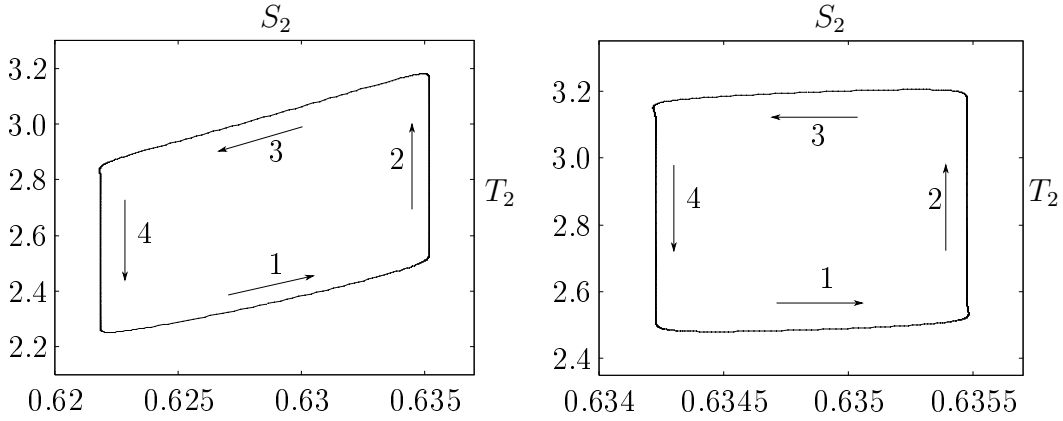

Figure 3.5.: Quantum Otto machine with artificial decoupling: ST-diagram run by the driven spin in heat pump mode, (left), cf. a classical Otto cycle, and if approaching $\Delta T_{\text{crit}}^{\text{id}}$ (right), cf. Carnot cycle.

The critical temperature gradient is obtained from (3.20), too:

$$\Delta T_{\text{crit}}^{\text{id}} = T_c \left(\frac{\Delta E_1}{\Delta E_3} - 1 \right) \tag{3.21}$$

For the given parameters it follows that $\Delta T_{\text{crit}}^{\text{id}} = 0.714$ as approved in Figs. 3.2 and 3.3. For differently chosen energy gaps of the bath contact spins the Quantum Otto heat pump efficiency would be found at $\tilde{\eta}_{\text{p}}^{\text{id}}$ and thus the critical temperature gradient would decrease to $\Delta \tilde{T}_{\text{crit}}^{\text{id}}$ (see also [16]).

Heat Currents and ST-Cycles

For the Quantum Otto heat pump with artificial decoupling the heat currents $J_h < 0$ from the system into the hot bath and $J_c > 0$ from the cold bath into the system are calculated with the help of (2.78) and displayed in Fig. 3.4, both over one period $\tau = 2\pi/\omega$. Since we deal with a non-equilibrium scenario here, $J_h \neq -J_c$, contrary to the stationary case. For a heat engine the signs of both curves would simply change.

The numbers 1 to 4 refer to the cycle steps described in Sec. 3.2.2. If the driven spin becomes resonant to one of the the bath contact spins, the corresponding spin-spin coupling is "switched on". In succession both spins immediately swap due to the big mutual temperature difference and since the spin-spin interaction is much stronger here than the one between the system and the baths, i. e. $\lambda \gg \kappa$. As a consequence, the heat currents between the system and the baths increase considerably.

After the coupling has been "switched off" again, any back-float of heat is suppressed. Thus, the respective bath spin exponentially relaxes back into its canonical equilibrium state due to the decohering bath influence, cf. [26].

In the left part of Fig. 3.5 the ST-diagram of the ideal Quantum Otto cycle running as heat pump is illustrated. Again the numbers 1 to 4 refer to the cycle steps from Sec. 3.2.2. Spin 2 runs two adiabats (2,4) where its entropy S_2 remains constant, and

two isochores (1,3) where both entropy and temperature T_2 change with zero work performance. Hereby the entropy and temperature of the gas spin 2 result from (2.70) and (2.73), respectively.

The engine scenario qualitatively would yield the same course in opposite direction. Towards the critical temperature gradient $\Delta T_{\mathrm{crit}}^{\mathrm{id}}$, the ST-diagram takes more and more a rectangle shape like in a Carnot cycle as illustrated in the right part of Fig. 3.5, since also the Quantum Otto efficiency approaches the Carnot efficiency. At the same time the shape of the ST-diagram and thus the work decrease to zero (note the difference in the scaling of the S_2 axes).

Summarizing, this numerical model is able to simulate adequately a three-spin system running an ideal Quantum Otto cycle under nearly perfectly controlled cycle steps. Discussion and analysis of the dynamically driven three-spin machine at permanent coupling can be found in [15, 16].

4. Parallel Quantum Machine Circuits

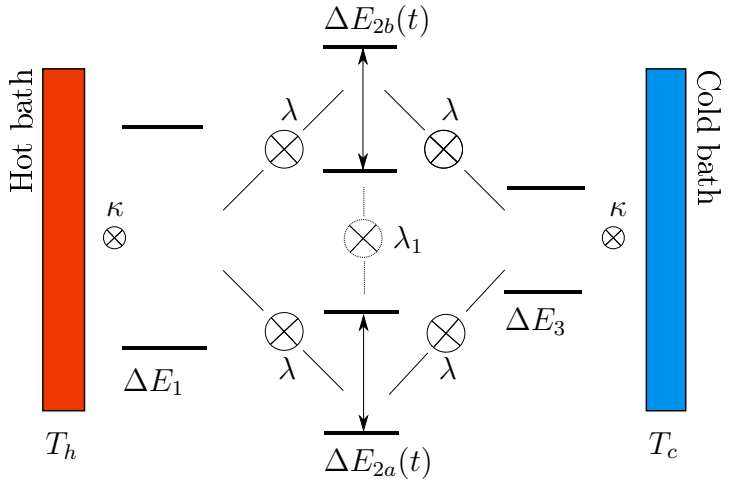

Figure 4.1.: Model of the parallel quantum machine circuit. ΔE_ν are local spin energy gaps. Big circles stand for Heisenberg spin coupling (λ) and small ones for system-bath interaction (κ). The coupling λ_1 is optional.

After it has been shown in the previous chapter and in [16, 15] that a Heisenberg chain of three spins between to heat reservoirs may be enabled to run a Quantum Otto cycle, it is now of interest in how far this concept is extendable to more complex quantum machine networks such as parallel and serial circuits of quantum machines. In this case also the question for common characteristics and differences between the different models arises. To give an answer, this chapter deals at first with a model of a quantum machine circuit where two gas spins are coupled in parallel. Serial machine circuits will be investigated in Ch. 5.

The parallel quantum machine circuit is depicted in Fig. 4.1. Here spins $2a$ and $2b$ are driven and therefore take the role of the working gas. Both are coupled in parallel to the bath spins 1 and 3 where again the interaction is of Heisenberg type. The Hamiltonian for this model is obtained via Eq. (3.8),

$$\hat{H} = \sum_{\mu=1,2a,2b,3} \frac{\Delta E_\mu}{2} \hat{\sigma}_z^\mu + \lambda_1 \sum_{i=x,y,z} \lambda_1 \hat{\sigma}_i^{2a} \otimes \hat{\sigma}_i^{2b} + \lambda \sum_{i=x,y,z} \hat{\sigma}_i^1 \otimes \hat{\sigma}_i^{2a} + \hat{\sigma}_i^1 \otimes \hat{\sigma}_i^{2b} + \hat{\sigma}_i^{2a} \otimes \hat{\sigma}_i^3 + \hat{\sigma}_i^{2b} \otimes \hat{\sigma}_i^3 \quad (4.1)$$

In the course of this chapter several dynamical driving scenarios are considered. The gas spins may either be driven in-phase (see Sec. 4.2) or with a relative phase shift (Sec. 4.3). In both cases they are mutually uncoupled by default ($\lambda_1 = 0$).

The effects of a strong coupling between the gas spins ($\lambda_1 \neq 0$) are investigated in Sec. 4.2.2. Finally, the dependence of the process characteristics on the driving frequency ω is discussed in Sec. 4.2.1.

4.1. Static Heat Current Scenario

Before investigating the mentioned dynamic quantum machine scenarios, the static heat current behavior in the parallel four-spin circuit has to be analyzed in order to verify whether the statements cited in Sec. 2.5.3 also hold in this case, even if a a different behavior compared to a linear spin chain setup is not expected. In particular, the dependence of the heat currents on the local energy gaps in terms of spin chain resonance is of interest. In the following, corresponding numerical examinations are performed qualitatively by means of concrete examples.

First, the local energy gaps of the bath contact spins are chosen $\Delta E_1 = \Delta E_3 = 1.0$, and the bath temperatures are $T_h = 2.63$ and $T_c = 2.5$, whereas the splittings of the middle spins, ΔE_{2a} and ΔE_{2b} are simultaneously varied.

The resulting stationary heat currents J_h^4 from the hot bath into the system and J_c^4 from the system into the cold bath are calculated with the help of (2.78) and depicted in Fig. 4.2. Both approach zero for a strong detuning and reach their respective maxima at overall resonance where $\Delta E_{2a} = \Delta E_{2b} = 1.0$, in analogy to the explanations given in Sec. 2.5.3. As expected, the relation $J_c = -J_h$ is fulfilled anytime.

For reasons of comparison, Fig. 4.2 also shows the developing of the corresponding heat currents J_h^3 and J_c^3 in a three-spin chain in dependence of the detuning of the middle spin, cf. [16].

In a first order approximation both systems obviously exhibit the same stationary heat current characteristics. Hence one may conclude that the bath contact spins 1 and 3 act as filters only allowing for a limited heat throughput which does not predominantly depend on the internal configuration of the spin system, the more so as the system-bath coupling strength remains unchanged. Since there are no heat sinks or sources within the system, the heat current is conserved. Thus, depending on the spin chain resistance in terms of the detuning of $\Delta E_{2a,2b}$, the heat current J_h splits up into two partial currents running through the "branch" spins $2a$ and $2b$ [41].

At this point analogies to electric current and the Kirchhoff node rule for electric circuits can be deduced, comparing the former to heat current and the spins in a spin chain to resistances in a parallel electric circuit, the more so as electrical current is conserved as well and would thus split up into partial currents at a branching point, depending on the strength of the resistances in the branches.

The small but not negligible discrepancies between both curves in Fig. 4.2 result from the different forming of correlations, comparing the simpler geometry of a three-spin chain to the more complex one in a paralleled spin chain. Correlations such as entangle-

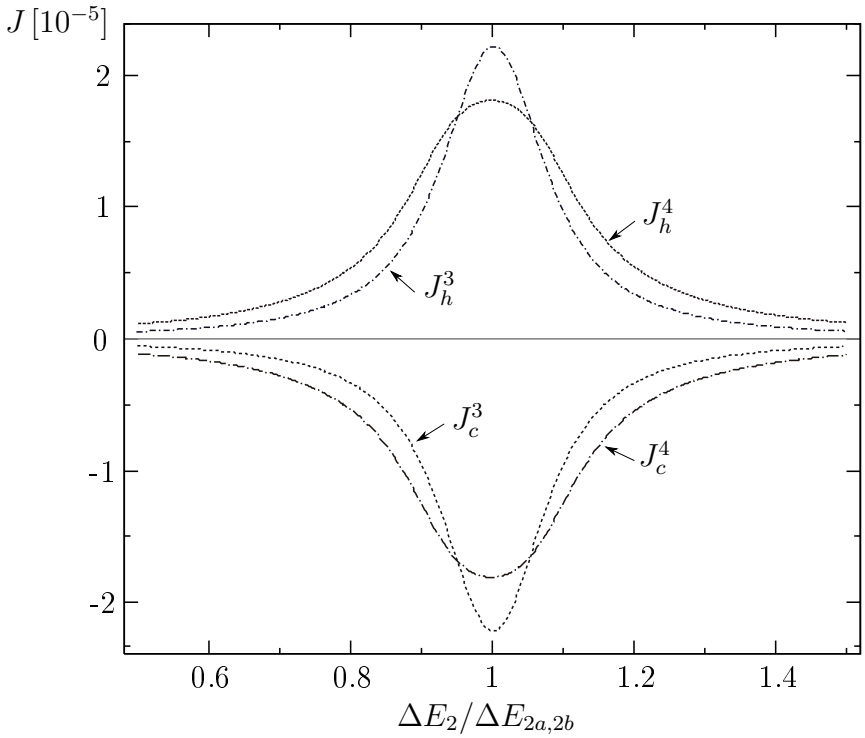

Figure 4.2.: Static heat currents $J^4_{h,c}$ through the parallel four-spin circuit as functions of the variation of ΔE_{2a} and ΔE_{2b}, compared to the currents $J^3_{h,c}$ through a 3-spin chain as function of the energy splitting ΔE_2 of the middle spin.

ment typically arise in anti-ferromagnetic Heisenberg chains at low temperatures. Their magnitude crucially depends on temperature as well as on the local magnetic fields. This is shown e. g. in [35] with the help of the Bures distance measure given in (2.35).

A concrete example for the relationship between the heat current and correlations in the parallel four-spin circuit is shown in Fig. 4.3. Here only ΔE_{2a} is varied while $\Delta E_{2b} = 1.0$ remains constant and $\Delta E_1 = \Delta E_3 = 1.0$ as above. Over a wide range of detuning the stationary heat current J_h^{2a} takes the maximal resonance value of J_h^3 found for the three-spin chain, whereas for $\Delta E_{2a} = 1.0 = \Delta E_{2b}$ the maximum current of J_h^4 found in the four-spin circuit for overall resonance is achieved, cf. Fig. 4.2. The analog holds for $J_c^{2a} = -J_h^{2a}$, omitted here.

Obviously, in the case only one of the middle spins is strongly detuned, all heat transport would obviously happen via the other one being in resonance with the bath spins, since the total current approximately equals that through a three-spin chain, cf. Fig. 4.2. Once again this resembles very much the behavior of electrical current in a parallel circuit with two branches, say. If one branch featured a high resistance while the resistance of the other branch was low, the major amount of electrical current would run through the latter.

Comparing J_h^{2a} to the Bures distance measure for the parallel four-spin circuit (cf. (2.35)),

$$D^2 = \mathrm{Tr}\big\{\big(\hat{\varrho}_\mathrm{S} - (\hat{\varrho}_1 \otimes \hat{\varrho}_2 \otimes \hat{\varrho}_3 \otimes \hat{\varrho}_4)\big)^2\big\}$$

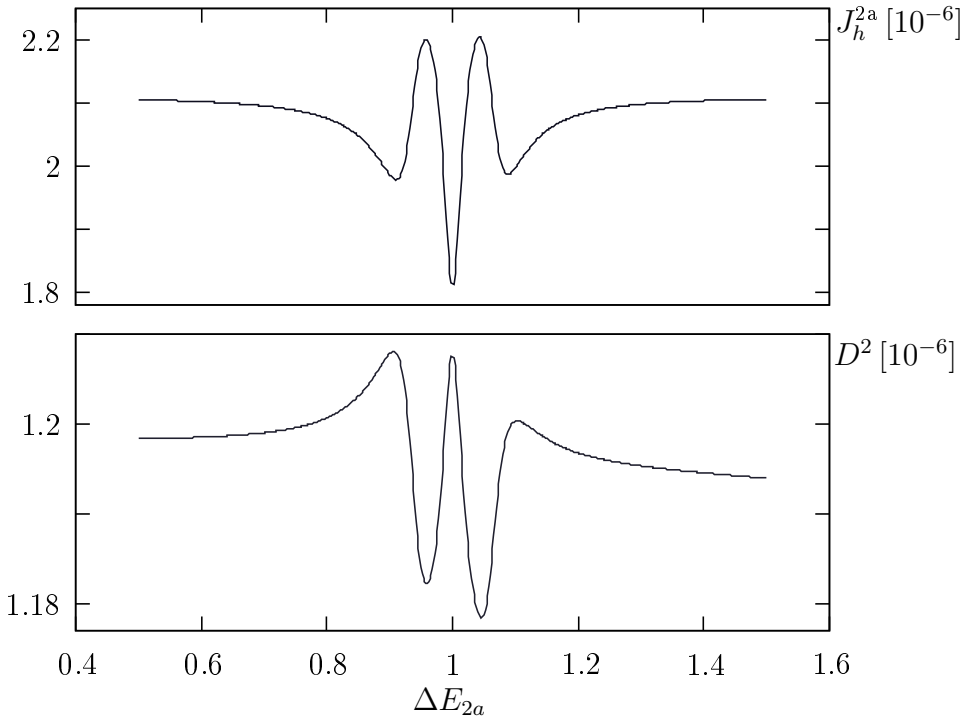

Figure 4.3.: Static heat current J_h^{2a} through the parallel four-spin circuit (upper part) and Bures distance D^2 (lower part, see text), both as functions of the variation of the energy gap ΔE_{2a} of spin $2a$ only

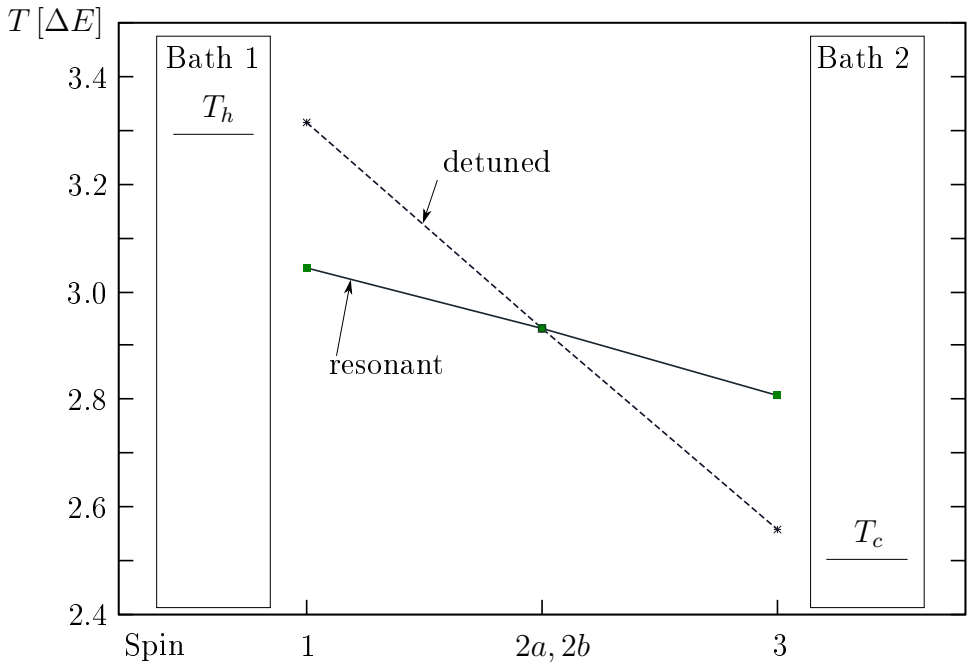

Figure 4.4.: Linear temperature gradient in the parallel four-spin circuit for overall resonance (solid) and if both middle spins $2a, 2b$ are detuned (dashed). The temperatures of the middle spins approximately coincide.

yields that both qualitatively exhibit the same characteristics. Thus, Fig. 4.3 reveals again that the difference in heat conductivity between the three-spin chain and the four-spin circuit is associated with the differing forming of correlations in both systems.

It must be noted that at present neither the effects of classical nor quantum correlations on the treated non-equilibrium scenarios are included in the model description on a quantitative level yet. A promising ansatz for this purpose is given in [43], linking heat currents in a spin chain to entanglement, which in turn is a function of the global temperature gradient and the local spin energy splittings.

In analogy to Sec. 2.5.3 all spins in the parallel circuit are always found in local equilibrium states and thus exhibit local temperatures. The validity of Fourier's law for the present scenario is again verified qualitatively by exemplarily choosing the bath temperatures as $T_h = 3.3$ and $T_c = 2.5$, the local energy gaps of the bath spins as $\Delta E_1 = \Delta E_3 = 1.0$ and the coupling parameters as $\lambda = 0.01$ and $\kappa = 0.001$. Fig. 4.4 shows that an internal linear temperature gradient is found in the system, depending on the detuning of $\Delta E_{2a,2b}$. In all cases The temperatures of spins $2a$ and $2b$ are both found at about the same value and close to the average temperature $T_{2a,2b} \simeq 2.9 = \frac{1}{2}(T_h + T_c)$.

A stronger detuning of both spins, e. g. $\Delta E_{2a} = \Delta E_{2b} = 1.3$ compensates the internal coupling strength in the spin chain. The bath contact spins 1 and 3 thus approach the respective bath temperatures $T_{h,c}$ but are shifted to slightly higher values (dashed line). The external and internal temperature gradients approximately coincide as it would be the case for a weaker internal coupling strength, e. g. $\lambda = 0.001$. Following Fig. 4.2 the corresponding stationary heat current is very small. Reference is made here to [35].

On the other hand, if all spins are resonantly split, $\Delta E_{2b} = \Delta E_{2a} = 1.0$ the internal temperature gradient is flatter (solid line) due to the stronger internal coupling, coming along with strong heat currents.

All in all, it has become evident that, as general property of spin chain systems between two heat baths, the bath contact spins act as filters limiting the heat current through the chain. In a first order approximation the heat currents do not depend on the internal configuration of the spin system. This limitation will come up again in the following sections, presenting numerical results of the dynamically driven parallel four-spin circuit.

4.2. Dynamically Driven Parallel Four-Spin Circuit

This section deals with the scenario of driving the four-spin circuit depicted in Fig. 4.1 dynamically by modulating the middle spins $2a$ and $2b$ periodically in time. The motivation hereof is to demonstrate that both driven spins run a Quantum Otto cycle each, corresponding to the cycle steps listed in Sec. 3.2.2, and to draw comparisons to the three-spin machine cycle.

In the following, spins $2a$ and $2b$ are sinusoidally modulated with a frequency $\omega = 1/128$ and zero relative phase ($\varphi = 0$). Initially they are uncoupled ($\lambda_1 = 0$). Again the cold reservoir temperature is set constant, $T_c = 1/\beta_c = 2.5$ while T_h is varied. The local spin energy gaps are chosen as $\Delta E_1 = 2.25$, $\Delta E_{2a}(t) = \Delta E_{2b}(t) = 2.0 + 0.25 \sin \omega t$ and

ΔE_1 (hot bath)	ΔE_3 (cold bath)	ω	T_h	T_c	λ	κ
2.25	1.75	1/128	2.5 - 5.0	2.5	0.01	0.001

Table 4.1.: Standard parameters for the quantum machine setups in the present work, given in units of local energy splittings ΔE

$\Delta E_3 = 1.75$, fulfilling the resonance condition

$$\Delta E_1 \geq \Delta E_{2a,2b}(t) \geq \Delta E_3 \,.$$

It becomes clear that both spins indeed perform Quantum Otto cycles with consecutive isochoric and adiabatic steps, see Sec. 3.2.1 and Sec. 3.2.2. During the isochores the driven spins simultaneously come into resonance with the same bath spin, resulting in a heat flux between the system and the respective bath. In between, during the adiabats, the local energy gaps of the gas spins are modulated and thus brought out of resonance with the bath spins why heat currents are negligibly small. In the following this behavior will be substantiated by numerical simulations.

Table 4.1 lists some standard parameters which from now on will be used for the various models treated this work if not mentioned otherwise.

Fig. 4.5 shows the heat currents $J_h < 0$ and $J_c > 0$, obtained via (2.78) for the case the dynamically driven parallel circuit works as heat pump. The numbers 1 to 4 denote the four cycle steps, cf. Sec. 3.2.2. Heat transfer between the system and the hot and cold bath occurs during the isochoric steps 1 and 3, respectively, while steps 2 and 4 are adiabats.

A major difference to the idealized scenario with artificial decoupling described in Sec. 3.3.1 arises in the symmetric shape of the currents. The reason hereof is a leakage current J_L floating from the hot to the cold bath. Due to the permanent coupling between the driven and bath spins a uncontrollable back-flow of heat current within the spin chain occurs during the isochoric steps, causing a leakage heat transfer of $Q_L = \oint_0^\tau J_L \mathrm{d}t$ per cycle. In all models treated in this work we consider a net current balance, i. e. J_L is always included in the total heat currents.

As a consequence, the net heat currents are smaller in magnitude and decay to zero much faster than seen in Fig. 3.4 for the artificial decoupling scenario since a considerable amount of heat floats back into the direction of the internal temperature gradient in an uncontrolled manner whereas, in the case of a heat pump, heat is to be transported into the opposite direction.

On the one hand, leakage is responsible for reduced heat transport which also means less work to be applied or released. For this reason, the absolute values and therewith the inclinations of the heat and work functions depending on the global temperature gradient are decreased as seen later on. On the other hand, additional work has to be applied to the driven spins in order to compensate losses. Since this work is effectively dissipated, the dynamically driven Quantum Otto cycle is an irreversible process lack of full check on the cycle steps.

In particular, the presence of losses is indicated by the dips observed in the ST-diagrams of the driven spins $2a$ and $2b$. These are depicted in Fig. 4.6 for the cases the circuit runs as heat pump and heat engine, respectively, where the temperatures T_{2a} and T_{2b} are obtained with (2.73) and the entropies S_{2a} and S_{2b} with (2.70). At the end of the isochoric steps, heat evidently flows into the direction of the temperature gradient in the system. Thus, losses are especially profound in the case of a heat pump since, based on the dip size, more work performance is lost.

In Fig. 4.6 only one corresponding ST-diagram is shown for both gas spins. Since the modulation is symmetrical, it is found that both run the same thermodynamic cycle, that is, they both receive and deliver one half of the total of heat current and thus exert or consume the same amount of work $\Delta W_{2a} = \Delta W_{2b}$, adding up to the total system work ΔW_{tot}. This is indicated in Figs. 4.9 and 4.10.

As a consequence, the efficiencies of the entire circuit and those of the single driven units are all identical, $\eta_{\mathrm{en/p}}^{\mathrm{tot}} = \eta_{\mathrm{en/p}}^{\mathrm{2a}} = \eta_{\mathrm{en/p}}^{\mathrm{2b}}$.

Another interesting aspect arises from the filtering nature of the bath spins, mentioned in Sec. 4.1, and from the description of the ideal Quantum Otto cycle in Sec. 3.3. Hence the characteristic system properties such as critical temperature gradient, heat, work and efficiencies should basically be governed by the bath temperatures and the local energy gaps of the bath spin splittings and not predominantly depend on the internal spin chain configuration. In particular, the ideal Quantum Otto efficiencies given by Eq. (3.18) take the same values for the parallel four-spin circuit as for a linear chain.

The heat pump and heat engine efficiencies of the dynamically driven parallel four-spin circuit are obtained via Eq. (3.7) and depicted in Fig. 4.7 as functions of the temperature gradient $\Delta T = T_h - T_c$, together with the Carnot efficiencies. Fig. 4.9 shows the related heat ΔQ_h and ΔQ_c, obtained by (3.5), the local work ΔW_{2a} and ΔW_{2b} of the single driven units $2a$ and $2b$, obtained via (3.4) and, finally, the total circuit work $\Delta W_{\mathrm{tot}} = \Delta W_{2a} + \Delta W_{2b}$. Fig. 4.10 is a zoom into the same.

The critical temperature gradient lies at $\Delta T_{\mathrm{crit}} = 0.63$, being smaller than the ideal value of $\Delta T_{\mathrm{crit}}^{\mathrm{id}} = 0.714$ obtained with (3.21). Here the machine is idle, $\Delta W_{\mathrm{tot}} = \Delta W_{2a} = \Delta W_{2b} = 0$ and likewise the stationary case only a leakage current J_L and thus a stationary heat transport $\Delta Q_L = \Delta Q_h = -\Delta Q_c$ remain. Moreover, the engine and pump efficiencies are always inferior to the respective Carnot bounds and decay to zero on approach to ΔT_{crit}. For $\Delta T \to 0$ the heat pump efficiency η_{p} does not diverge since asymmetry within the system persists, introduced by the inhomogeneous spin chain splitting.

Following Fig. 4.10, ΔQ_c changes sign before ΔQ_h does, which is due to leakage. In the region where ΔQ_h and ΔW_{tot} are both positive, all work input is dissipated to compensate losses.

In Fig. 4.8 the efficiencies of the dynamically driven circuit are compared to those of an ideal Quantum Otto cycle which after (3.18) take the values $\eta_{\mathrm{p}}^{\mathrm{Otto}} = 4.5$ and $\eta_{\mathrm{en}}^{\mathrm{Otto}} = 0.222$ for the bath spin energy splittings being $\Delta E_1 = 2.25$ and $\Delta E_3 = 1.75$. Although the latter are supposed to be upper bounds, the dynamical heat pump efficiency η_{p} may obviously exceed $\eta_{\mathrm{p}}^{\mathrm{Otto}}$ for small ΔT. Apparently the attribute 'ideal' must be handled carefully with regard to the Quantum Otto cycle.

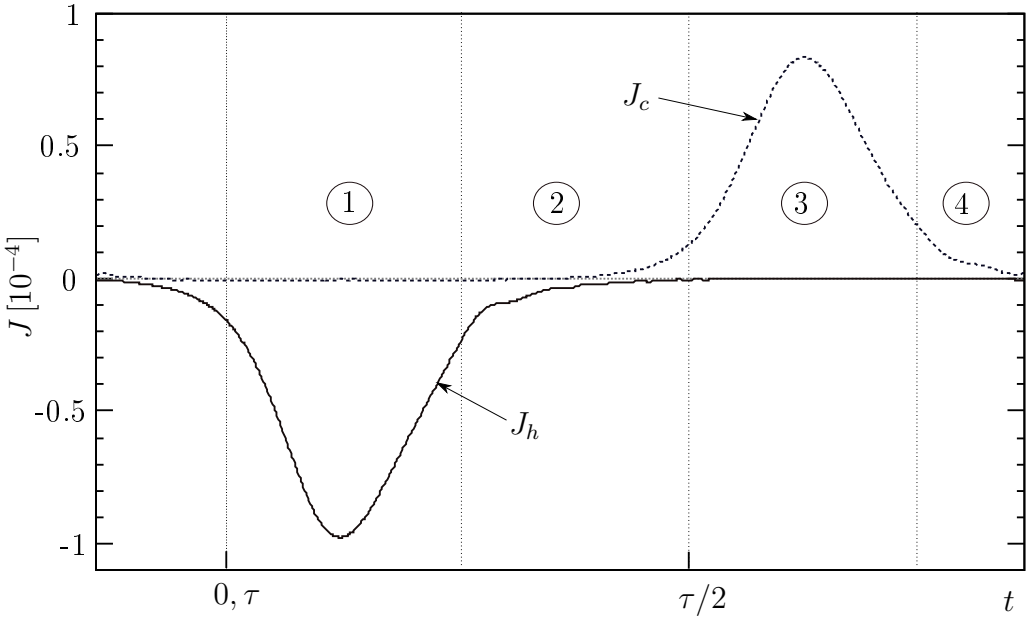

Figure 4.5.: Heat currents over one period τ if the entire parallel four-spin circuit works as heat pump ($\Delta T = 0.13$) without relative driving phase between the gas spins.

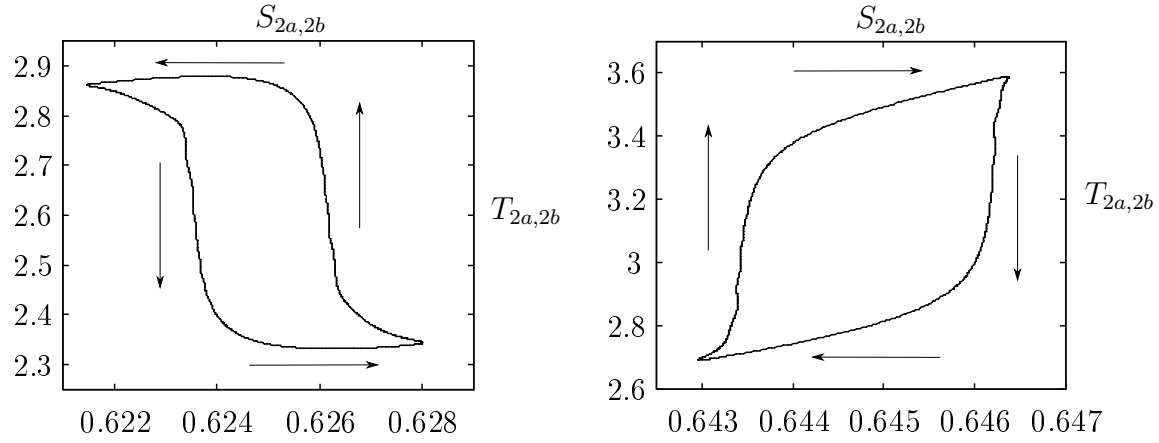

Figure 4.6.: ST-diagrams if the entire parallel four-spin circuit is driven in-phase and works as heat pump (left diagram) or as heat engine (right diagram). Only one ST-diagram for both driven spin is displayed.

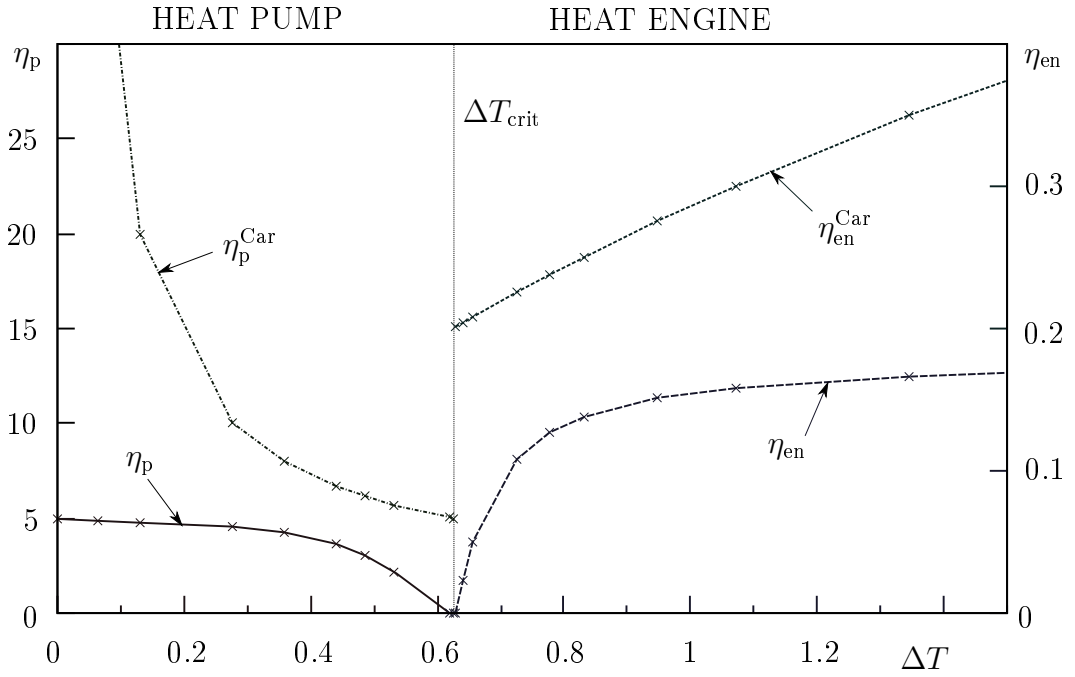

Figure 4.7.: Parallel four-spin circuit driven in-phase ($\varphi = 0$): Efficiencies of the heat engine $\eta_{\rm en}$ and heat pump, $\eta_{\rm p}$ and Carnot bounds $\eta_{\rm en/p}^{\rm Car}$ as functions of ΔT.

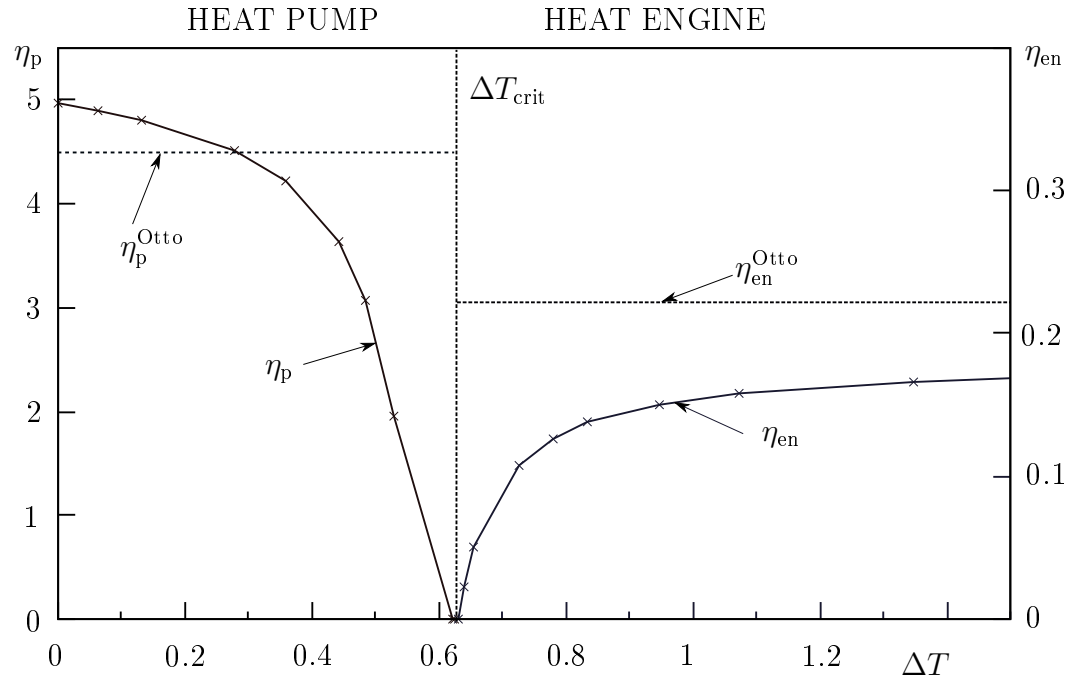

Figure 4.8.: Parallel circuit driven in-phase: Efficiencies of the heat engine and heat pump, $\eta_{\rm en/p}$ and corresponding Quantum Otto efficiencies $\eta_{\rm en/p}^{\rm Otto}$ as functions of ΔT.

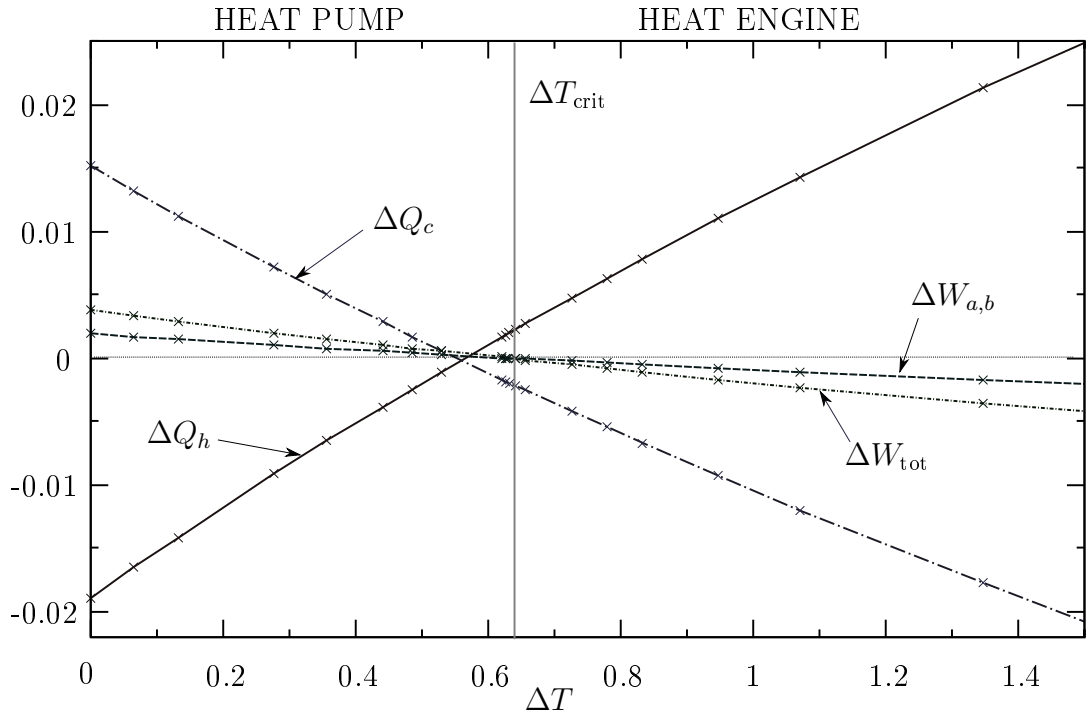

Figure 4.9.: Parallel circuit driven in-phase: Heat ΔQ_h and ΔQ_c, work of the entire circuit ΔW_{tot} and work of the single gas spins ΔW_a, ΔW_b as functions of ΔT.

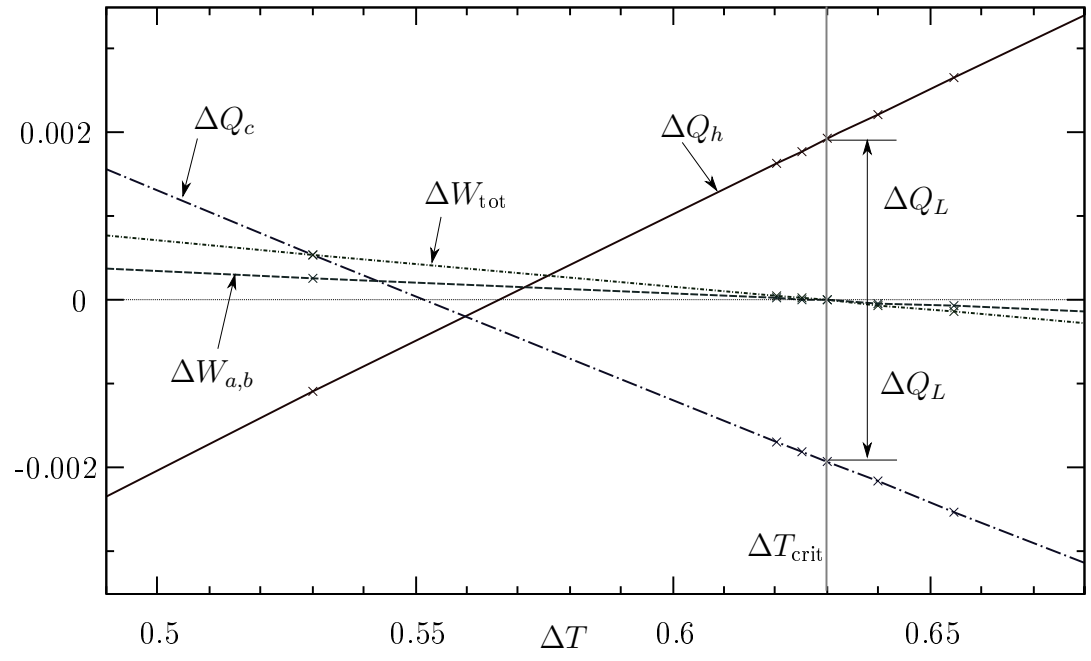

Figure 4.10.: Zoom into Fig. 4.9: At $\Delta T_{\text{crit}} = 0.63$ the circuit is idle, $\Delta W_{\text{tot}} = 0$. Only the leakage Q_L remains.

The losses underlying the described deviations from the behavior originally expected for a Quantum Otto cycle may be introduced from a phenomenological point of view [16]. Here the gas spins are assumed to approach a thermal state which is not in accordance with the respective bath temperatures. By consequence ΔQ_h and ΔQ_c are decreased. On the other hand also less work is done, which explains the possibility that $\eta_{\mathrm{p}}^{\mathrm{qm}}$ may exceed $\eta_{\mathrm{en}}^{\mathrm{Otto}}$. In general, these losses are asymmetric since they are always directed towards the temperature gradient in the system. This feature finally makes the heat pump and engine efficiencies vanish on approaching ΔT_{crit} which usually is inferior to $\Delta T_{\mathrm{crit}}^{\mathrm{th}}$. Thus, effectively, the emergence of the engine function is favored.

Comparing the numerically found properties of the parallel four-spin circuit to those of the linear three-spin machine [15, 16], one finds good accordance. Thus, in first order approximation it is feasible to map both models on each other in that both systems run equivalent Quantum Otto cycles and exhibit the same characteristics provided the bath temperatures and the energy gaps of the bath spins are identically chosen.

Though, discrepancies between the different systems remain which are unexplained yet. In order to obtain a more convenient theoretical description it will become necessary to include the effects of correlations on the heat currents cf. [43].

In particular, it is presumably inappropriate to assume ideal heat exchange under perfect contact equilibrium if two spins are coupled in parallel to a third one. As mentioned already in Sec. 4.1, in the case of a spin "ladder" correlations will form in a different manner than in a simple spin chain. Nevertheless, contact equilibrium does develop up to a certain degree, that is why the machine finally works.

4.2.1. Impact of the Driving Frequency

As sketched in Sec. 3.2.3, our quantum machine circuits run on finite time scales. In contrast to an ideal classical process the work turns zero in the quasi-static limit ($\omega \to 0$), corresponding to the stationary scenario described in Sec. 4.1. On the other hand, following condition (3.12) a too fast driving speed ($\omega \to \infty$) would also lead to a breakdown since the dynamical timescale of the system would then approach that of the baths, inhibiting sufficient damping.

In the following the dependence of some heat pump and the heat engine characteristics on the driving frequency ω are discussed by means of the parallel four-spin circuit with the gas spins driven in-phase. We choose the temperature gradients as $\Delta T = 0.13$ and $\Delta T = 1.5$, respectively, and leave all other parameters as listed in table 4.1.

Fig. 4.11 shows the work ΔW^{en} released by the engine and the heat ΔQ_h^{p} transported to the hot reservoir by the pump. Both absolute values cease for slow and very fast driving frequencies and show a relative maximum around $\omega \simeq 1/2000$. It remains yet unclear down to what speed the machine can be run before the quasi-static limit is reached. A corresponding long enough periodic time $\tau = 2\pi/\omega$ has not even been reached for a lower-dimensional three-spin machine [41], consuming by far less numerical runtime.

In Fig. 4.12 the efficiencies of the heat engine and heat pump are depicted as functions of ω. While η_{en} decays quasi-monotonically with decreasing ω, η_{p} exhibits a max-

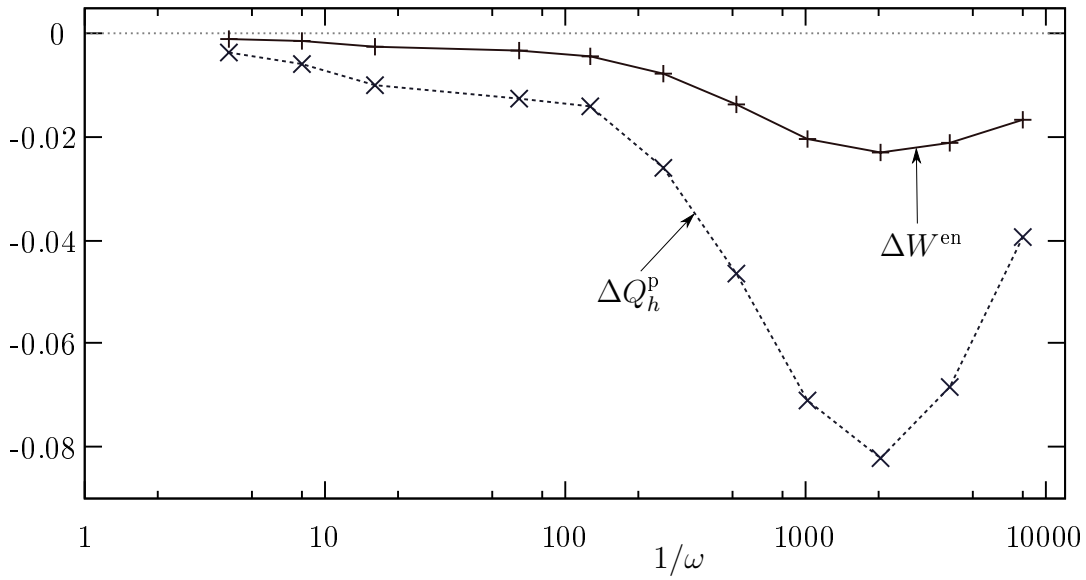

Figure 4.11.: Work $\Delta W^{\mathrm{en}} < 0$ released by the heat engine and heat $\Delta Q_h^{\mathrm{p}} < 0$ transported by the heat pump per cycle, both as functions of the driving frequency ω

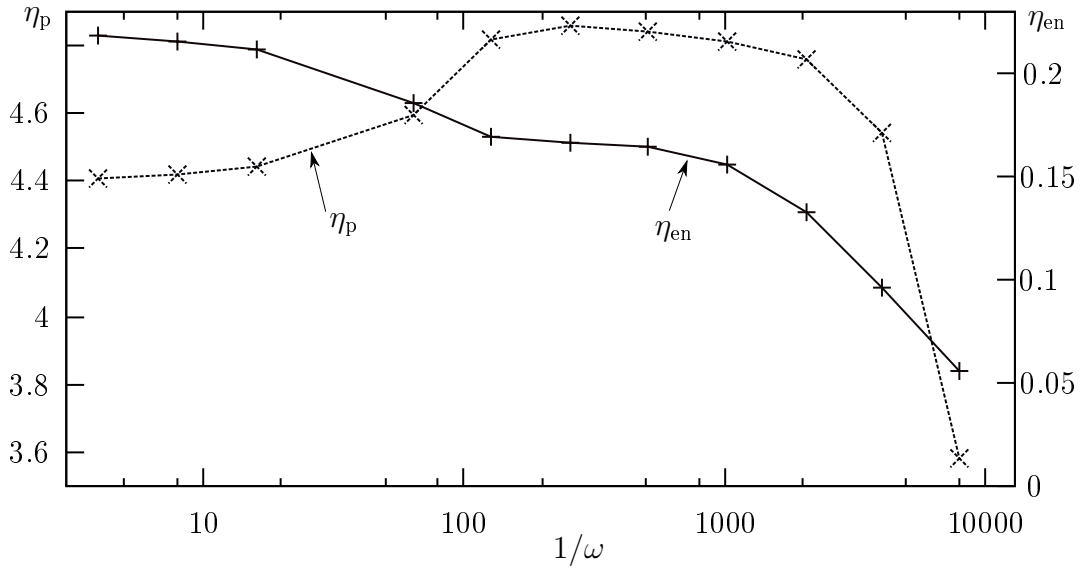

Figure 4.12.: Efficiency $\eta_{\mathrm{p}} = -\Delta W/\Delta Q_h^{\mathrm{p}}$ of the heat pump (left scale) and $\eta_{\mathrm{en}} = \Delta Q_h^{\mathrm{en}}/\Delta W$ of the heat engine (right scale) as functions of ω

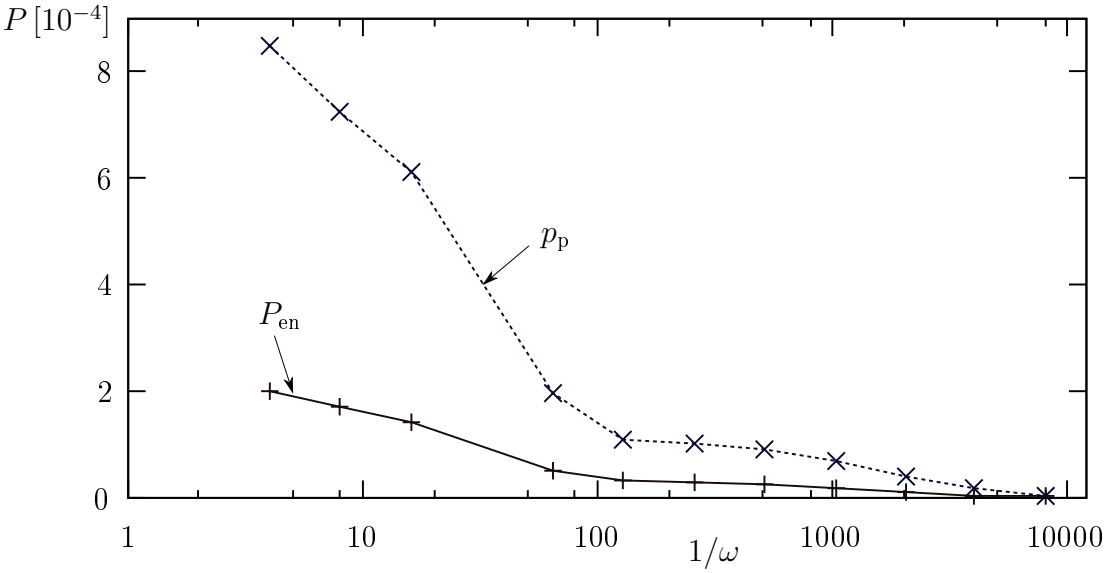

Figure 4.13.: Power output of the heat engine, $P_\mathrm{en} = -\omega\Delta W^\mathrm{en}$ and heat pump, $p_\mathrm{p} = -\omega\Delta Q_h^\mathrm{p}$ as functions of ω

imum plateau starting at $\omega \simeq 10^{-2}$ where also work and heat are still sufficiently large (cf. Fig. 4.11). This justifies the choice of $\omega = 1/128$ as driving frequency if the other system parameters are comparably selected.

The power characteristics is given in Fig. 4.13. For the engine, power is defined as $P_\mathrm{en} = -\Delta W^\mathrm{en}\omega$, for the heat pump $p_\mathrm{p} = -\Delta Q_h^\mathrm{p}\omega$. In both cases the power decreases monotonically with ω. From an economic point of view a higher driving frequency in agreement with (3.12) is thus favorable for the engine, whereas the heat pump should be operated at lower speed to reduce work input, cf. Fig. 4.12.

Beyond this qualitative analysis it would be favorable to know the efficiency of the endoreversible Quantum Otto cycle at maximum power output rather than trying all possible sets of parameters. In other words, we are looking for an expression analog to the Curzon-Ahlborn efficiency (2.1.3) in the case of a Carnot cycle. Although a corresponding relationship is not yet available, it supposedly would have to depend from the bath contact energy splittings as well as from the bath temperatures.

4.2.2. Driven Spin Pair with Mutual Coupling

In this section we discuss the impacts of coupling the driven spins in the parallel four-spin circuit by means of a coupling constant λ_1. Otherwise the circuit is equivalent to that of Sec. 4.2, using the standard parameters from Tab. 4.1. The gas spins are driven in-phase, i. e. $\varphi = 0$.

As a consequence, heat is now transported by a pair of spins labeled $2ab$ which, due to the mutual coupling, is found in a canonical state as a whole and can thus be assigned a local spin group temperature T_{2ab}, to be calculated by the fitting routine `TempFit` [44]

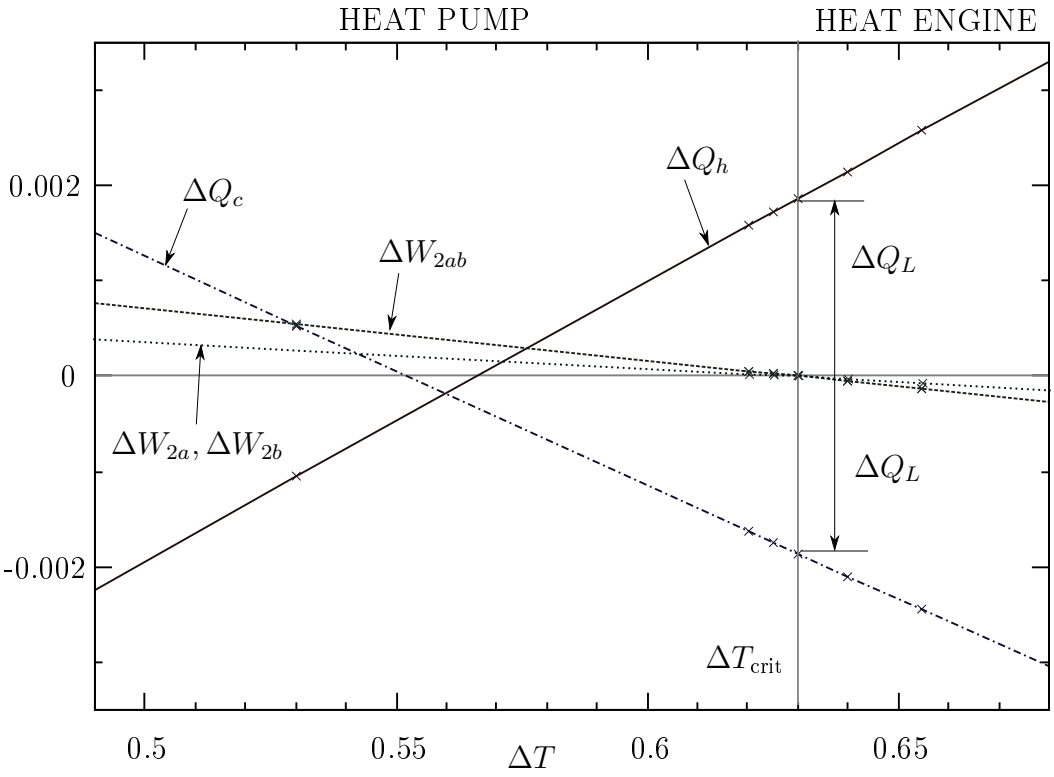

Figure 4.14.: Work and heat per period with strong mutual coupling of the gas spins. The work of the driven spins is additive, $\Delta W_{2ab} \simeq \Delta W_{2a} + \Delta W_{2b}$

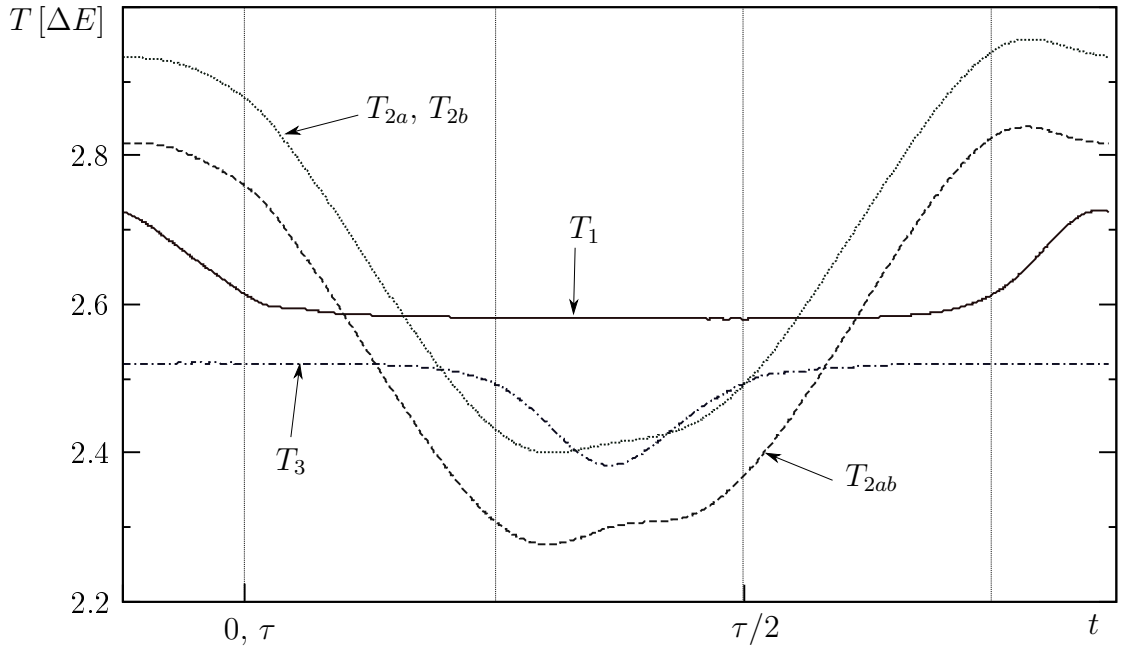

Figure 4.15.: Local temperatures over one period τ: The local spin temperatures T_{2a}, T_{2b} are increased due to correlations, while the temperature T_{2ab} of the spin pair is rather descriptive here.

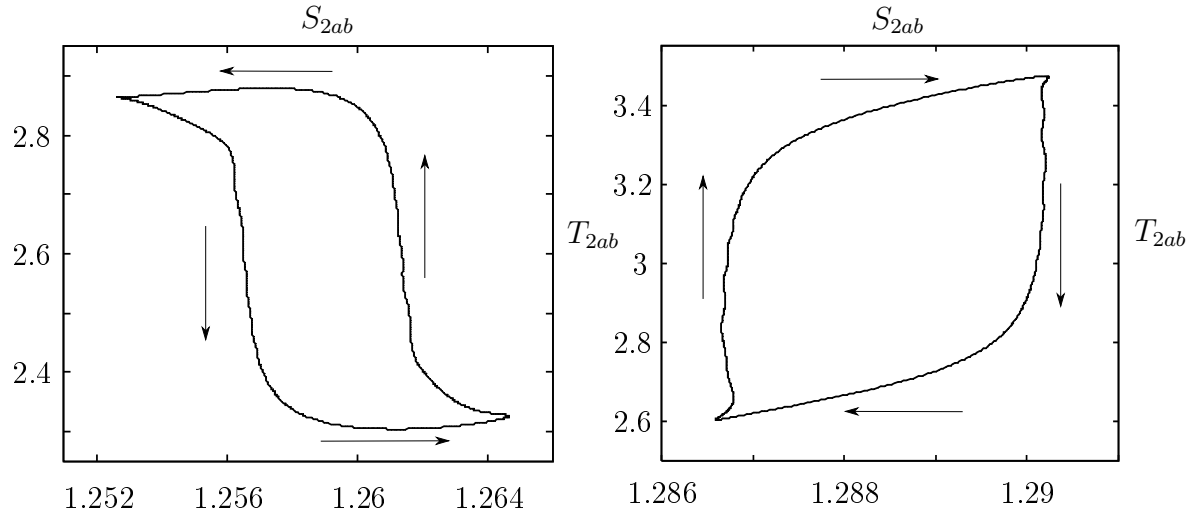

Figure 4.16.: ST-diagrams of the driven spin pair $2ab$ working as heat pump (left) and heat engine (right)

out of the energy eigenvalues of the spin group Hamiltonian,

$$\hat{H}_{2ab} = \sum_{\mu=2a,2b} \frac{\Delta E_\mu}{2} \hat{\sigma}_z^\mu + \lambda_1 \sum_{i=x,y,z} \hat{\sigma}_i^{2a} \otimes \hat{\sigma}_i^{2b}$$

and the reduced state $\hat{\varrho}_{2ab}$.

It turns out that, for rather weak coupling ($\lambda_1 = \lambda = 0.01$) the canonical temperature T_{2ab} is equivalent to the local spin temperatures T_{2a} and T_{2b} obtained via (2.73).

Setting $\lambda_1 = 0.1$ changes the situation drastically, though. Now, the local temperatures of the single spins are higher than the spin pair temperature, i. e. $T_{2a} = T_{2b} > T_{2ab}$, to be observed in Fig. 4.15. This behavior is plausible due to the explanations in 2.4.2, according to which the local temperature of a spin or group of spins is descriptive only in the case of weak interaction with neighbored groups, say $\lambda = 0.01$. Else correlations make local entropies increase, why local temperatures are no longer intensive.

Fig. 4.16 shows the ST-diagrams of the spin pair $2ab$ running its own thermodynamic cycle as heat pump or heat engine, where T_{2ab} is obtained as described above and S_{2ab} results from (2.29). At the same time the single spins $2a$ and $2b$ still run their individual cycles, cf. Sec. 4.2. The dependencies of heat, work and efficiencies on ΔT turn out to be the same as for the uncoupled case where $\lambda_1 = 0$. Despite of the presence of strong correlations between the driven spins, it is found that the work performed by the single gas spins simply adds up to that of the spin pair, $\Delta W_{2a} + \Delta W_{2b} \simeq \Delta W_{2ab}$ as shown in Fig. 4.14. Hence the increase in local temperatures and entropies caused by correlations only leads to an approximately constant offset in the ST-diagrams which rules out on integration.

Summarizing, this scenario is rather equivalent to the uncoupled case and obviously does not furnish any improvement, which one could have assumed because of the internal symmetry.

4.3. Driving with Relative Phase Shift

In Sec. 4.2 it was discussed that driving the gas spins in the parallel four-spin circuit with zero relative phase would yield the same result as for a comparable three-spin machine, i. e. no improvement could be achieved by an additional spin due to the filtering function of the bath spins determining the system. It shows, however, that this can be circumvented by introducing a relative phase shift $\varphi \neq 0$ into the modulation of the gas spin energy gaps.

In this section the implications hereof are investigated by means of a relative phase $\varphi = \pi$. The modulation functions of the energy gaps become $\Delta E_{2a}(t) = 2.0 + 0.25 \cos \omega t$ and $\Delta E_{2b}(t) = 2.0 - 0.25 \cos \omega t$. Hence both driven spins alternately come into resonance with the bath spins and therefore receive the "full" heat quantity per period as it would also be the case for a three-spin machine. For that reason the model can be interpreted as combination of two independent three-spin machines rather than as parallel circuit.

In the following this feature and its consequences are demonstrated numerically. Fig. 4.19 displays the heat currents for the case the entire system works as heat pump. Since heat is transferred between the system and each heat bath twice per period, both current curves now exhibit two peaks, each with about the same magnitude as if the gas spins were driven in-phase. In accordance, both ST-diagrams given in Fig. 4.17 approximately comprehend twice the shape compared to Fig. 4.6. Hence each driven spin transports about the double heat quantity and also performs the double of work per period since the modulation is still uniform. The oscillations observed in both diagrams result from transitions in the spin system induced by the baths during the adiabats due to the permanent system-bath coupling.

Correspondingly, one would expect the total work and heat per period to scale by about factor two, compared to the three-spin machine and the four-spin circuit driven in-phase. This behavior is indeed confirmed by Fig. 4.21 and Fig. 4.22. Each of the spins coupled in parallel now transports about the same amount of heat and exerts or consumes the same work per period than the single driven spin in a three-spin machine would do. Thus, the heat engine power output $P = \Delta W/\tau = \Delta W \omega / 2\pi$ is also doubled, making the parallel four-spin circuit with phase-shifted modulation about twice as good as a three-spin machine. However, in a possible experimental setup this would inevitably combined with higher effort as two external modulation fields within a narrow range would be needed.

As a further consequence, Fig. 4.20 shows that the engine and heat pump efficiencies for phase-shifted driving qualitatively show the same characteristics compared to in-phase driving, except the critical temperature gradient is marginally shifted to $\Delta T_{\mathrm{crit}} = 0.675$.

It must be noted that the found scaling behavior of heat and work by factor two is not exact. The deviations hereof may again be traced back to correlations. In Sec. 4.1 it was shown that the stationary heat currents decrease for a spin "ladder" configuration at overall resonance, compared to the case where only one spin is detuned. Although this behavior cannot be simply mapped one-to-one to the present dynamical scenario, analogies do exist.

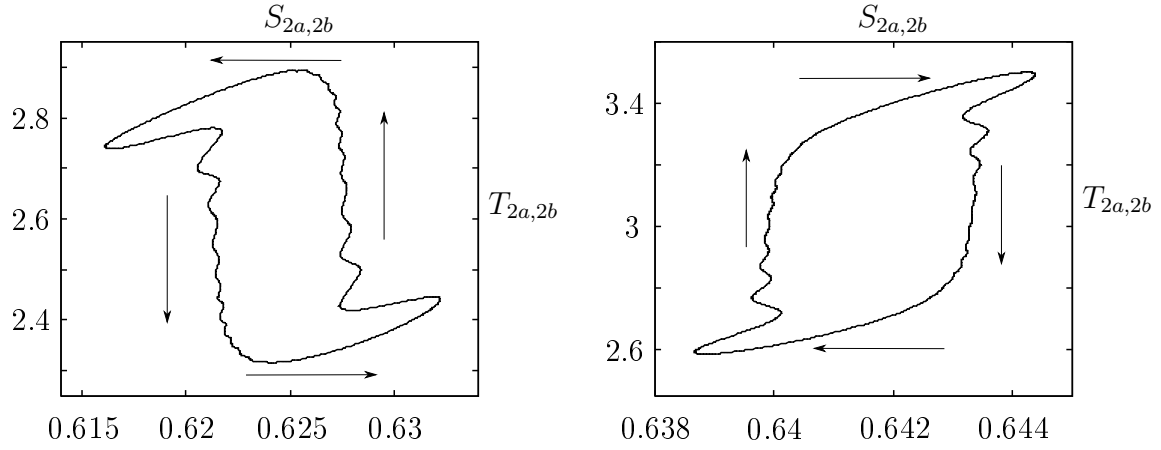

Figure 4.17.: Parallel four-spin circuit driven with phase shift $\varphi = \pi$: ST-diagrams (identical for both gas spins $2a, 2b$) if the circuit works as heat pump (left) or heat engine (right).

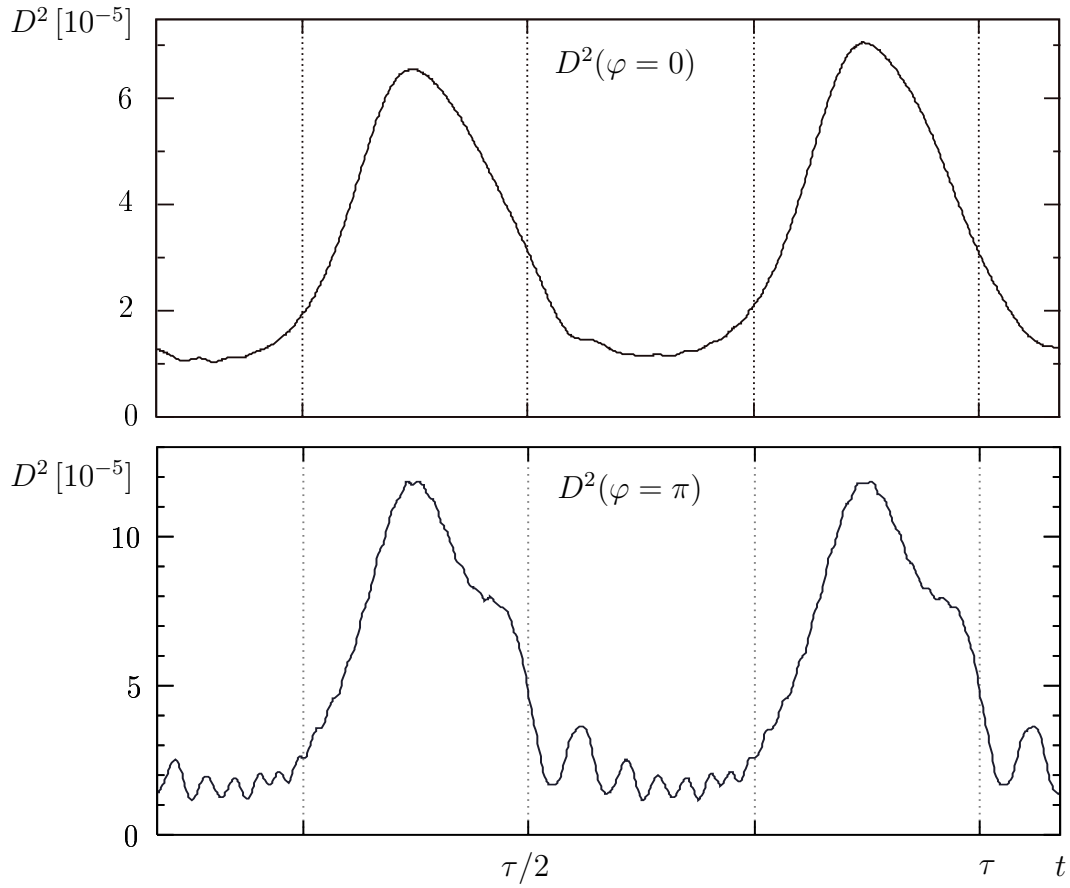

Figure 4.18.: Parallel four-spin circuit working as heat pump ($\Delta T = 0.13$): Bures measure over one period τ if driven in-phase ($\varphi = 0$, upper part) and with phase shift ($\varphi = \pi$, lower part), where correlations are higher. Compare the related heat currents displayed in Fig. 4.5 and Fig. 4.19.

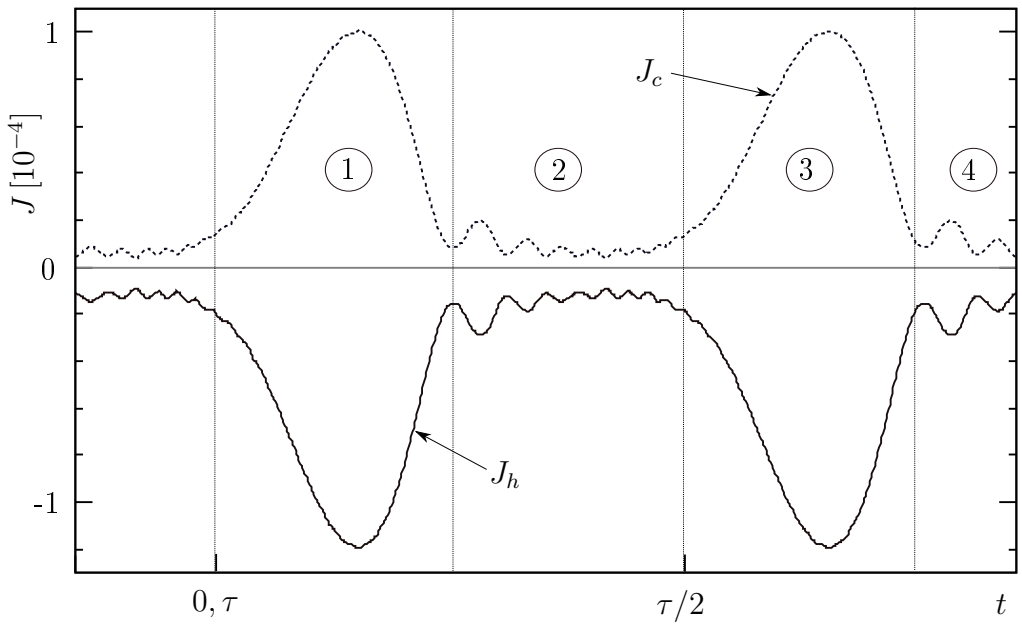

Figure 4.19.: Parallel four-spin circuit driven with phase shift $\varphi = \pi$ and working as heat pump ($\Delta T = 0.13$): Heat currents J_h and J_c, each exhibiting two peaks since the system interacts twice with each bath per period τ.

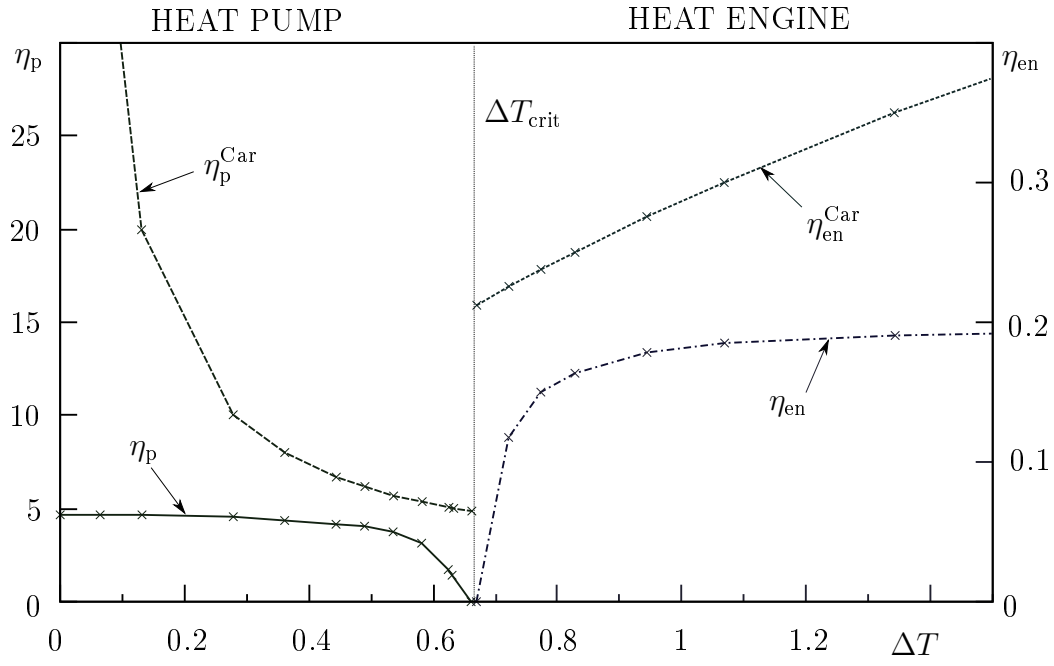

Figure 4.20.: Parallel four-spin circuit driven with phase shift $\varphi = \pi$: Efficiencies of the heat engine η_en and heat pump, η_p and Carnot bounds $\eta_\mathrm{en/p}^\mathrm{Car}$ as functions of ΔT. The Quantum Otto efficiencies $\eta_\mathrm{p}^\mathrm{Otto} = 4.5$ (heat pump) and $\eta_\mathrm{en}^\mathrm{Otto} = 0.222$ (heat engine) are not displayed.

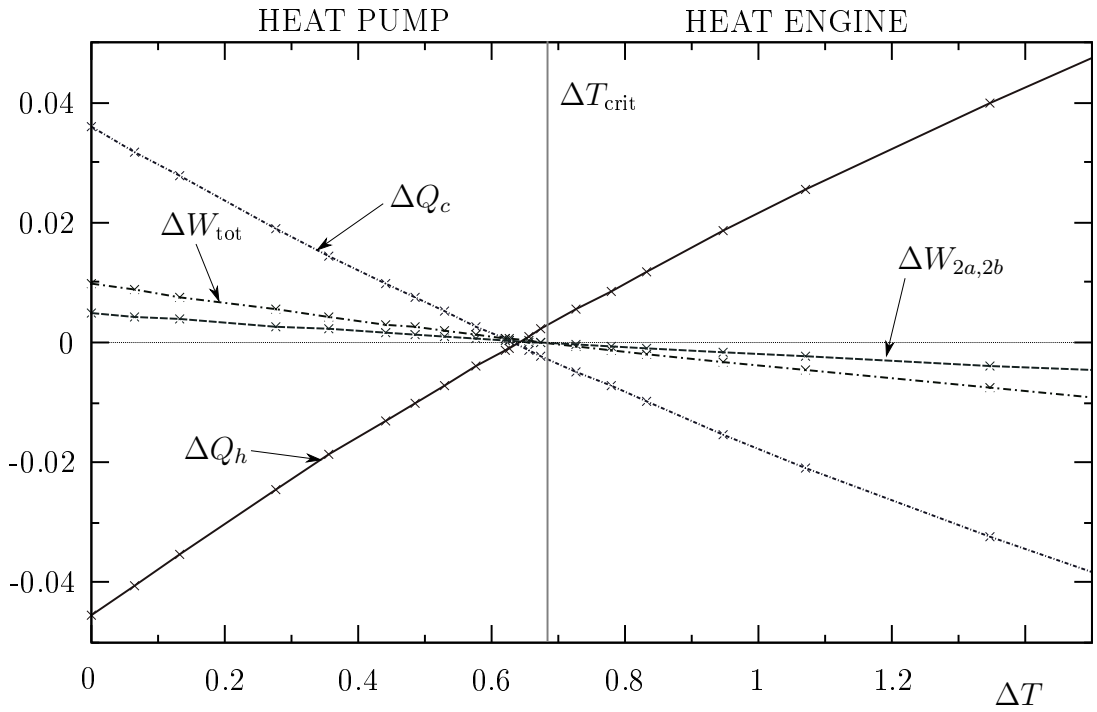

Figure 4.21.: Parallel four-spin circuit driven with phase shift $\varphi = \pi$: Work $\Delta W_{\rm tot}$ (entire system), $\Delta W_{2a,2b}$ (single gas spins), and heat $\Delta Q_{h,c}$ as functions of ΔT.

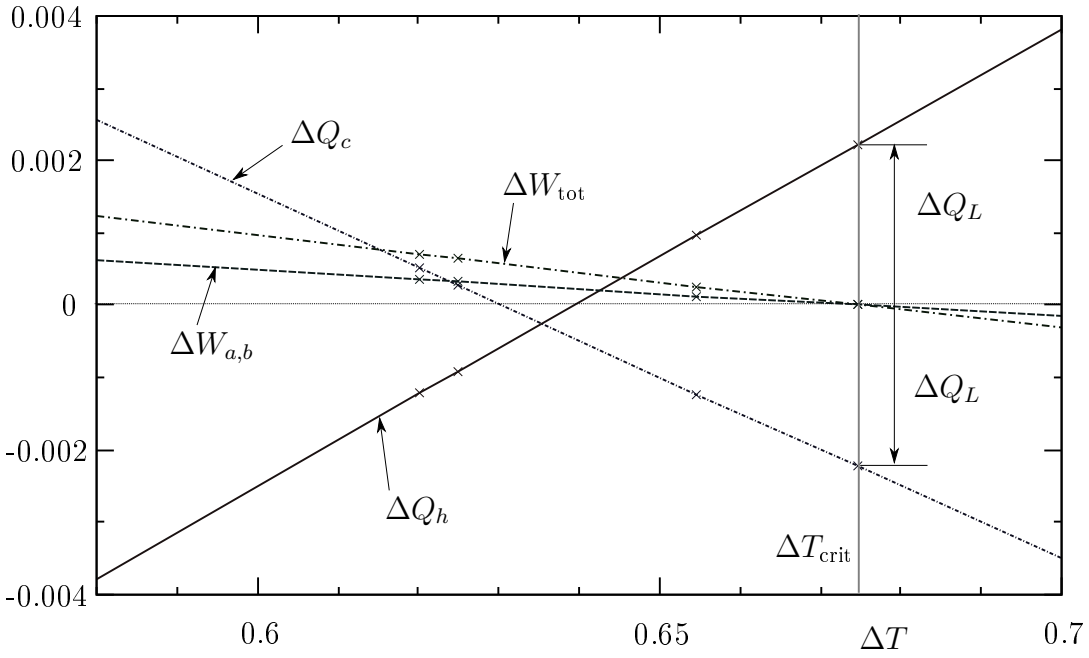

Figure 4.22.: Zoom into Fig. 4.21. At $\Delta T_{\rm crit}$, $\Delta W = 0$ and only the leakage heat ΔQ_L remains.

If the gas spins are driven with relative phase-shift and alternately exchange heat with the reservoirs, the heat current flux through the system and thus heat and work are more than only doubled, compared to the case where both gas spins are driven in-phase. This can be interpreted as a consequence from the static scenario and is confirmed by comparing the respective heat currents for the cases the gas spins are either driven in-phase (Fig. 4.5) or with relative phase shift (Fig. 4.19).

Moreover, the respective Bures measures for both cases plotted in Fig. 4.18 over one period yield the double amount of correlations for driving with phase-shift. They also trace the oscillations resulting from bath-induced transitions and being more distinctive for phase-shifted driving.

At this point a clear relationship between heat currents on the one hand and the spin chain geometry and correlations on the other hand appears, where, in comparison, the latter are linked to different conductivities for both driving scenarios. So far an analytical description hereof is not available, but a promising ansatz is provided by [43].

5. Serial Quantum Machine Circuits

In this chapter the interest is pointed at serial quantum machine circuits, that is, several machine units such as discussed in Sec. 3.2.1 shall be connected in series in order to obtain a linear machine chain with more than one driven spin. For computational reasons we restrict ourselves to compounds of two serially connected units. As displayed in Fig. 5.1 our model consists of a chain of five Heisenberg-coupled, inhomogeneously split spins between two heat baths, two of which are driven. The system Hamiltonian is that of the Heisenberg spin chain, given by extending (3.8) to five spins.

Based on numerical simulations it shall be pointed out that each of the subunits A and B and thus the circuit as a whole run a Quantum Otto cycle for given resonance conditions between adjacent spins. Similarly the other models investigated so far, the cycle characteristics such as work, heat etc. mainly depend on the local energy gaps and temperatures of the outermost spins in the chain locally coupled to the baths. Depending on their respective canonical distributions, the entire circuit either works as heat engine or as heat pump. As it will turn out, the local working mode of units A and B are globally determined as well.

5.1. Circuit of Oppositely Directed Quantum Machines

We consider first the spin chain setup depicted in Fig. 5.1. Due to the particular internal energetic geometry of this model, spins A and B are expected to run oppositely directed cycles, i. e. one works as heat pump while the other runs as heat engine. In this context a particular role devolves to spin 3 in the middle. Imagine that, if the local energy gaps of spins 2 and 4 are decreased during an adiabatic step, their temperatures T_2 and T_4 are lowered also unless they arrive in resonance with spin 3. With regard to a system attractor state it is therefore plausible that spin 3 is found at a lower temperature than the baths, i. e. $T_3 < T_c < T_h$. Provided that both units run ideal Quantum Otto cycles, the temperature T_3 corresponds to the average canonical distribution out of those of the bath spins. These exhibit the same temperatures as the baths they are coupled to, respectively.

For this reason it is justified to consider spin 3 as a finite effective cold bath via which units A and B exchange heat. Although it certainly has nothing in common with an infinite heat reservoir, i. e. is not a heat source or sink, spin 3 nevertheless acts as environment, shielding the hot reservoir from unit B and the cold reservoir from unit A. Due to the tapered internal temperature gradients resulting hereof, the cycles performed by the gas spins 2 and 4 are indeed of opposite direction.

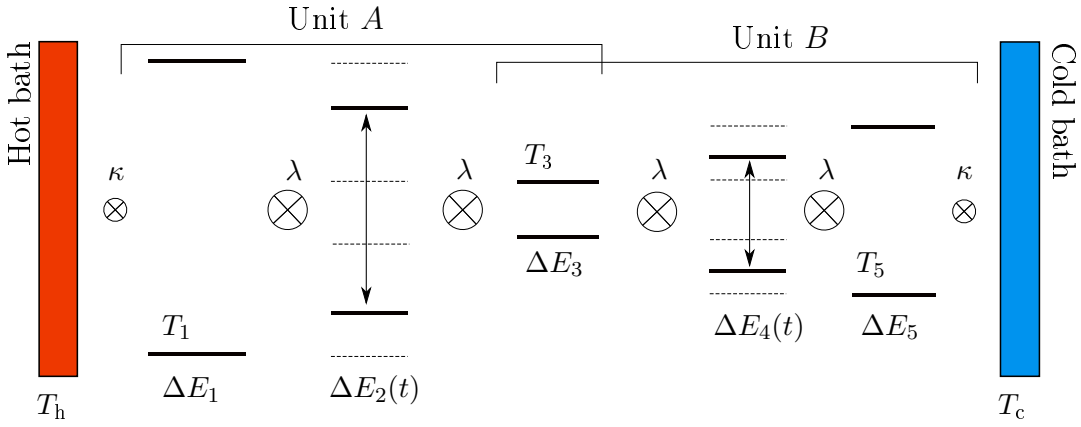

Figure 5.1.: Serial circuit of two quantum machine units A and B between two heat baths, working as heat pump and heat engine, respectively. Symbol notations are same as above.

Because of energy conservation, the heat current entering the effective bath from one side must re-emerge on the other side. In particular, the Gibbs relation for the entire circuit, $\Delta Q_h + \Delta Q_c + W_A + W_B$ is always fulfilled, where W_i is the work done or consumed by unit i.

The bath contact spins 1 and 5 and the central spin 3 feature constant energy splittings, here chosen as $\Delta E_1 = 2.25, \Delta E_3 = 1.25$ and $\Delta E_5 = 1.75$ while spins 2 and 4 are both sinusoidally driven with $\omega = 1/128$. All other parameters are as listed in Tab. 4.1. The resonance conditions for the driven spins are fulfilled according to

$$\begin{aligned} &\Delta E_1 \geq \Delta E_2(t) = 1.75 + 0.5 \sin \omega t \geq \Delta E_3 \qquad \text{and} \\ &\Delta E_3 \leq \Delta E_4(t) = 1.5 + 0.25 \sin \omega t \leq \Delta E_5 \,. \end{aligned}$$

For the case the serial circuit works as heat pump and transports heat from the cold to the hot bath, the Quantum Otto cycle steps shall be recapitulated in analogy to Sec. 3.2.2:

1. Isochoric step: Spins 2 and 4 are in resonance with spin 3. A heat current flows from spin 4 to spin 2 until local equilibrium is reached. The work is zero since the spectrum is not deformed.

2. Adiabatic step: The energy gaps of the driven spins are increased, both carrying the same average occupation as spin 3. During this step work is released. Heat currents between the system and the baths as well as inside the system are negligible.

3. Isochoric step: Spins 2 and 4 are in resonant contact with the bath spins 1 and 5, resulting in heat currents $J_c > 0$ and $J_h < 0$ from the cold bath into the system and from the system into the hot bath, respectively. Again no work is applied or released.

4. Adiabatic step: The local energy gaps of spins 2 and 4 are decreased with constant occupation probabilities, that is, work has to be applied while heat currents are suppressed.

5.1.1. Serial Circuit Efficiencies

In the serial Quantum Otto circuit both subunits A, B exhibit local efficiencies as they effectively transport heat between two heat reservoirs each. Let now the entire circuit work as heat engine with net transport from the hot to the cold reservoir. Then, during one period the heat quantity $\Delta Q_h > 0$ flows from the hot reservoir into subunit A, working as heat engine between the hot reservoir and the cold effective bath spin 3. Thus, an amount of work $\Delta W_A < 0$ is released and, via the effective bath, the heat quantity $\Delta Q^* = \Delta Q_h - \Delta W_A$ reaches subsystem B working as heat pump. Here the amount of work $\Delta W_B > 0$ has to be reinvested to transport the heat $\Delta Q_c < 0$ to the cold bath, according to our sign conventions. The local engine efficiencies then yield, according to (3.7),

$$\begin{aligned}\eta_A^{\mathrm{en}} &= -W_A/Q_h > 0\\ \eta_B^{\mathrm{en}} &= -W_B/(Q_h + W_A) \equiv -W_B/(-Q_c + W_B) < 0\end{aligned}$$

Note that, since subsystem B works as heat pump, it is assigned a negative engine efficiency because we are interested in the engine efficiency of the entire circuit. As expected, with (2.12) the global engine efficiency becomes

$$\eta_{\mathrm{tot}}^{\mathrm{en}} = -(W_A + W_B)/Q_h \quad (> 0)$$

and, for a heat pump, $\eta_{\mathrm{tot}}^{\mathrm{p}} = -Q_h/(W_A + W_B)$.

The ideal Quantum Otto efficiency for the serial heat pump/engine circuit is obtained similarly. If we assume perfectly controlled cycle steps and energy conservation with regard to heat transport through spin 3, the heat current from spin 2 to spin 4 must satisfy

$$J_{2\to 3} = -J_{3\to 4} \tag{5.1}$$

or, according to Eq. (3.17),

$$\frac{\Delta E_3}{2}\left(\tanh\frac{\Delta E_1}{2T_h} - \tanh\frac{\Delta E_3}{2T_3}\right) = \frac{\Delta E_3}{2}\left(\tanh\frac{\Delta E_3}{2T_3} - \tanh\frac{\Delta E_5}{2T_c}\right). \tag{5.2}$$

Compared to (2.72) this leads to a normalized average energy expectation value $\langle E_3^*\rangle$ constant in time,

$$\frac{1}{\Delta E_3}\langle E_3^*\rangle = \tanh\frac{\Delta E_3}{2T_3} = \frac{1}{2}\left(\tanh\frac{\Delta E_1}{2T_h} + \tanh\frac{\Delta E_5}{2T_c}\right) \tag{5.3}$$

and hence to the average temperature

$$T_3^* = \Delta E_3\left[2\,\mathrm{arctanh}\left[\frac{1}{2}\left(\tanh\frac{\Delta E_1}{2T_h} + \tanh\frac{\Delta E_5}{2T_c}\right)\right]\right]^{-1} \tag{5.4}$$

With the help of (5.3) the ideal Quantum Otto efficiencies of the heat engine and heat pump for units A and B become, in analogy to Sec. 3.3,

$$\begin{aligned} \eta_{en,A}^{\mathrm{Otto}} &= 1 - \frac{\Delta E_3}{\Delta E_1} = 0.444 \qquad & \eta_{p,A}^{\mathrm{Otto}} &= \frac{\Delta E_1}{\Delta E_1 - \Delta E_3} = 2.25 \\ \eta_{en,B}^{\mathrm{Otto}} &= 1 - \frac{\Delta E_3}{\Delta E_5} = 0.286 \qquad & \eta_{p,B}^{\mathrm{Otto}} &= \frac{\Delta E_5}{\Delta E_5 - \Delta E_3} = 3.5 \end{aligned} \tag{5.5}$$

where the values of the ΔE_i from Sec. 5.1 have been inserted.

The ideal Quantum Otto efficiencies for the entire serial circuit are obtained with Eq. (2.12),

$$\eta_{en}^{\mathrm{Otto}} = 1 - \frac{\Delta E_5}{\Delta E_1} = 4.5 \qquad \eta_{p}^{\mathrm{Otto}} = \frac{\Delta E_1}{\Delta E_1 - \Delta E_5} = 0.22 \tag{5.6}$$

It is remarkable that these expressions only depend on the energy splittings of the bath spins but not of ΔE_3. The same holds for the critical temperature gradient, taking again the value $\Delta T_{\mathrm{crit}}^{\mathrm{id}} = 0.714$ after (3.21).

These criteria may be checked for comparing different quantum machine models featuring the same boundary configurations. As it will get clear below, this manner of description partially fails to describe dynamic scenarios in some serial circuit setups and has to be improved.

5.1.2. Dynamic engine-pump scenario

Now the serial five-spin circuit presented in the previous two sections shall be run dynamically, using the listed parameters. In the following, the results of corresponding numerical calculations are presented.

For the case the entire system works as heat pump, the heat currents are shown in Fig. 5.2. Relating to the cycle steps described in Sec. 5.1, the visible current peaks represent heat transfer between the circuit and the hot and cold reservoir during the second isochoric step. On the other hand, internal heat transfer is not resolved since it is not considered in (2.78). The current peaks are not of equal height due to the asymmetric energetic geometry set by the local energy gaps. Further on they are of weaker magnitude compared to corresponding three- and four-spin machine cycles. First of all this is due to the spin chain "resistance" which is expected to increase with each spin added and the more different frequencies are present in the system [41]. Secondly, as will be revealed further on, the local energy gap and the temperature of the effective bath spin 3 are decisive here.

After heat transfer between the system and the reservoirs, oscillations occur which can again reduced to bath-induced transitions. This effect is also visible on the adiabats in the ST-diagrams depicted in Fig. 5.4. As anticipated, spins 2 and 4 work as heat pump and heat engine, respectively, both running Quantum Otto cycles corresponding to the cycle steps in Sec. 5.1, while the entire circuit pumps heat from the cold to the hot reservoir. Likewise before, the characteristic dips in the ST-diagrams indicate the

emergence of leakage currents. While the large dips represent losses occurring during the bath contacts, the small ones indicate the presence of internal losses during the driven spins exchange heat via the effective bath spin.

Fig. 5.3 shows the serial circuit efficiencies $\eta_{\mathrm{en/p}}$ of the heat engine and heat pump as well as the respective Quantum Otto efficiencies $\eta_{\mathrm{en/p}}^{\mathrm{Otto}}$, both as functions of the global temperature gradient ΔT. Like for comparable three- and four-spin machines the corresponding Carnot efficiencies $\eta_{\mathrm{en/p}}^{\mathrm{Car}}$ are never exceeded. As expected, the characteristics of $\eta_{\mathrm{en/p}}$ are similar as for different models with identical bath spin configurations. Minor differences arise in that the heat pump efficiency is significantly smaller whereas the engine efficiency reaches higher values. The reason hereof is found in Fig. 5.5 showing the heat $\Delta Q_{h,c}$, the global circuit work ΔW_{tot} and the local subunit work $\Delta W_{\mathrm{A,B}}$. While the quantity of work consumed or exhausted per cycle remains in the same range compared to other similar models, the heat transfer between the system and the reservoirs is substantially smaller here. This goes along with the reduced intensity of the heat current peaks as shown above.

Fig. 5.6 shows that, unexpectedly, the subunits change their local modes of operation at different temperature gradients. With increasing ΔT, first unit B switches from heat engine to heat pump mode at $\Delta T_{\mathrm{crit}}^{B} = 0.71$ where ΔW_B changes sign. Then the signs of ΔQ_c and ΔQ_h change, and finally $\Delta W_A = 0$ follows at $\Delta T_{\mathrm{crit}}^{A} = 0.77$. As a consequence hereof the transition of the entire circuit where the total work $\Delta W_{\mathrm{tot}} = \Delta W_A + \Delta W_B$ changes sign is significantly shifted rightwards to $\Delta T_{\mathrm{crit}} = 0.833 > \Delta T_{\mathrm{crit}}^{\mathrm{id}} = 0.714$.

For $\Delta T_{\mathrm{crit}}^{B} \leq \Delta T \leq \Delta T_{\mathrm{crit}}^{A}$ both units A and B work as heat pumps. Primarily, a work quantity $W_{A/B} > 0$ has to be inserted per cycle to compensate losses due to leakage currents in the direction of the internal temperature gradients. Since spin 3 is a finite heat bath and cannot be cooled down or heated up arbitrarily, it is evidently impossible that both heat pumps could work against each other in an efficient way. Thus all work input is dissipated within this range of ΔT, and the energy of spin 3 remains effectively unchanged after one performed cycle.

For $\Delta T_{\mathrm{crit}}^{A} \leq \Delta T \leq \Delta T_{\mathrm{crit}}$ both units work as heat engine and heat pump, respectively. However, a smaller amount of work $\Delta W_A < 0$ is released from unit A than the quantity $\Delta W_B > 0$ to be applied to the latter. This is due to dissipation arising from the mutual influence of both units as explained later on. Hence $\Delta W_{\mathrm{tot}} > 0$ and $\Delta Q_h > 0$ at the same time, therefore the circuit heat pump efficiency η_{p} is arbitrarily set to zero in Fig. 5.3.

In Fig. 5.7 the local heat pump (p) and heat engine (en) efficiencies of units A and B are depicted, defined as

$$\begin{aligned} \eta_{\mathrm{p}}^{\mathrm{A}} &= -\Delta Q_h/\Delta W_A \qquad & \eta_{\mathrm{p}}^{\mathrm{B}} &= -\Delta Q_c/\Delta W_B \\ \eta_{\mathrm{en}}^{\mathrm{A}} &= -\Delta W_A/\Delta Q_h \qquad & \eta_{\mathrm{en}}^{\mathrm{B}} &= -\Delta W_B/\Delta Q_c\,. \end{aligned} \tag{5.7}$$

Again it is visualized that, between the local critical temperature gradients $\Delta T_{\mathrm{crit}}^{B}$ and $\Delta T_{\mathrm{crit}}^{A}$ both units work as heat pumps. Far from these values, however, the local Quantum Otto efficiencies obtained with (5.5) are approached and may even be exceeded.

Hence both units do behave like three-spin machines, and consequently the entire circuit does so. At those ΔT where $\Delta W_B > 0$ and $\Delta Q_c > 0$ in Fig. 5.6 the heat pump

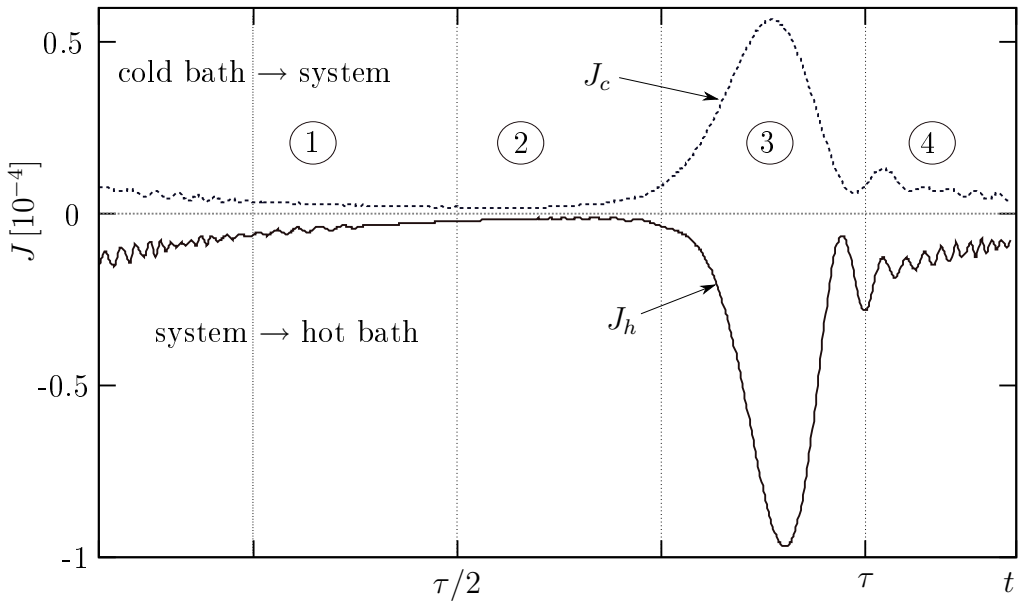

Figure 5.2.: Serial five-spin circuit working as heat pump ($\Delta T = 0.13$): Heat currents $J_{h,c}$ over one cycle $\tau = 2\pi/\omega$. Spins 2 and 4 are driven in-phase. Cycle steps: see Sec.5.1. Current peaks: heat transfer between system and reservoirs.

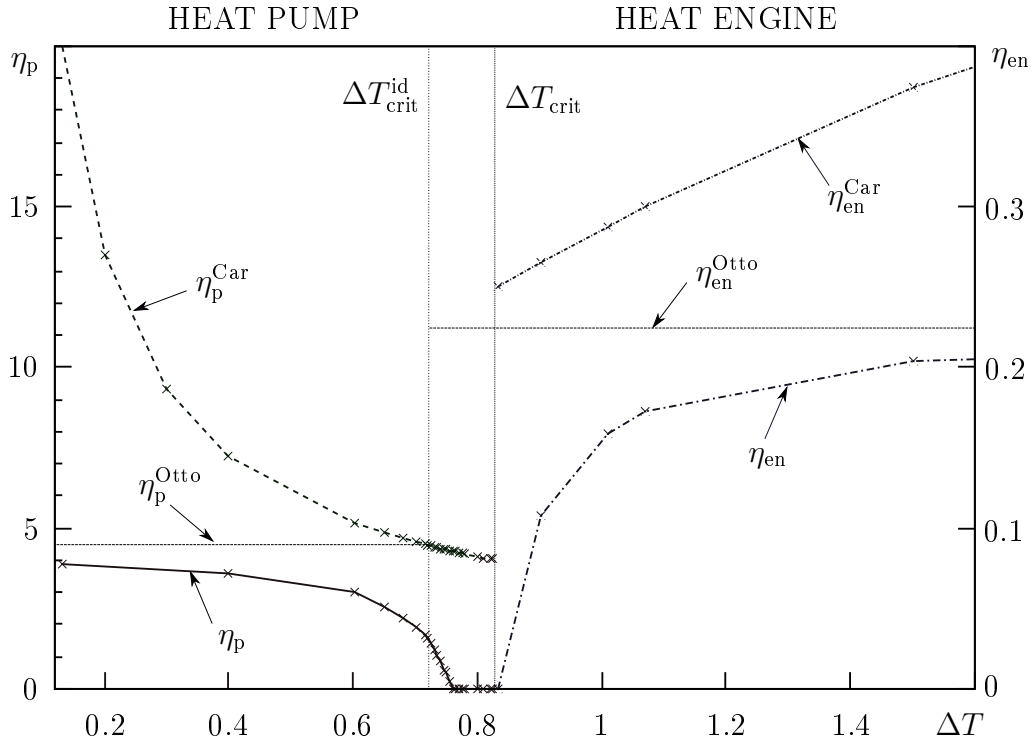

Figure 5.3.: Efficiencies of the serial circuit $\eta_{\rm en/p}$ working as heat engine (en) and heat pump (p), the ideal Quantum Otto cycle, $\eta^{\rm Otto}_{\rm en/p}$ and Carnot cycle, $\eta^{\rm Car}_{\rm en/p}$. The critical temperature gradient $\Delta T_{\rm crit} = 0.83$ is right-shifted compared to the ideal one, $\Delta T^{\rm id}_{\rm crit} = 0.714$.

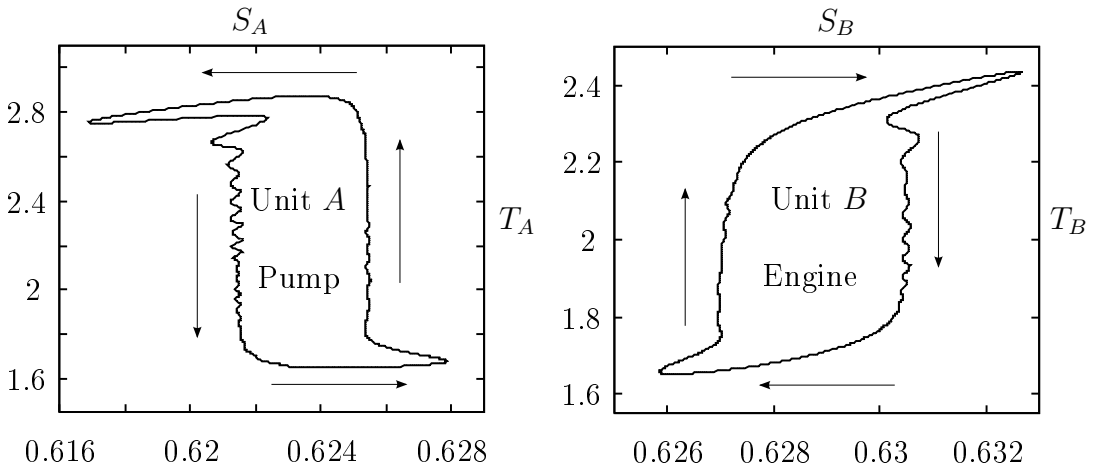

Figure 5.4.: Serial circuit working as heat pump ($\Delta T = 0.13$): ST-diagrams of the driven spins of units A and B, working as heat pump and heat engine, respectively.

efficiency $\eta_{\mathrm{p}}^{\mathrm{B}} = -\Delta Q_c/\Delta W_B$ of unit B would be negative and is set to zero. With regard to unit A the same holds for those ΔT where $\Delta W_A > 0$ and $\Delta Q_h > 0$. In these cases all work input is over-compensated by losses.

The reason why the subunits switch between heat engine and heat pump mode at different temperature gradients is founded in a slight increase of the otherwise nearly constant temperature T_3 of the effective finite heat bath spin 3. This is illustrated in Fig. 5.9 by means of the energy expectation values of spins $i = 1, 3, 5$, all normalized to ΔE_3, $\langle \tilde{E}_i \rangle = \frac{\Delta E_3}{\Delta E_i} \tanh \frac{E_i}{2T_i}$ and plotted as functions of the global temperature gradient ΔT, together with the ideally supposed average energy (see (5.3)),

$$\langle E_3^* \rangle = \frac{1}{2} \left(\langle \tilde{E}_1 \rangle + \langle \tilde{E}_5 \rangle \right) = \frac{\Delta E_3}{2} \tanh \frac{\Delta E_3}{2T_3} = \frac{\Delta E_3}{4} \left(\tanh \frac{\Delta E_1}{2T_h} + \tanh \frac{\Delta E_5}{2T_c} \right) . \quad (5.8)$$

This holds because, assuming ideal adiabats, the driven spins 2 and 4 carry the same occupation probabilities as the respective bath spins 1 and 5 just before heat transfer via spin 3, i. e. $\langle \tilde{E}_2 \rangle = \langle \tilde{E}_1 \rangle$ and $\langle \tilde{E}_4 \rangle = \langle \tilde{E}_5 \rangle$. If spin 3 featured the ideal average energy $\langle E_3^* \rangle$, the entire circuit as well as both units would simultaneously switch their respective modes of operation at $\Delta T_{\mathrm{crit}}^{\mathrm{id}}$ where the canonical distributions of both bath spins are equal. In this case, $\langle E_3^* \rangle = \langle \tilde{E}_1 \rangle = \langle \tilde{E}_5 \rangle$.

However, spin 3 is found with an energy $\langle \tilde{E}_3 \rangle > \langle E_3^* \rangle$. The offset

$$C' = \langle \tilde{E}_3 \rangle - \langle E_3^* \rangle = 0.0064\,[\Delta E]$$

only marginally depends on ΔT over a wide range. This considerably changes the situation.

Following Fig. 5.9, for $\Delta T \leq \Delta T_B$ the entire circuit works as heat pump due to the energetic order of the involved spins,

$$\langle \tilde{E}_5 \rangle = \langle \tilde{E}_4 \rangle > \langle \tilde{E}_3 \rangle > \langle \tilde{E}_2 \rangle = \langle \tilde{E}_1 \rangle$$

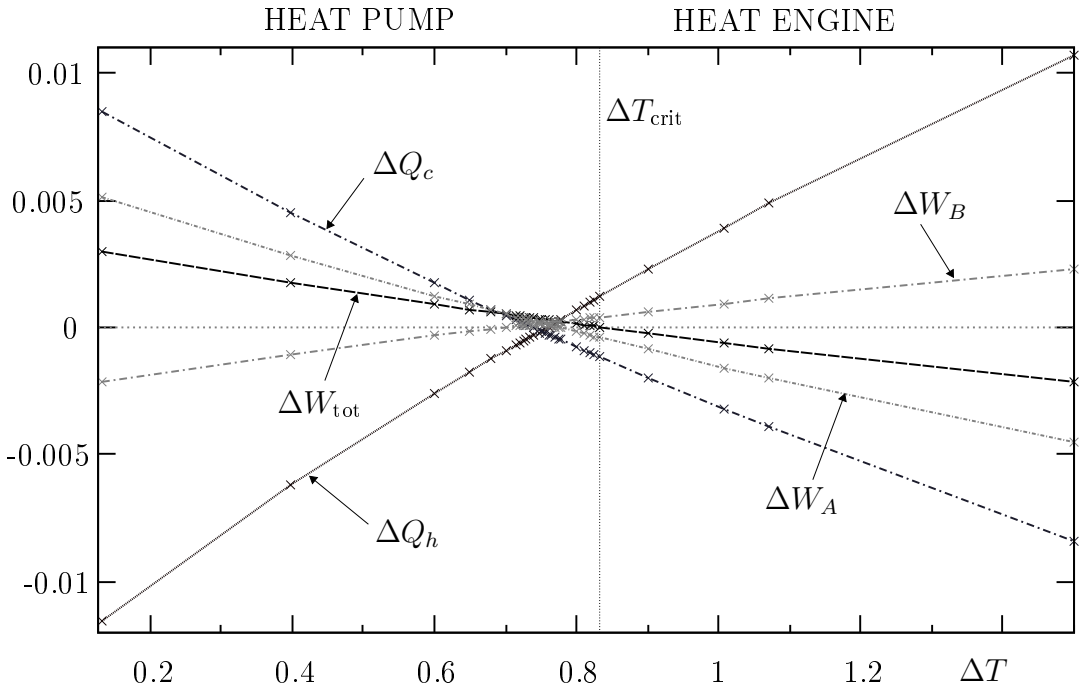

Figure 5.5.: Serial circuit: Heat ΔQ_h and ΔQ_c, work $W_{\rm tot}$ of the entire circuit and work $W_{A/B}$ of the local units A and B during one period τ.

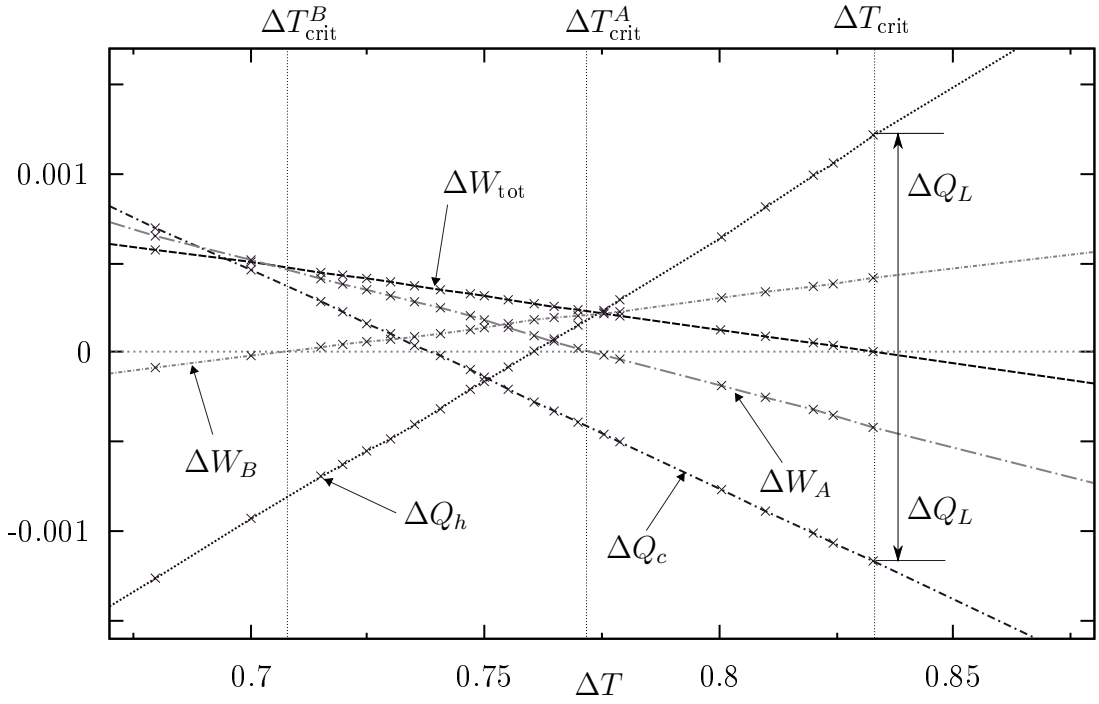

Figure 5.6.: Zoom into Fig. 5.5. The work functions $W_{A/B}$ of units A and B change sign at different critical gradients $\Delta T^A_{\rm crit} = 0.77 > \Delta T^B_{\rm crit} = 0.71$. The work function $W_{\rm tot}$ of the entire circuit finally changes sign at $\Delta T_{\rm crit} = 0.83$.

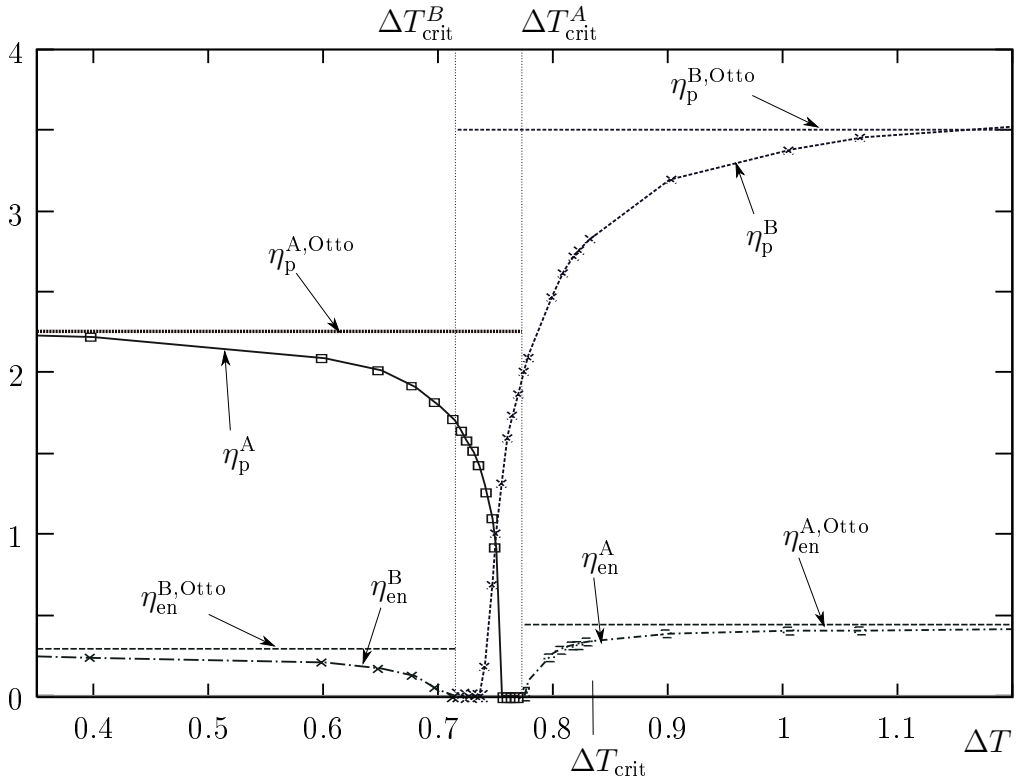

Figure 5.7.: Serial circuit: Local heat pump and engine efficiencies of units A and B, $\eta_{\rm en/p}^{A/B}$ compared to local ideal Quantum Otto efficiencies $\eta_{\rm en/p}^{A/B,\,\rm Otto}$. The units switch their modes of operation at different critical gradients $\Delta T_{\rm crit}^{A/B}$.

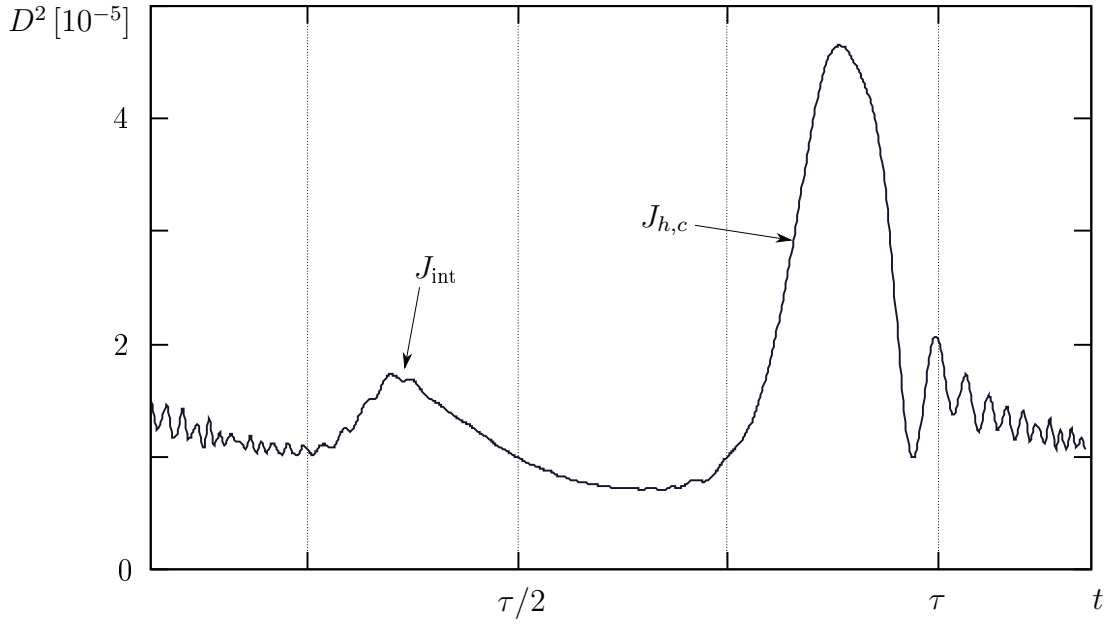

Figure 5.8.: Bures distance measure D^2 over one period τ. Heat current transfer $J_{\rm int}$ via spin 3 (internal) and $J_{h,c}$ with the reservoirs are marked by peaks.

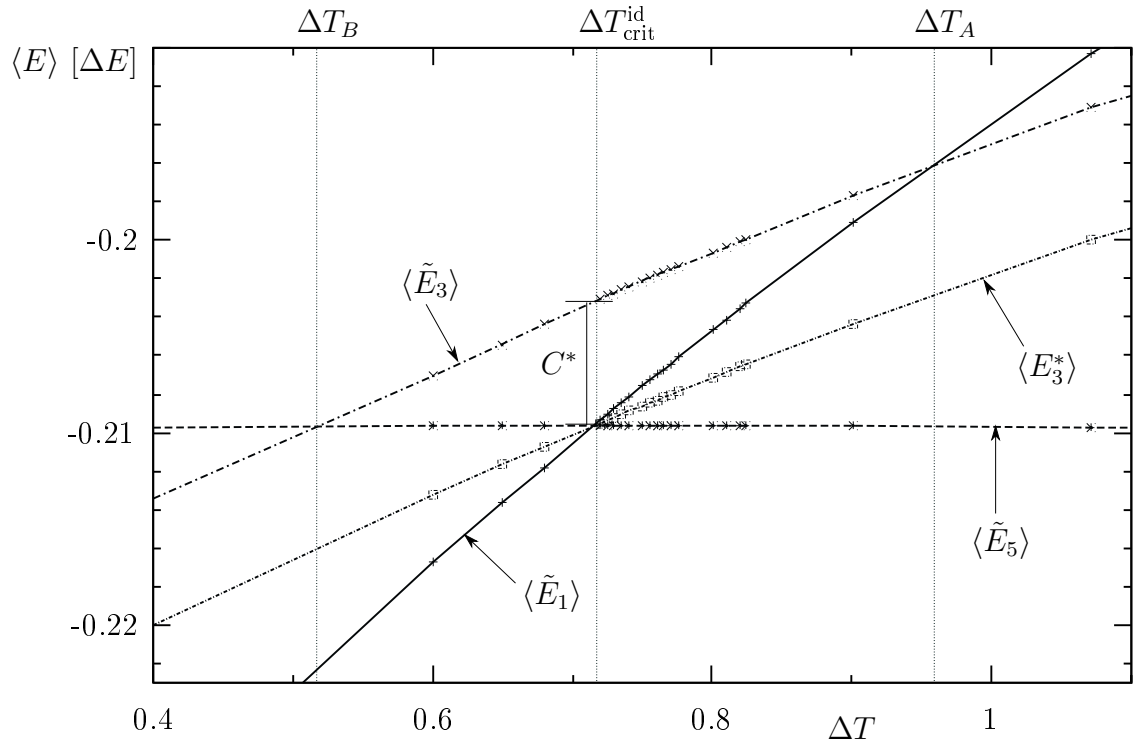

Figure 5.9.: Energy expectation values $\langle \tilde{E}_i \rangle$, $i = 1, 3, 5$ and $\langle E^*_3 \rangle$ (ideal). Due to the energetic up-shift $C^* = 0.0064\,[\Delta E]$ (with (5.10): $C = 0.0205$), units A, B should switch operation modes at $\Delta T_A = 0.96$ and $\Delta T_B = 0.52$, respectively.

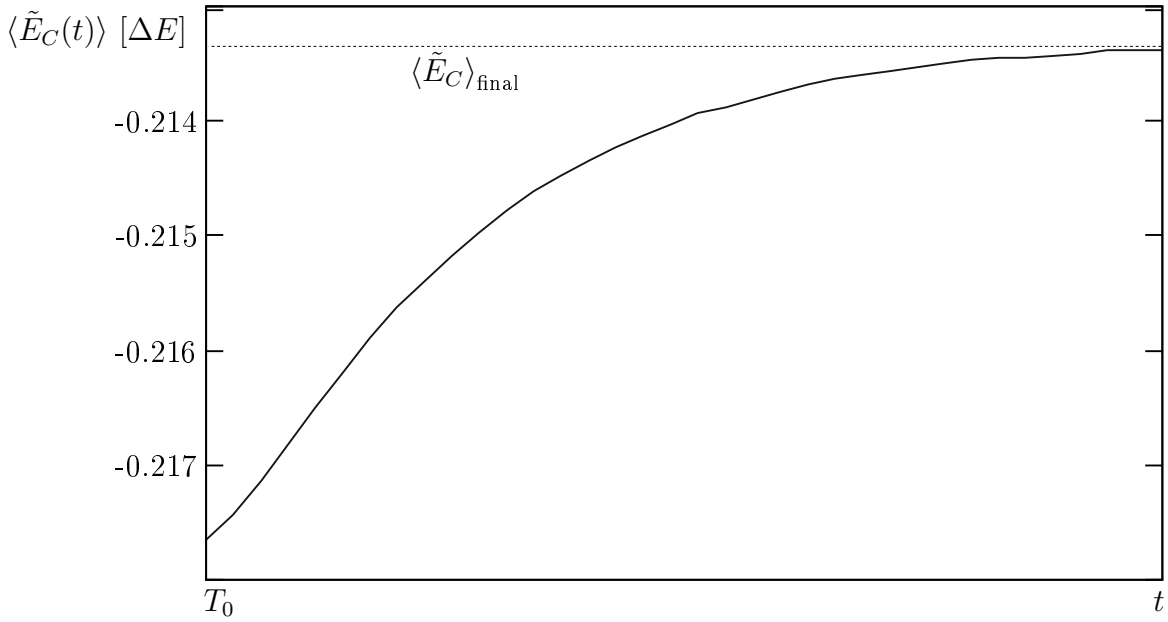

Figure 5.10.: The energy $\langle \tilde{E}_E(t) \rangle$ of spin 3 for $\Delta T = 0.4$ asymptotically approaches a stable value $\langle \tilde{E}_3 \rangle_{\mathrm{final}} \simeq -0.2135[\Delta E]$ during the temporal evolution of the system into its nonequilibrium attractor state.

At $\Delta T_B = 0.52$ the canonical distributions of spins 3 and 5 are equal, which marks the expected switch from heat engine to heat pump mode in unit B. For unit A the heat pump should emerge at $\Delta T_A = 0.96$ where $\langle \tilde{E}_1 \rangle = \langle \tilde{E}_3 \rangle$.

Comparing Fig. 5.9 and Fig. 5.6 one would expect that $\Delta T_B = \Delta T_{\text{crit}}^B$ and $\Delta T_A = \Delta T_{\text{crit}}^A$. Due to the presence of leakage currents, however, both transition points are shifted towards lower internal temperature gradients which, for unit B, corresponds to a higher global temperature gradient. For this reason, Fig. 5.6 shows the actual situation. In addition, the zero points of $\Delta Q_{h,c}$ are displaced as well. This behavior is the same as for the three- and four-spin models described above where leakage currents cause the breakdown of the heat pump and the emergence of the engine function at smaller critical temperature gradients than ideally expected. Furthermore, since heat and work functions are proportional to each other, their absolute values and inclinations decrease, compared to the case of lossless transport in the ideal Quantum Otto cycle.

The energetic increase C' in spin 3 is of magnitude 10^{-2} in units of the local energy splittings ΔE . To check whether this can be attributed to the weak but present correlations within the spin chain, the Bures distance measure between the actual state and the product of the uncorrelated local states (cf. (2.35)),

$$D^2 = \mathrm{Tr}\big\{ \left(\hat{\varrho}_{\mathrm{S}} - (\hat{\varrho}_1 \otimes \hat{\varrho}_2 \otimes \hat{\varrho}_3 \otimes \hat{\varrho}_4 \otimes \hat{\varrho}_5) \right)^2 \big\}$$

is plotted in Fig. 5.8 over one period τ, yielding only a magnitude of $10^{-5}[\Delta E]$. This is much too small to explain the mentioned up-shift effect since also the spin-spin interaction has been chosen in the weak coupling limit ($\lambda = 0.01$). Nevertheless, strong similarities to the characteristics and magnitude of the heat currents (Fig. 5.2) are observable, indicating clear mutual dependencies. The smaller peak in Fig. 5.8 represents the internal heat current J_{int} via the effective bath spin which is invisible in the heat current characteristics. Only the higher peak can be directly linked to the heat currents $J_{h,c}$ between the system and the hot and cold reservoir.

The explanation for the up-shift C' may finally be founded in that during the evolution of the system towards its non-equilibrium attractor state some of the heat transported through the chain effectively remains stuck in the "bottleneck" spin 3 due to internal leakage currents. As shown in Fig. 5.10, the energy expectation value of spin 3 $\langle \tilde{E}_3(t) \rangle$ asymptotically approaches the stable average energy $\langle \tilde{E}_3 \rangle_{\text{final}} \simeq -0.2135[\Delta E]$ for an initial energy $\langle E_3^* \rangle \simeq -0.22$ and $\Delta T = 0.4$. For better visibility oscillations of $\langle \tilde{E}_3(t) \rangle$ are omitted.

We remark that the driven spins could also be modulated with other relative phases than done here. The best heat transport through this kind of serial circuit has however been found for the case that both driven spins simultaneously are in resonant contact with spin 3, since only in this case the latter features a constant energy and temperature, allowing for easier investigation. If otherwise the driven spins alternately exchange heat with the effective bath, its energy and temperature oscillates around an average value.

Finally the setup as in figure 5.1 could be altered such that two identical subunits had to work against each other. Then $\Delta W_A = -\Delta W_B$ and, as claimed by the Curie principle for the absence of any asymmetry, the total work would vanish and solely an effective

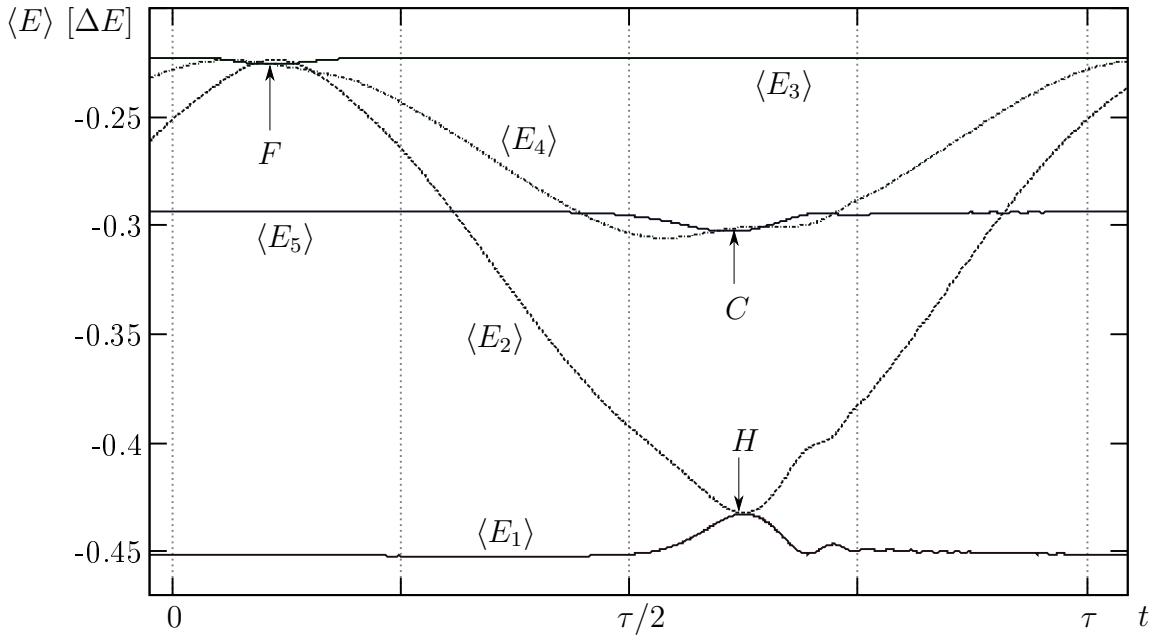

Figure 5.11.: Energy expectation values $\langle E_i \rangle$ of spin i for $\Delta T = 0.13$. Losses occur due to long times of resonant contact between adjacent spins, labeled F, H and C (see text). While spins 2,3 and 4 equilibrate (F), Spin 2 does not reach the energy level of spin 1 (H).

leakage transport from the hot to the cold bath would remain, effectively reducing the machine function to a pure transport phenomena.

If, in addition, both reservoirs had the same temperatures, the resulting highly symmetrical configuration might be used to cool the middle spin down to a minimal temperature determined by the canonical distributions of the bath spins. The same could also be achieved with a driven three-spin chain coupled to one heat bath only [41].

5.1.3. Extensions of the Ideal Quantum Otto Cycle

As indicated above, the description of the ideal Quantum Otto cycle does correctly predict the Quantum Otto efficiencies of the engine-pump circuit with "bottleneck" but is obviously unable to give an adequate estimate for the global critical temperature gradient without further modifications.

First of all, the conservation of energy for the heat current running through the effective bath (5.2) does not seem to work any more for any average temperature other than T_3^* from (5.4). However, remedy is found in Fig. 5.11 where the energy expectation values of all spins are plotted over one period for the case the entire circuit works as heat pump. During heat transfer via the effective bath spin marked F, spins 2,3 and 4 are in resonant contact and their energies approximately equal. Thus, even for more than two spins the intuitive view of contact equilibrium holds at least up to a certain degree, even in a dynamical scenario. While the energies of spins 4 and 5 approach each other

as well during heat inflow from the cold bath (labeled C), the energy of spin 2 does not fully reach that of spin 1 although both interact (labeled H). It is generally found that, if unit A works as heat pump and B as engine, spin 2 features a higher temperature than it would under idealized conditions, i. e. optimal heat transfer. The same happens to spin 4 in the contrary case. For $\Delta T_B \leq \Delta T \leq \Delta T_A$ where units A and B work as heat pumps (see Fig. 5.6) both gas spins do not fully equilibrate with the bath spins.

As pointed out in the following, Eq. (5.2) remains valid for $T_3 \neq T_3^*$ by a phenomenological modification. Firstly, Eq. (5.3), giving the distribution of spin 3, is rewritten as

$$\tanh \frac{\Delta E_3}{2T_3} = \frac{1}{2}\left(\tanh \frac{\Delta E_1}{2T_h} + \tanh \frac{\Delta E_5}{2T_c} - C\right) \tag{5.9}$$

where

$$C = 4C^*/\Delta E_3 \tag{5.10}$$

with C^* taken from figure 5.9 and introduced as a phenomenological constant. For the presently used parameters the value $C = 0.0192$ is found. The local critical gradients ΔT_B and ΔT_A are now given by

$$\tanh \frac{\Delta E_1}{2T_h} = \tanh \frac{\Delta E_3}{2T_3} \quad \Longrightarrow \Delta T_A = \frac{\Delta E_1}{2\,\mathrm{arctanh}\left(\tanh \frac{\Delta E_5}{2T_c} - C\right)} - T_c > \Delta T_{\mathrm{crit}}^{\mathrm{id}}\,, \tag{5.11}$$

$$\tanh \frac{\Delta E_5}{2T_c} = \tanh \frac{\Delta E_3}{2T_3} \quad \Longrightarrow \Delta T_B = \frac{\Delta E_1}{2\,\mathrm{arctanh}\left(\tanh \frac{\Delta E_5}{2T_c} + C\right)} - T_c < \Delta T_{\mathrm{crit}}^{\mathrm{id}}\,. \tag{5.12}$$

These expressions only depend on the initially unknown parameter C to be obtained from the numerics and, in general, are supposed to be a function of ΔE_3, the driving frequency ω and the other constant model parameters (see table 4.1).

Over a wide range a slight dependence on ΔT is visible which, however, may be neglected within the frame of this phenomenological ansatz. If $C = 0$ it would be again

$$\Delta T_B = \Delta T_{\mathrm{crit}}^{\mathrm{id}} = \Delta T_A = T_c(\Delta E_1/\Delta E_5 - 1)\,.$$

On the other hand, the elevated energy that e. g. spin 4 exhibits after having been in resonant contact with spin 5 is included by assuming the cold bath at a raised temperature T_c^*. The altered continuity condition now reads

$$\frac{\Delta E_3}{2}\left(\tanh \frac{\Delta E_1}{2T_h} - \tanh \frac{\Delta E_3}{2T_3}\right) = \frac{\Delta E_3}{2}\left(\tanh \frac{\Delta E_3}{2T_3} - \tanh \frac{\Delta E_5}{2T_c^*}\right) \tag{5.13}$$

leading to the following distribution of spin 4 for $\Delta T \geq \Delta T_A$:

$$-2\left\langle E_5^*\right\rangle/\Delta E_5 = \tanh \frac{\Delta E_5}{2T_c^*} = \tanh \frac{\Delta E_5}{2T_c} - C \tag{5.14}$$

An analog expression is obtained for spin 2 if $\Delta T \leq \Delta T_B$:

$$-2\left\langle E_1^* \right\rangle / \Delta E_1 = \tanh \frac{\Delta E_1}{2T_h^*} = \tanh \frac{\Delta E_1}{2T_h} - C \tag{5.15}$$

From a physical point of view, the spin system evolves into a stationary non-equilibrium state where either spin 2 or 4 do not sufficiently equilibrate with the respective bath contact spins. Eventually this can be explained as well with the occurrence of leakage currents. Even if unit A works as engine at $\Delta T > \Delta T_A$, spin 2 transports less heat due to the raised constant average temperature of spin 3 why, in turn, spin 4 engages towards a state with increased temperature in order that (5.13) is fulfilled. The analog inverse holds if the entire circuit works as heat pump for $\Delta T < \Delta T_B$. In between, if $\Delta T_B \leq \Delta T \leq \Delta T_A$, both units work as heat pumps and consume work only to compensate losses. Here, both the hot and cold reservoir are assumed to feature elevated temperatures T_h^{**} and T_c^{**}, respectively. This may be modeled by

$$\tanh \frac{\Delta E_1}{2T_h^{**}} = \tanh \frac{\Delta E_1}{2T_h} - (1-a)C \tag{5.16}$$

$$\tanh \frac{\Delta E_5}{2T_c^{**}} = \tanh \frac{\Delta E_5}{2T_c} - aC \tag{5.17}$$

where a for the rest is an unknown function of ΔT and the other system parameters, and $0 \leq a \leq 1$ for $\Delta T_B \leq \Delta T \leq \Delta T_A$.

Finally, the critical temperature gradients for units A and B calculated above lead to the one for the entire system. Taking into account that $W_B = 0$ at ΔT_B, the work function $\Delta W_B(\Delta T = T_h - T_c)$ of unit B writes

$$\Delta W_B(\Delta T) = \frac{1}{4}\left(\Delta E_5 - \Delta E_3\right)\left(\tanh \frac{\Delta E_5}{2T_c} - \tanh \frac{\Delta E_1}{2(\Delta T + T_c)} + C\right) \tag{5.18}$$

This function is also assumed to hold for $\Delta T \geq \Delta T_A$, taking into account the dissipation originating from the excess work to be applied to system B since here the driven and bath spin do not fully equilibrate. Otherwise T_c could be replaced by T_c^* from Eq. (5.14) which would give rise again to the ideal critical gradient $\Delta T_{\mathrm{crit}}^{\mathrm{id}}$.

In analogy to this, the work function $\Delta W_A(\Delta T)$ becomes

$$\Delta W_A(\Delta T) = \frac{1}{4}\left(\Delta E_1 - \Delta E_3\right)\left(\tanh \frac{\Delta E_1}{2(\Delta T + T_c)} - \tanh \frac{\Delta E_5}{2T_c} + C\right) \tag{5.19}$$

and finally, the entire work function gets

$$\begin{aligned}\Delta W_{\mathrm{tot}}(\Delta T) &= \Delta W_A(\Delta T) + \Delta W_B(\Delta T) \\ &= \frac{1}{4}\left(\Delta E_1 - \Delta E_5\right)\left(\tanh \frac{\Delta E_1}{2(\Delta T + T_c)} - \tanh \frac{\Delta E_5}{2T_c}\right) + \frac{C}{4}\left(\Delta E_1 + \Delta E_5 - 2\Delta E_3\right)\end{aligned} \tag{5.20}$$

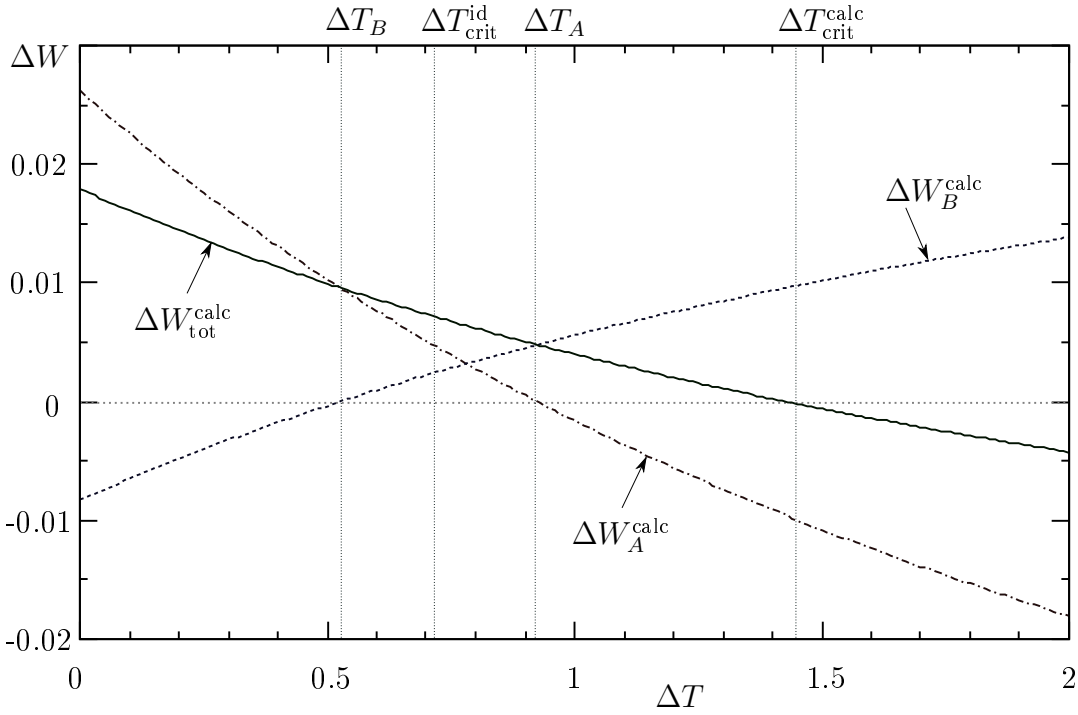

Figure 5.12.: Work $\Delta W_{A/B}^{\rm calc}$ of units A, B and total circuit work $\Delta W_{\rm tot}^{\rm calc}$, calculated with Eqns. (5.18) - (5.20) for $\Delta E_3 = 1.25$ and $C = 0.0192$. $\Delta W_{\rm tot}^{\rm calc}$ changes sign at $\Delta T_{\rm crit}^{\rm calc} = 1.45$, cf. Eq. (5.21).

The transition point where $\Delta W_{\rm tot} = 0$ is obtained as

$$\Delta T_{\rm crit} = \frac{\Delta E_1}{2}\left[\operatorname{arctanh}\left(\tanh\frac{\Delta E_5}{2T_c} - \frac{C(\Delta E_1 + \Delta E_5 - 2\Delta E_3)}{\Delta E_1 - \Delta E_5}\right)\right]^{-1} - T_c \qquad (5.21)$$

This expression depends on the internal geometry in terms of ΔE_3 as well as on the energetic up-shift in spin 3 read out from Fig. 5.9 with (5.10).

For $C > 0$ and $\Delta E_3 < \Delta E_1$, ΔE_5 we have $\Delta T_{\rm crit} > \Delta T_{\rm crit}^{\rm id}$. As a result, the mutual influence between the subunits via the effective bath spin causes the entire circuit to change its mode of operation at a higher critical temperature gradient than ideally expected. This is also clarified by considering the energy expectation values $\langle \tilde{E}_i \rangle$ normalized to ΔE_3. Globally seen, work is released only if

$$(\Delta E_1 - \Delta E_3)\left(\langle \tilde{E}_1 \rangle - \langle \tilde{E}_3 \rangle\right) > (\Delta E_5 - \Delta E_3)\left(\langle \tilde{E}_3 \rangle - \langle \tilde{E}_5 \rangle\right)$$

Moreover, the factor 1/4 appearing in the expressions derived for $\Delta W_{A/B}$ indicates a general reduction of both work and transported heat due to the presence of spin 3, even if $C = 0$. This also applies to other models containing an effective bath spin (see Sec. 5.2) and can be linked to the elevated resistance of the five-spin chain. Considering e. g. a three-spin machine, the factor 1/2 rules instead, cf. (3.4), (3.5).

All in all, the given ansatz is rather phenomenological but, at least, it can roughly explain the shift of the global critical temperature gradient in a "bottleneck" model. Compared to the description of the ideal Quantum Otto cycle, only one additional extension has been introduced, namely C.

A plot of the work functions for the entire circuit and both subunits, calculated with (5.18), (5.19) and (5.21), is depicted in Fig. 5.12 for $\Delta E_3 = 1.25$ and $C = 0.0192$. As expected, the zero points $\Delta T_{A/B}$ coincide with the intersection points from Fig. 5.9. While, qualitatively, the calculated work functions are quite similar to the numerically obtained ones displayed in Fig. 5.5 and Fig. 5.6, the obtained critical temperature gradient of the entire circuit, $\Delta T_{\mathrm{crit}}^{\mathrm{calc}} = 1.45$ is much too large compared to the actual value of $\Delta T_{\mathrm{crit}} = 0.83$.

Hence, the effects of leakage currents must necessarily be taken into account. As mentioned, this will induce shifts of the local critical gradients $\Delta T_{A/B}$ and also a downscaling of the work functions. Up to now, however, this can only be done with other ad-hoc approaches, introducing more correction terms such as scaling factors and zero shifts $\Delta T \rightarrow \Delta T \pm \Delta$ to $\Delta W_{A/B}$ into Eqns. (5.18) - (5.20), likewise the approach in [16].

As it will be shown below, the offset C changes if ΔE_3 is altered. This behavior and its impacts on the global circuit characteristics will now be investigated further by means of some more examples.

5.1.4. Modified Circuit Configurations – Variation of the Energetic Geometry

In order to determine the dependence of the circuit characteristics on the local energy splittings, we examine an additional example where the local energy gap of spin 3 is set to $\Delta E_3 = 0.25$ and the amplitudes of spins 2 and 4 are adjusted in order to to agree with the new resonance conditions. This model, referred to as circuit 2, is found to exhibit a substantially different behavior than the prior one.

For the case the circuit works as heat pump, the ST-diagrams of units A, B are displayed in Fig. 5.13. Compared to the previously investigated circuit (Fig. 5.4) their shapes are rather rectified, indicating that leakage currents are considerably suppressed here. In particular, the small dips related to leakage within the spin chain factually vanish.

This quasi-rectification follows from the low value of ΔE_3, leading to faster "stroke velocities" of the gas spin energy gaps and thus to shortened resonance times between neighbored spins. In physical terms the time derivatives of the local Hamiltonian of gas spins 2 and 4 read

$$\dot{\hat{H}}_{2,4} = \tfrac{1}{2}\,\omega \Delta E_{2,4}^{0} \cos \omega t \tag{5.22}$$

with increased amplitudes $\Delta E_{2,4}^{0} = \frac{1}{2}\,(\Delta E_{1,5} - \Delta E_3)$. In the following we concentrate on the influence of variations of ΔE_3 on the system characteristics whereas the impacts of different driving frequencies ω has not been researched yet.

The reduction of leakage is also apparent from the heat currents depicted in Fig. 5.14, featuring asymmetric shapes with flat slopes. This is quite similar to the model with

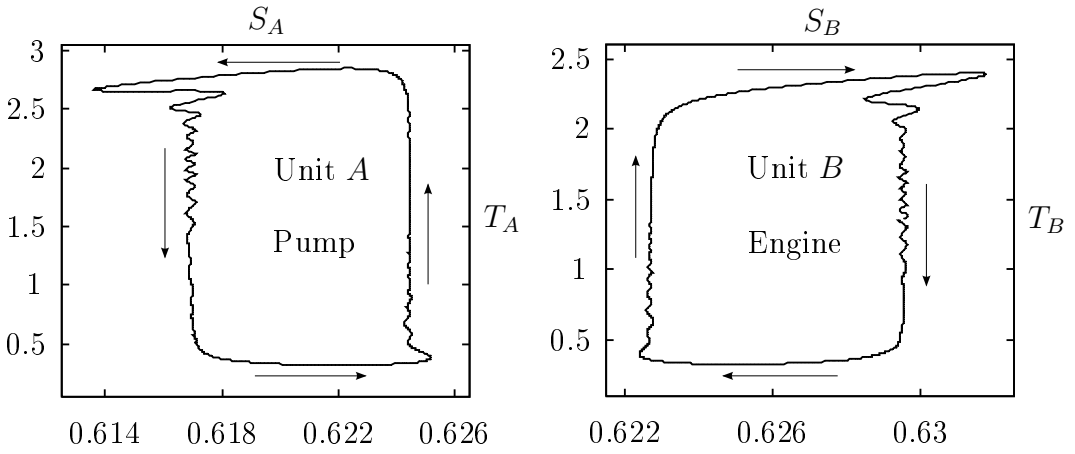

Figure 5.13.: Circuit 2 (defined on p. 66) working as heat pump ($\Delta T = 0.13$): ST-diagrams of the driven spins of units A and B, working as heat pump and heat engine, respectively.

artificial decoupling discussed in Sec. 3.3.1, cf. Fig. 3.4). After the isochoric step where heat is exchanged with the reservoirs, the heat currents into and out of the system may decay slowly since the gas spins are rapidly driven out of resonance and therefore backflow is inhibited. Nonetheless the driven spins remain coupled to the baths which is indicated by the ubiquitous oscillations during the adiabats.

The altered system geometry neither leaves the characteristics of the work and heat functions unchanged. Both are almost doubled as the comparison of figures 5.15 and 5.5 yields. The increase of heat goes in hand with heat current peaks of higher magnitude than those for the prior model (cf. Fig. 5.2).

In contrast, the efficiencies $\eta_{\mathrm{en/p}}$ of the whole circuit drawn in Fig. 5.17 remain qualitatively unaltered in essence. They approach the ideal Quantum Otto efficiencies $\eta_{\mathrm{en}}^{\mathrm{Otto}} = 0.222$ and $\eta_{\mathrm{p}}^{\mathrm{Otto}} = 4.5$ for values of ΔT afar the critical gradient for the entire circuit, being right-shifted again to $\Delta T_{\mathrm{crit}} = 0.87$ where the circuit efficiencies decay to zero.

The actual difference to the previous model turns out in Fig. 5.20, displaying the local heat engine and pump efficiencies $\eta_{\mathrm{en/p}}^{A/B}$ of units A, B together with the corresponding local Quantum Otto efficiencies. These take the values $\eta_{\mathrm{en}}^{\mathrm{A,Otto}} = 0.889$ and $\eta_{\mathrm{p}}^{\mathrm{A,Otto}} = 1.125$ for unit A and $\eta_{\mathrm{en}}^{\mathrm{B,Otto}} = 0.857$ and $\eta_{\mathrm{p}}^{\mathrm{B,Otto}} = 1.167$ for unit B. Both units switch much more abruptly between heat engine and heat pump mode and their efficiencies converge faster towards the local ideal Quantum Otto bounds since internal leakage currents are widely suppressed. Otherwise the slopes of the decaying efficiency functions would be much flatter, cf. Sec. 4.2 and [16].

In analogy, Fig. 5.16 shows that for both subunits the work and heat functions equal zero at the same temperature gradients, i. e. $\Delta W_B = \Delta Q_c = 0$ at $\Delta T_{\mathrm{crit}}^B = 0.7$ and $\Delta W_A = \Delta Q_h = 0$ at $\Delta T_{\mathrm{crit}}^A = 0.743$, revealing again that locally dissipation is minimized.

Globally seen, however, the situation remains unchanged. For $\Delta T_{\mathrm{crit}}^B \leq \Delta T \leq \Delta T_{\mathrm{crit}}^A$ both subsystems again work as heat pumps and consume work only to compensate losses.

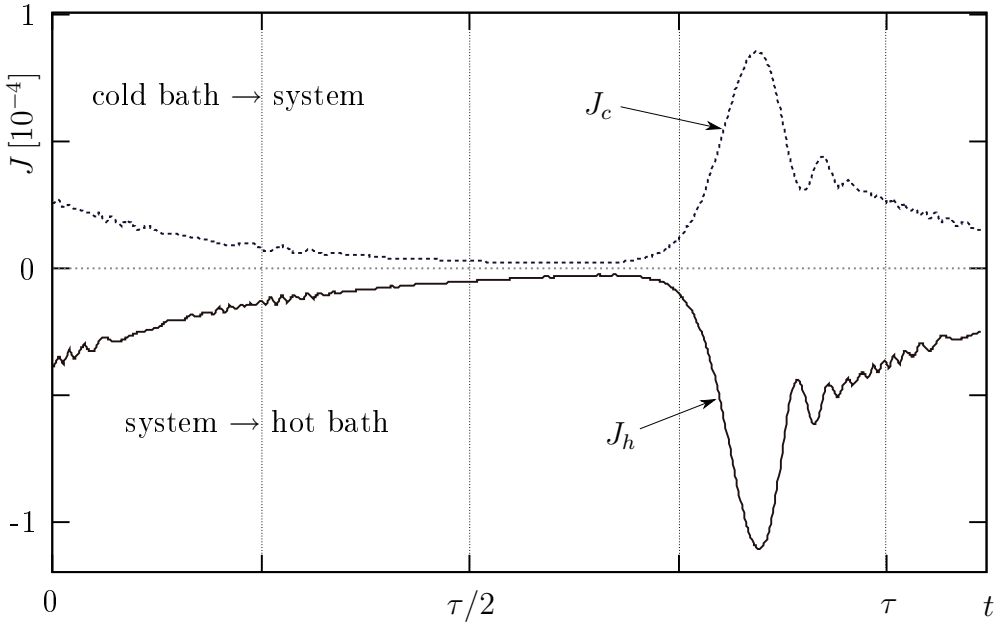

Figure 5.14.: Circuit 2 (p. 66) working as heat pump ($\Delta T = 0.13$): Heat currents $J_{h,c}$ between system and baths over one cycle.

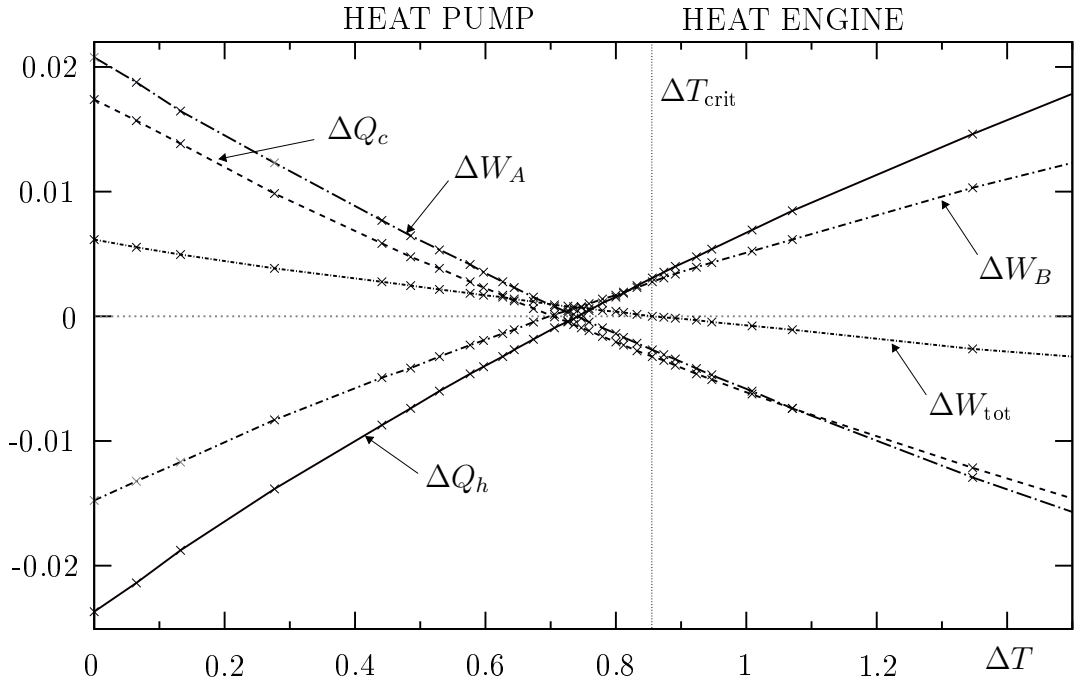

Figure 5.15.: Circuit 2 (p. 66): Heat $\Delta Q_{h,c}$, total circuit work $\Delta W_{\rm tot}$ and work $\Delta W_{A/B}$ of the subunits per period τ.

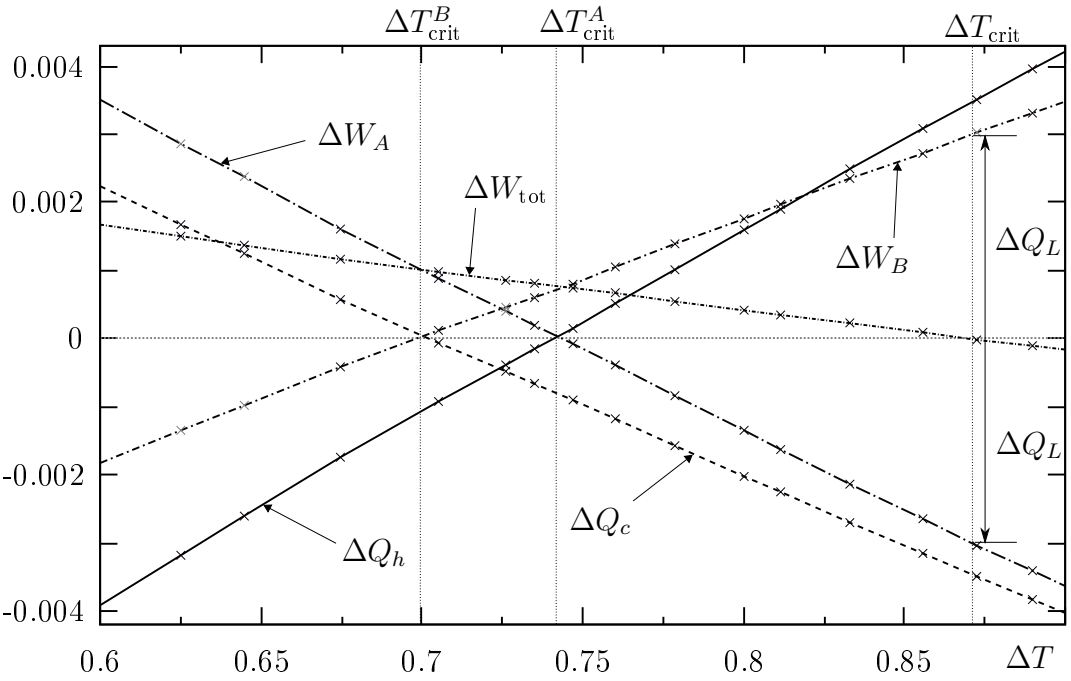

Figure 5.16.: Zoom into Fig. 5.15. One finds $\Delta Q_c = \Delta W_B = 0$ at $\Delta T^B_{\rm crit} = 0.7$ and $\Delta Q_h = \Delta W_A = 0$ at $\Delta T^A_{\rm crit} = 0.743$ (see text). The critical gradient for the entire circuit is $\Delta T_{\rm crit} = 0.87$, here only the leakage heat ΔQ_L remains.

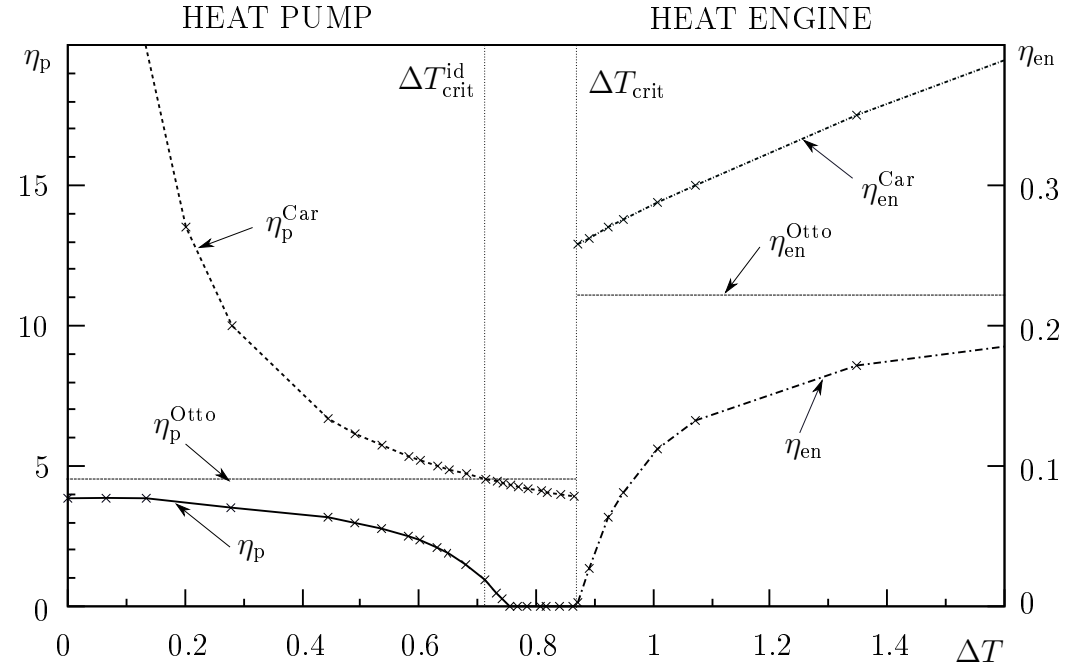

Figure 5.17.: Circuit 2 (p. 66): efficiencies of global engine and pump $\eta_{\rm en/p}$, ideal Quantum Otto bounds $\eta^{\rm Otto}_{\rm en/p}$ and Carnot bounds $\eta^{\rm Car}_{\rm en/p}$. Now, $\Delta T_{\rm crit} = 0.87 > \Delta T^{\rm id}_{\rm crit} = 0.714$.

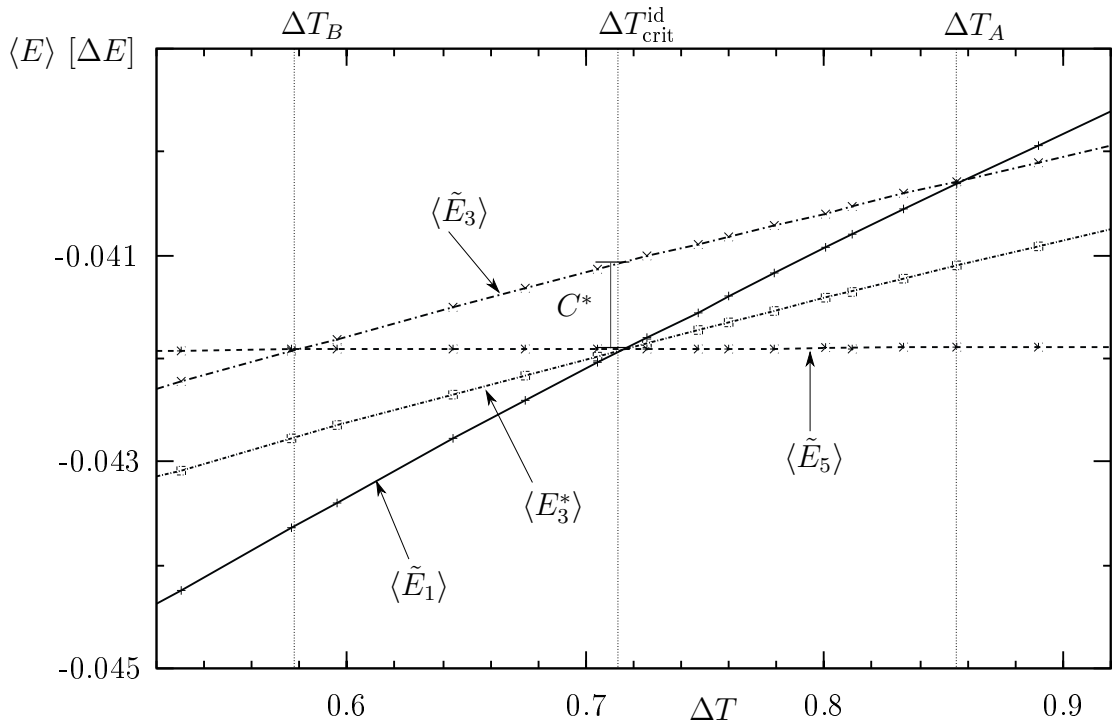

Figure 5.18.: Energy expectation values for circuit 2 (p. 66): $\langle \tilde{E}_i \rangle$, $i = 1, 3, 5$ and $\langle E_3^* \rangle$ (ideal). Definitions are analogous to p. 57. We find $C^* = 0.0008$ and thus $C = 0.013$ after Eq. (5.10).

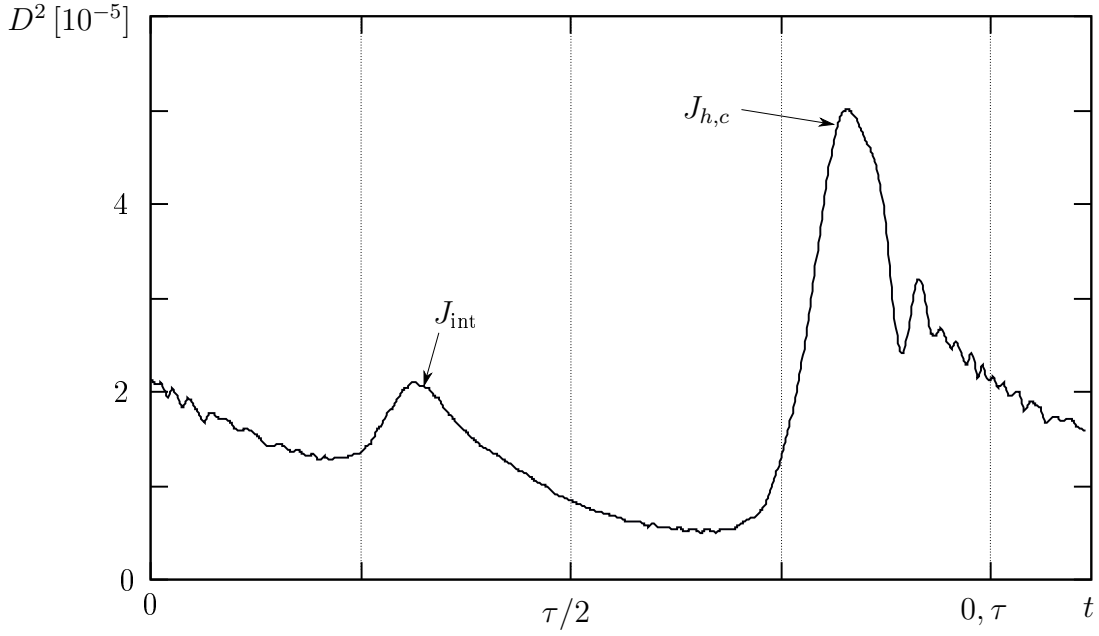

Figure 5.19.: Bures distance measure D^2 over one period τ for circuit 2 (p. 66). Peaks mark the presence of internal (J_{int}) and external heat currents ($J_{h,c}$), cf. Fig. 5.14.

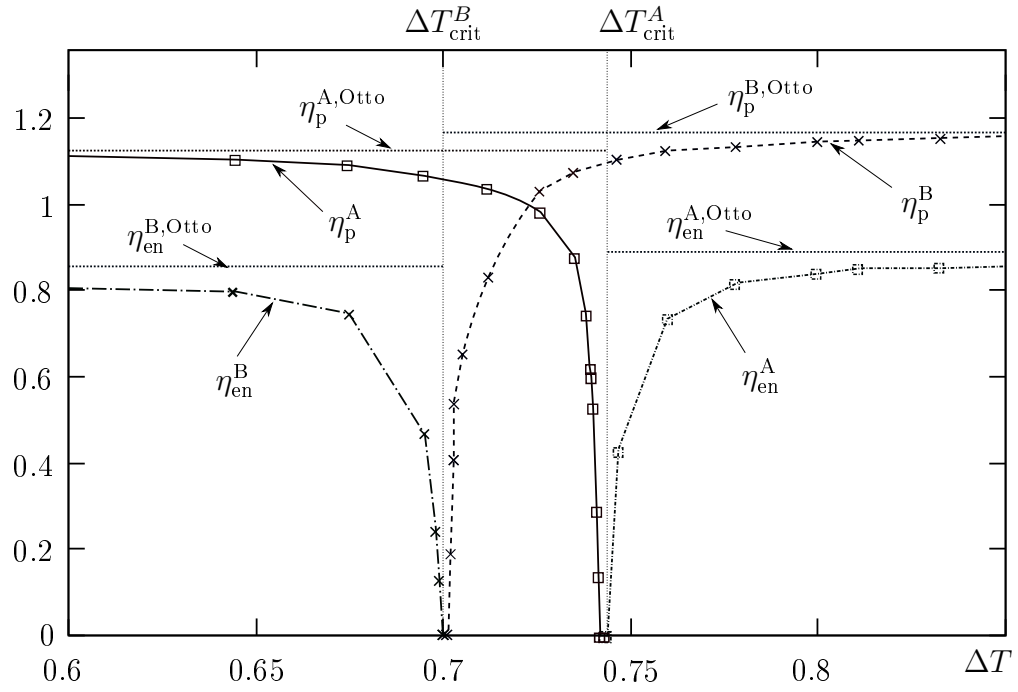

Figure 5.20.: Circuit 2 (p. 66): Local efficiencies of units A, B, $\eta_{\rm en/p}^{A/B}$ and ideal Quantum Otto efficiencies $\eta_{\rm en/p}^{A/B\,\rm Otto}$. Due to reduced losses, local operation modes switch abruptly at $\Delta T^{A,B}_{\rm crit}$.

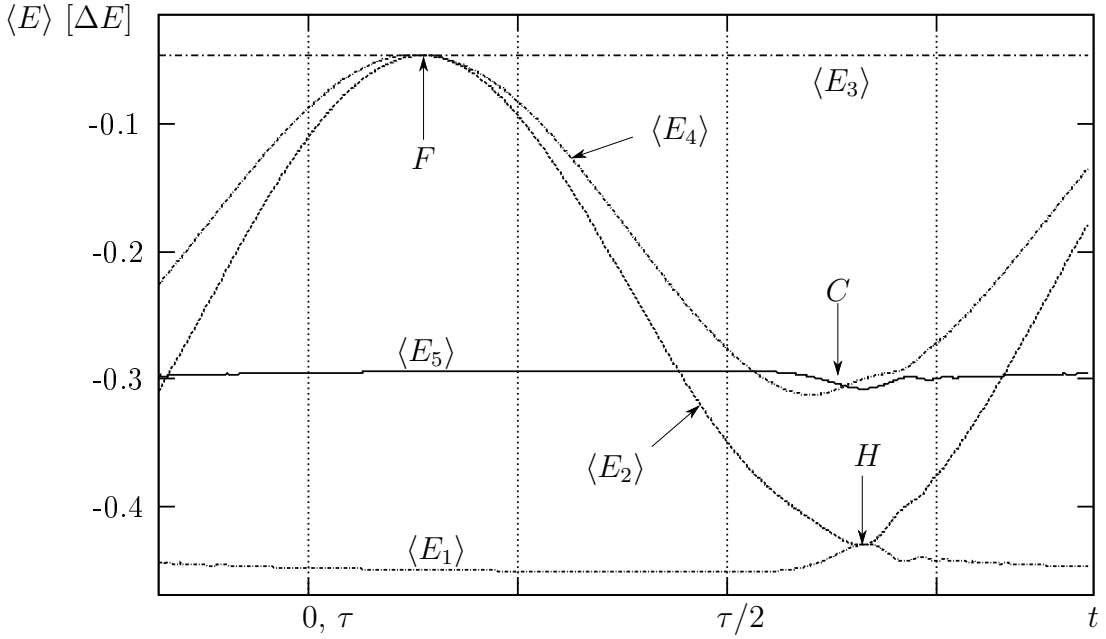

Figure 5.21.: Circuit 2 (p. 66) working as heat pump ($\Delta T = 0.13$): Energy expectation values $\langle E_i\rangle$ of spins i. Due to short resonance times between adjacent spins, labeled F, H and C, internal leakage currents are reduced. Spins 1 and 2 do not equilibrate energetically ($\rightarrow H$).

As mentioned, this is necessary to keep the effective bath spin 3 on its constant average energy.

Likewise, within $\Delta T^A_{\rm crit} \leq \Delta T \leq \Delta T_{\rm crit}$ subsystem A works as heat engine and B as pump. Again, $\Delta Q_h > 0$ and $\Delta W_{\rm tot} > 0$ because of $\Delta W_B > -\Delta W_A$, i. e. unit B consumes more work than A releases and, effectively, work must be expended to transport heat from the hot to the cold reservoir.

For the present model the energetic up-shift $C^* = 0.0009[\Delta E]$ of spin 3 is found from in Fig. 5.18, yielding $C = 4C^*/\Delta E_3 = 0.014$ which is smaller than before. As indicated above, the reduced value of ΔE_3 leads to a raised "stroke" velocity and thus to shortened resonance times since driving is effectively faster. Consequently, internal leakage currents are more effectively suppressed and the heat quantity stuck in the bottleneck spin is therefore reduced. As a result, the difference in canonical distributions between the bath spins on the one hand and spin 3 on the other hand is increased, leading to increased heat transport through the circuit via spins 2 and 4 which, in relation, release or consume even more work due to the larger internal energy gradients. At the same time, Fig. 5.17 indicates that more work has to be expended for dissipation balance in unit B since, for $\Delta T > \Delta T_{\rm crit}$ the global engine efficiency $\eta_{\rm en}$ undergoes its pendant from the prior model.

Following Eq. (5.11) and (5.12), the zero points of the local subunit work functions $\Delta W_{A/B}$ should be shifted to lower local internal temperature gradients for smaller values of C as well, which is confirmed by Fig. 5.18. Compared to Fig. 5.16, additional leakage-induced adjustments in this sense appear also. However these are less distinctive since leakage currents are reduced. After (5.20) the zero point of the entire circuit work function $\Delta W_{\rm tot}(\Delta T)$ is expected at $\Delta T_{\rm crit} = 2.0$, being far too big to match with the actual value of $\Delta T_{\rm crit} = 0.87$ from Fig. 5.16. Hence, in order to obtain the right zero positions and slopes of $\Delta W_{A/B}$ and $\Delta W_{\rm tot}$ adequate correction factors reflecting losses are needed once more.

A closer look on the processes during the isochores is furnished in Fig. 5.21 by means of the energy expectation values $\langle E_i \rangle$ for all spins i plotted over one period $\tau = 2\pi/\omega$. Compared to Fig. 5.11, resonance times between adjacent spins are shortened here. During the internal isochoric step with heat transfer via spin 3, labeled F, the energies of spins 2,3 and 4 approach quite well, indicating sufficient contact equilibrium. However, like in the previous case, the driven spin 2 does not sufficiently approach the average energy level $\langle E_1 \rangle$ of spin 1 (labeled H) and thus remains at a higher temperature. Since this is related to dissipation in unit B, the engine function of the entire circuit emerges at an even more increased gradient $\Delta T_{\rm crit}$ where, finally, unit A starts to release more work than B can consume.

Finally, weak correlations of magnitude and characteristics comparable to the heat currents (Fig. 5.14) are found in the system, displayed in Fig. 5.19 by means of the Bures distance measure over one period (see (2.35)). Again the internal heat currents are made visible by peaks.

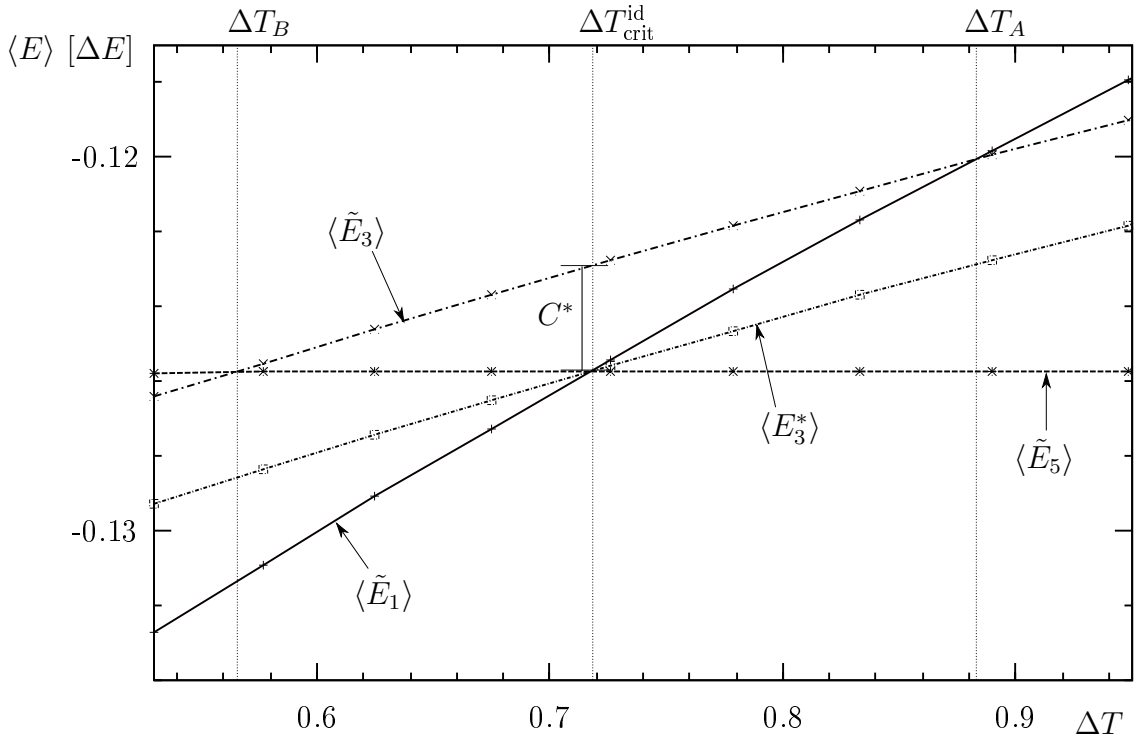

Figure 5.22.: Circuit 3 (p. 75) with $\Delta E_3 = 0.75$: Energy expectation values $\langle \tilde{E}_i \rangle$ and $\langle E^*_3 \rangle$ (ideal) , $i = 1, 3, 5$ (cf. p. 57). One finds $C^* = 0.0028$ and thus $C = 0.015$ (see (5.10)). Further, $\Delta T_A = 0.836$ and $\Delta T_B = 0.577$.

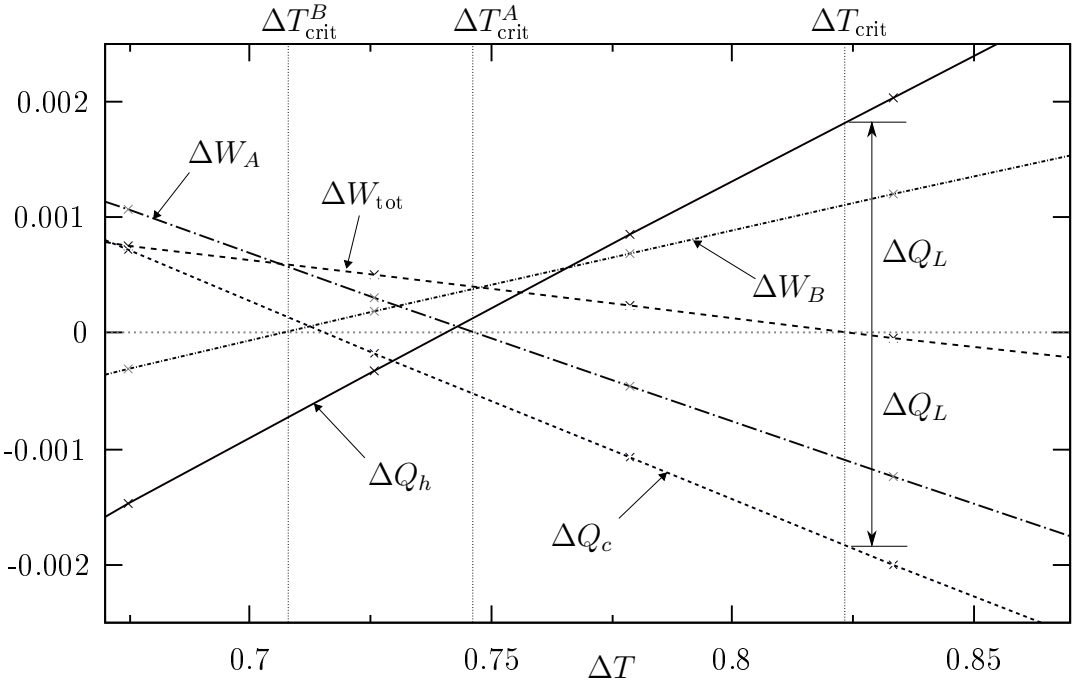

Figure 5.23.: Work and heat for circuit 3 (p. 75). Here $\Delta T^A_{\mathrm{crit}} = 0.747$, $\Delta T^B_{\mathrm{crit}} = 0.707$, and $\Delta T_{\mathrm{crit}} = 0.824$

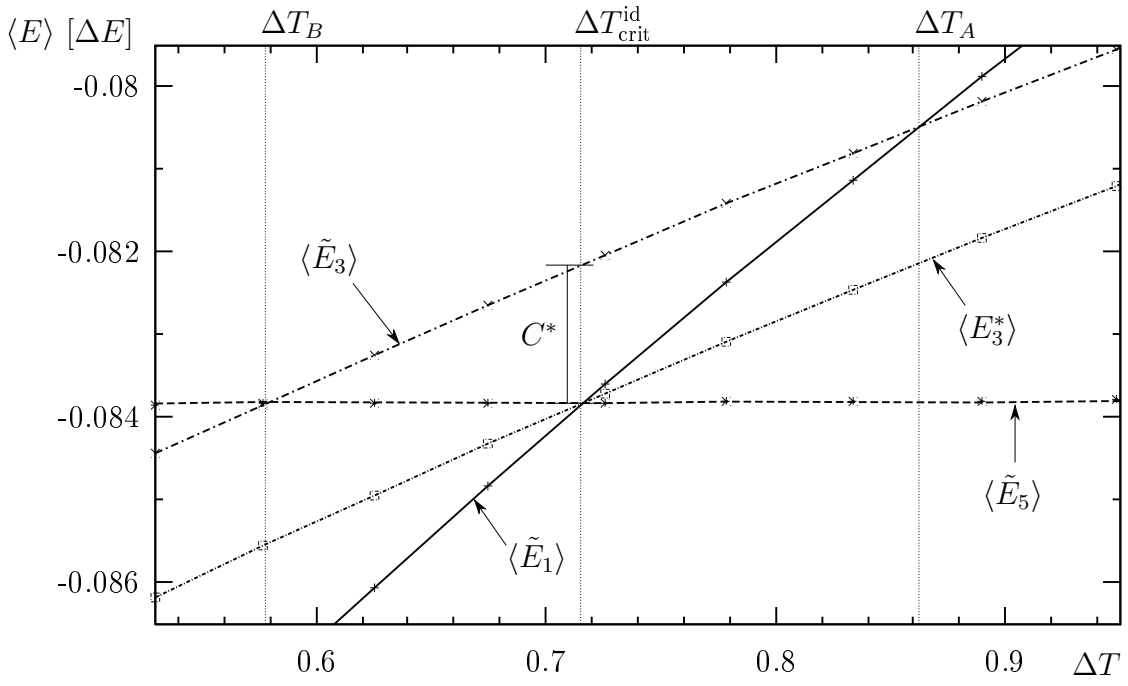

Figure 5.24.: Circuit 4 (p. 75) with $\Delta E_3 = 0.5$: Energy expectation values $\langle \tilde{E}_i \rangle$ and $\langle E_3^* \rangle$ (ideal), $i = 1, 3, 5$ (cf. p. 57). We find $C^* = 0.00168 \rightarrow C = 0.0135$ (Eq. (5.10)). Further on, $\Delta T_A = 0.836$ and $\Delta T_B = 0.577$.

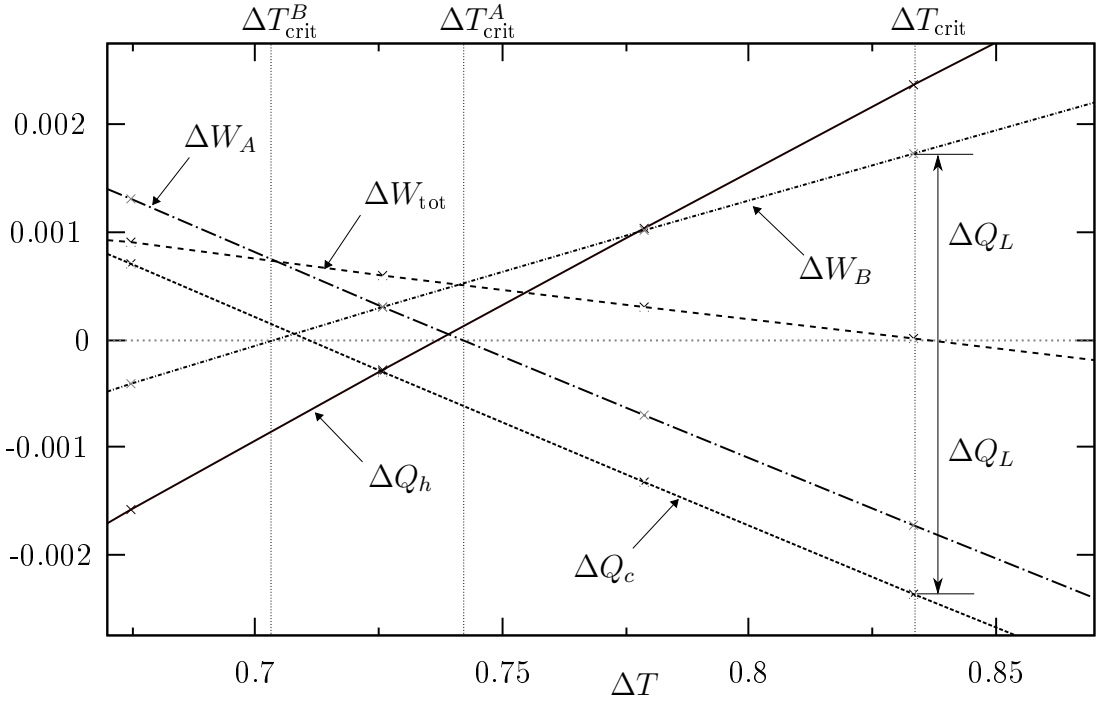

Figure 5.25.: Work and heat for circuit 4 (p. 75). Here $\Delta T^A_{\text{crit}} = 0.743$, $\Delta T^B_{\text{crit}} = 0.704$, and $\Delta T_{\text{crit}} = 0.836$.

ΔE_3	ω	C	ΔT_A	ΔT^A_{crit}	ΔT_B	ΔT^B_{crit}	ΔT_{crit}	with (5.21)
1.25	1/128	0.02	0.96	0.771	0.52	0.708	0.833	1.45
0.75	1/128	0.015	0.88	0.747	0.564	0.707	0.827	1.7
0.50	1/128	0.0135	0.863	0.743	0.577	0.704	0.836	1.8
0.25	1/128	0.013	0.859	0.743	0.581	0.7	0.87	2.0

Table 5.1.: Serial circuit: Characteristic results for different values of ΔE_3

Further Examples: Circuits 3 and 4

In a third example for a bottleneck model, referred to as circuit 3, we choose $\Delta E_3 = 0.75$ and adjust the amplitudes of the driven spins, whereas all other parameters are left unchanged, see Tab. 4.1. From Fig. 5.22 one finds the energy up-shift $C = 0.015$. Accordingly, $\Delta T_A \simeq 0.827$ and $\Delta T_B \simeq 0.564$. Provided that the driving frequency is unaltered, the stroke velocity decreases because of smaller internal energy gradients. This leads to longer spin contact times than in circuit 2 (p. 66), why internal leakage currents are invoked again. As displayed in Fig. 5.23, all heat and work functions equal zero at different ΔT and mainly come with absolute values in between those of circuits 1 and 2, according to the intermediate value of C.

Apparently, the parameter C crucially influences the heat transport capability in these systems and therefore is a resistance indicator. C definitely depends on ΔE_3 and, assumedly, also on ω which however is to be verified numerically yet.

Following Fig. 5.23, the actual critical temperature gradients $\Delta T^A_{\text{crit}} = 0.74$ and $\Delta T^B_{\text{crit}} = 0.71$ of the subunits are shifted inbound compared to $\Delta T_{A/B}$ from Fig. 5.22. The critical gradient of the whole circuit lies at $\Delta T_{\text{crit}} = 0.827$.

Example No. 4 comes with $\Delta E_3 = 0.5$ and $C = 0.0135$, taken from Fig. 5.24. Its heat and work functions provided in Fig. 5.25 only yield small discrepancies to those of circuit 3. Here, the critical gradient is found at $\Delta T_{\text{crit}} = 0.836$.

Summary and overview

The stroke velocities, given by the time derivatives of the local Hamiltonians of the driven spins 2 and 4 in Eq. (5.22) have been found to determine the spin resonance contact times which are decisive for the performance of heat transfer. Therefore they considerably affect the internal leakage current behavior and thus the parameter C. Expectedly, in addition to ΔE_3 the impact of the driving frequency ω on C is considerable as well, which is yet subject to verification. Depending on ΔE_3 (and ω), the heat conductivity of the circuit is altered by changing the resistance of spin 3 via the parameter C. On the other hand, the global circuit efficiencies are comparable for different sets of parameters.

An overview of obtained characteristic values depending on ΔE_3 for all presented examples is given in table 5.1. In first approximation, the actual critical temperature gradient obtained from the numerics can be considered independent of ΔE_3, although it is explicitly contained in (5.21) as well as via C. This is made plausible in that the investigated models feature about the same critical gradient ΔT_{crit}. Solely circuit 2

where $\Delta E_3 = 0.25$ breaks ranks. This, however, seems to be a special case since only here internal leakage currents are sufficiently suppressed.

For the rest, all other values in table 5.1 monotonously depend on ΔE_3. It is easily verified that the ansatz from Sec. 5.1.3 correctly describes the positions of the local critical gradients $\Delta T_{A/B}$ where $\Delta W_{A/B} = 0$. It takes into account the dissipation arising due to the fact that at least one of the driven spins does not equilibrate with the respective bath spin during heat transfer between the system and the acceptor bath. Additionally, one can state that, even if for this class of serial quantum machine circuits direct leakage currents from the hot to the cold bath are not present, the same effects arise as if this was the case since, in some sense, the circuit subunits work against each other due to the effective bath function of the "bottleneck" spin.

It must be noted that the right-shift of ΔT_{crit} cannot be exploited up to the full range like in models with linear energetic gradients because, within the critical range, all expended work is needed to balance dissipative losses.

In general, even if adequate fitting parameters for leakage currents can be found, the actual processes within these rather complex systems are difficult to characterize.

Summarizing, the serial five-spin circuit with a "bottleneck" spin does indeed run a Quantum Otto cycle, however, a better performance and more efficient heat transport is possible with a three-spin or four-spin machine, so as with the parallel four-spin circuit driven with relative phase shift.

5.2. Serial Circuit of Directed Quantum Machines

After having looked at oppositely directed quantum machines in the previous section, we investigate now a serial circuit with a funnel-shaped global energy gradient as depicted in Fig. 5.26. Differently to the "bottleneck" model, units A and B are expected to run Quantum Otto cycles in the same direction and work in unison either as heat engines or heat pumps due to the directed energetic gradient. This includes a directed temperature gradient within the circuit as well. The Quantum Otto cycle steps performed analogously to the description in Sec. 5.1.

Likewise before the circuit is a Heisenberg spin chain whose Hamiltonian is given by (3.8) extended to five spins. For numerical investigations the spin energy splittings are chosen as $\Delta E_1 = 3.0$, $\Delta E_2(t) = 2.75 + 0.25\cos\omega t$, $\Delta E_3 = 2.5$, $\Delta E_4(t) = 2.25 - 0.25\cos\omega t$ and $\Delta E_5 = 2.0$, fulfilling the resonance conditions

$$\Delta E_1 \geq \Delta E_2(t) \geq \Delta E_3 \geq \Delta E_4(t) \geq \Delta E_5$$

Similarly, for the local temperatures one finds

$$T_h = T_1 > T_3 > T_5 = T_c$$

Spins 2 and 4 are driven with a relative phase shift of half a period in order to bring them into resonance with spin 3 simultaneously, since in this case a considerable reduction of leakage currents is found and heat transport is improved. The temperature of the cold

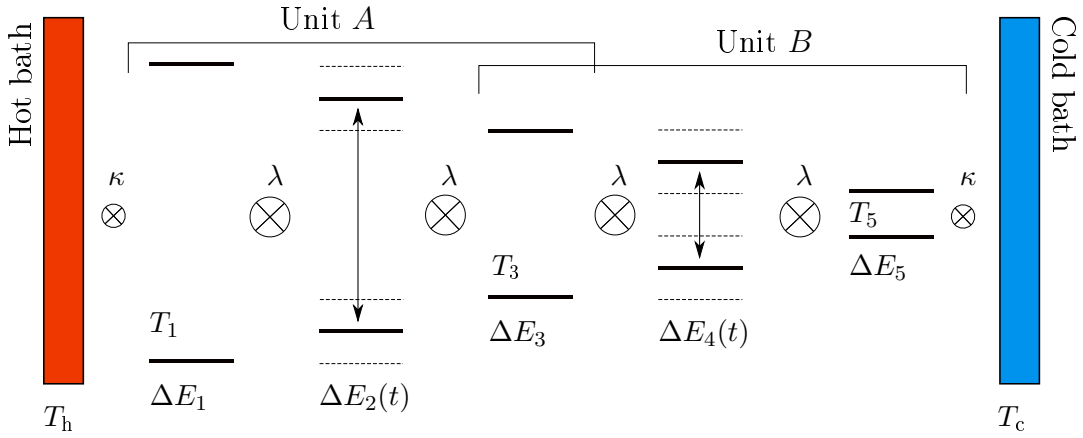

Figure 5.26.: Serial circuit of two quantum heat pumps/engines between two heat baths.

bath is constant, $\beta_c = 1/T_c = 0.7$ whereas that of the hot bath is varied. This set of parameters yields the same ideal critical temperature gradient as for all previous models, i. e. $\Delta T^{\mathrm{id}}_{\mathrm{crit}} = 0.714$, allowing for comparison. For ω and the coupling constants see table 4.1.

In Fig. 5.28 the heat engine and heat pump efficiencies $\eta_{\mathrm{en/p}}$ for the whole circuit are drawn as functions of ΔT. Both rapidly approach their ideal Quantum Otto bounds $\eta^{\mathrm{Otto}}_{\mathrm{en}} = 0.333$ and $\eta^{\mathrm{Otto}}_{\mathrm{p}} = 3$ and drop down steeply on approaching the critical temperature gradient found at $\Delta T_{\mathrm{crit}} = 0.68$, being very close to $\Delta T^{\mathrm{id}}_{\mathrm{crit}}$. These results imply that dissipative losses are small.

On the other hand, leakage currents do occur since the ST-diagrams depicted in Fig. 5.2 for the case both units work as heat pumps exhibit large typical leakage dips and strong oscillations on the adiabats, reflecting the bath influence. Furthermore, the peaks of the heat currents depicted in Fig. 5.30 are of symmetric shape, indicating internal heat current backflow, and also show the pertinent oscillations.

However, the apparent contradiction is resolved in that, up to a certain degree, the internal losses of spin 2 in the direction of the global temperature gradient are taken by spin 4 after internal isochoric heat transfer via spin 3. Since the ST-diagrams of both driven spins are roughly rotationally-symmetrical, one can conclude that the work dissipated in unit A due to losses is released again and thus sufficiently compensated in B, and vice versa. Contrarily, in a simple three-spin machine the leakage heat would simply vanish into the reservoirs and would therefore be lost.

Again the canonical distribution of spin 3 is about constant in time. In this case it approximately equals the ideal average of the bath spins (cf. Eq. (5.3)),

$$2\left\langle E_3\right\rangle/\Delta E_3 \equiv \tanh\frac{\Delta E_3}{2T_3} = \frac{1}{2}\left(\tanh\frac{\Delta E_1}{2T_h} + \tanh\frac{\Delta E_5}{2T_c}\right) \tag{5.23}$$

since there are no prerequisites for a constant energy up-shift such as for a "bottleneck" spin. $\langle E_3\rangle$ is the energy expectation value of spin 3 after 2.72.

Hence spin 3 takes again the role of an effective heat bath with a temperature in between of those of the baths, shielding both units from each other. However, the

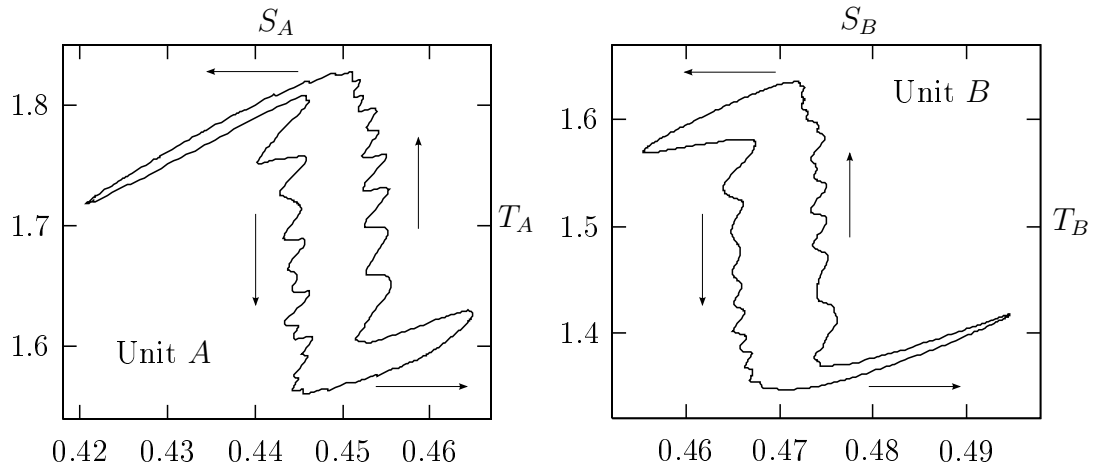

Figure 5.27.: ST-diagrams of two serially connected machine units A, B, working in unison as heat pumps here. The diagrams are roughly rotationally-symmetrical.

shielding capability is considerably reduced here due to the unidirectional temperature gradient.

In spite of the above said, losses are still present during heat transfer with the reservoirs as well as internally. This is learned from Fig. 5.29 and Fig. 5.31 where the heat and work functions $\Delta Q_{h,c}$ and ΔW are displayed. They are of similar magnitude as for comparable three- and four-spin models and change sign at different gradients ΔT. However, this happens on a much smaller scale and much closer to $\Delta T^{\mathrm{id}}_{\mathrm{crit}}$ than observed before. As indicated already by the ST-diagrams depicted in Fig. 5.2, units A and B run indeed the same thermodynamic cycle since the work functions $\Delta W_{A/B}$ carry the same sign. On larger scales it turns out that $\Delta W_A \approx \Delta W_B$, whereas the magnification in Fig. 5.31 shows that $\Delta W_A < \Delta W_B$ because a small amount of work in unit B is expended to compensate the losses emerging in A. As a consequence, both units change their modes of operation at slightly different temperature gradients $\Delta T^A_{\mathrm{crit}} \neq \Delta T^B_{\mathrm{crit}}$, symmetrically to ΔT_{crit}. For the rest, the Gibbs relation $\Delta Q_h + \Delta Q_c + \Delta W_A + \Delta W_B = 0$ is fulfilled.

Since the distribution of spin 3 equals about the ideal one (see (5.23)), it is easy to show that only half as much heat is exchanged between the system and the baths as it would be the case for a three-spin machine with the energetic gradient $(\Delta E_1 - \Delta E_5)$ and the same bath spin configurations $(\Delta E_1/T_h)$ and $(\Delta E_5/T_c)$. For the case the circuit runs as heat pump, this is now demonstrated by means of the ideal Quantum Otto cycle discussed in Sec. 3.3.

The heat flux from the cold bath into unit B is calculated as

$$\Delta Q_{h\to B} = \frac{\Delta E_5}{2}\left(\tanh\frac{\Delta E_5}{2T_c} - \tanh\frac{\Delta E_3}{2T_3}\right) = \frac{\Delta E_5}{4}\left(\tanh\frac{\Delta E_5}{2T_c} - \tanh\frac{\Delta E_1}{2T_h}\right) > 0$$

The work for the entire circuit becomes

$$\Delta W_{\mathrm{tot}} = \Delta W_A + \Delta W_B = \frac{1}{4}\left(\Delta E_1 - \Delta E_5\right)\left(\tanh\frac{\Delta E_5}{2T_c} - \tanh\frac{\Delta E_1}{2T_h}\right) > 0$$

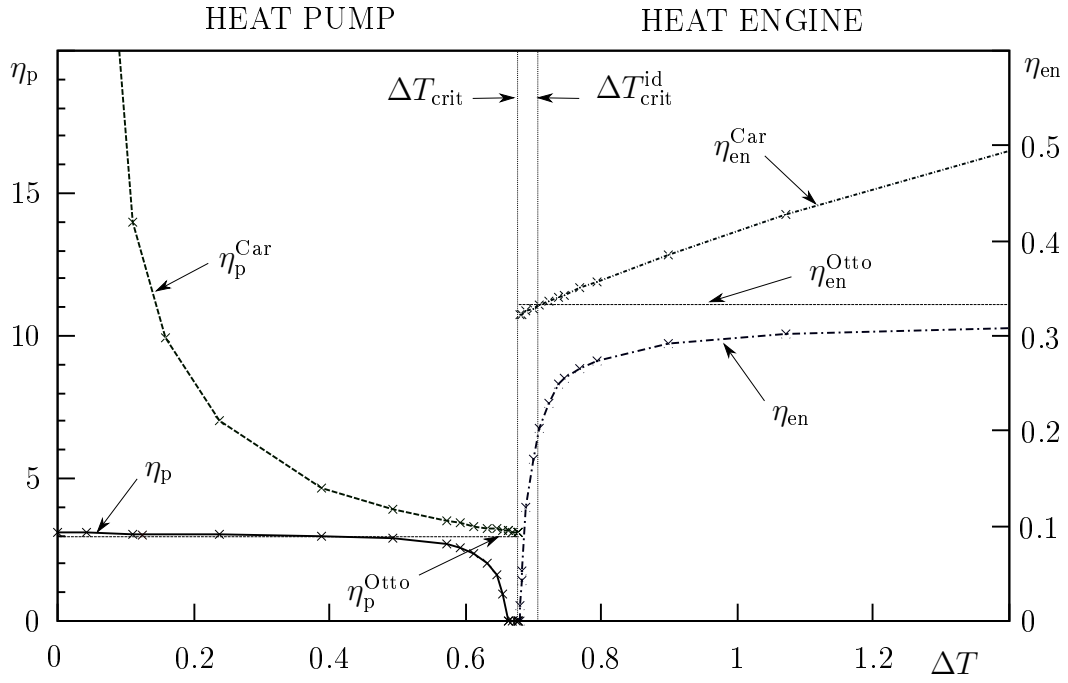

Figure 5.28.: Directed serial circuit: The efficiencies $\eta_{\rm en/p}$ of the heat engine and heat pump rapidly approach the ideal Quantum Otto bounds $\eta^{\rm Otto}_{\rm en/p}$ far from $\Delta T_{\rm crit} = 0.68$, close to $\Delta T^{\rm id}_{\rm crit} = 0.714$. The Carnot efficiencies are $\eta^{\rm Car}_{\rm en/p}$.

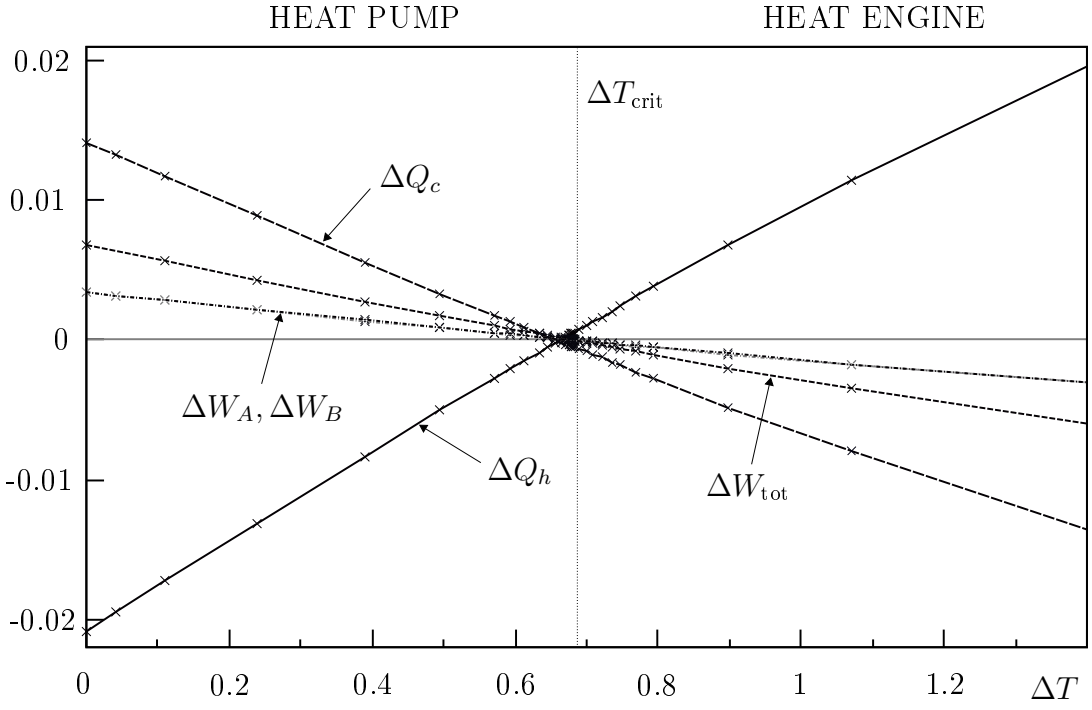

Figure 5.29.: Directed serial circuit: Heat $\Delta Q_{h,c}$, total circuit work $\Delta W_{\rm tot}$ and work $\Delta W_A \approx \Delta W_B$ of units A, B per period.

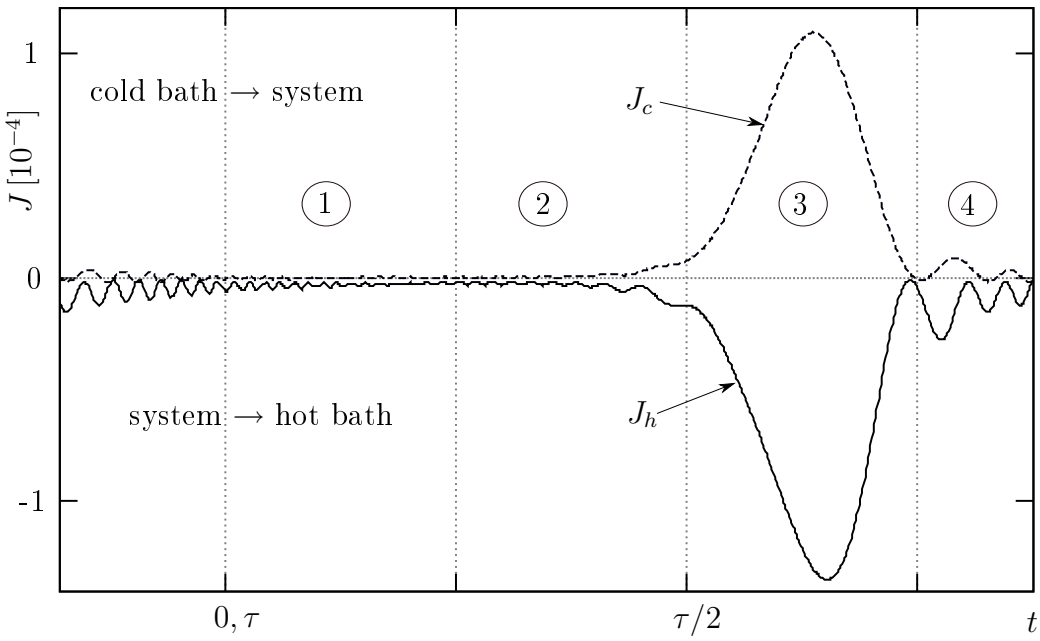

Figure 5.30.: Directed serial circuit running as heat pump ($\Delta T = 0.13$): Heat currents J_h, J_c over one period τ.

The heat floating from unit A into the hot bath, $\Delta Q_{A\to h}$ is obtained analogously.

All these function are reduced by a factor 2, compared to (3.17) and (3.16). Apparently, the additional spin in the middle leads to a downgrade in conductivity whereas, of course, the Quantum Otto efficiency $\eta_{\mathrm{p}}^{\mathrm{Otto}} = 3$ remains untouched since it only depends on ΔE_1 and ΔE_5. This limitation of heat throughput can be put on a level with a resistance to be assigned to spin 3. As discussed above, the same effect analogously arises in models with a "bottleneck" spin where it is further amplified by the mentioned energetic up-shift.

In comparison, a three-spin machine with the same canonical bath spin distributions but a smaller energetic gradient $\Delta E_1^* - \Delta E_5^* = x(\Delta E_1 - \Delta E_5)$, $0 < x < 1$ would transport more heat with the same work to be applied. Therefore, it would exhibit a higher ideal Quantum Otto efficiency for the heat pump and a lower one for the engine. Since, however, these efficiencies depend on concrete values of the bath spin splittings, a detailed comparison is not possible.

Fig. 5.32 shows the local heat engine and heat pump efficiencies $\eta_{\mathrm{en/p}}^{A/B}$ as well as the corresponding Quantum Otto efficiencies for units A and B which take the values $\eta_{\mathrm{p}}^{\mathrm{A,Otto}} = 6.0$, $\eta_{\mathrm{p}}^{\mathrm{B,Otto}} = 5.0, \eta_{\mathrm{en}}^{\mathrm{A,Otto}} = 0.167$ and $\eta_{\mathrm{en}}^{\mathrm{B,Otto}} = 0.2$.

Both heat pump efficiencies decease simultaneously to zero, whereas the emergence of the heat engine function in unit B is slightly shifted compared to that of unit A, i. e. $\Delta T_{\mathrm{crit}}^{B} > \Delta T_{\mathrm{crit}}^{A}$, since, as mentioned, a small work input into system B is required to compensate the losses in A (cf. Fig. 5.31). Far away from $\Delta T_{\mathrm{crit}}^{A/B}$ both heat pump efficiencies rapidly approach their respective Quantum Otto bounds, whereas the engine efficiencies also converge but effectively stay below. Following Fig. 5.28, the same

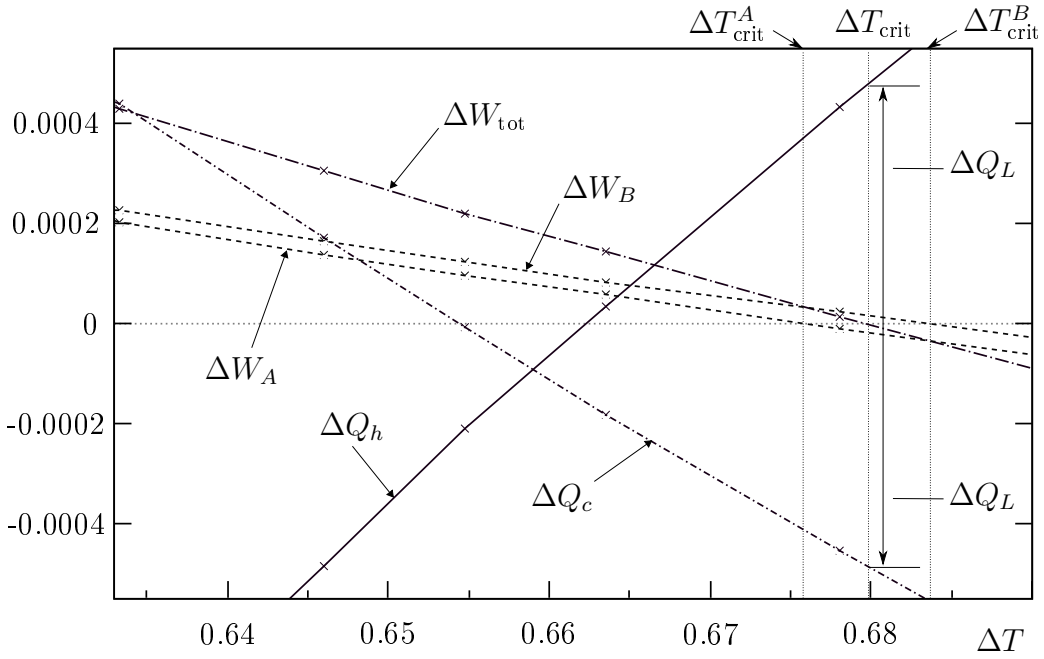

Figure 5.31.: Zoom into Fig. 5.29. The subunit work functions ΔW_A, ΔW_B. are mutually shifted and change sign symmetrically around $\Delta T_{\rm crit} = 0.68$ where the circuit is idle and only the leakage heat ΔQ_L persists.

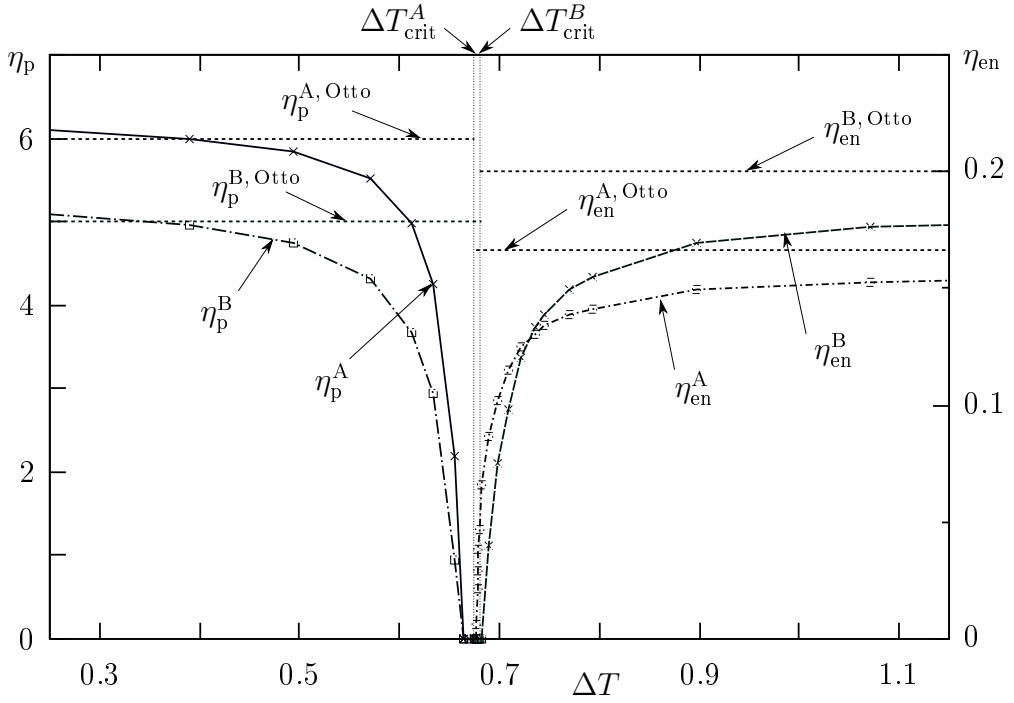

Figure 5.32.: Directed serial circuit: Local efficiencies of units A, B, coevally running as heat pumps, $\eta_{\rm p}^{A/B}$, or as heat engines, $\eta_{\rm en}^{A/B}$. Operation modes are switched at $\Delta T^A_{\rm crit} \approx \Delta T^B_{\rm crit} = 0.68$. For ΔT afar hereof the ideal Quantum Otto efficiencies $\eta_{\rm en/p}^{A/B,{\rm Otto}}$ are approached.

behavior is found for the entire circuit.

From a general point of view, the dependencies between global and local engine efficiencies are the same as in Sec. 5.1.1. A heat quantity ΔQ_h from the hot bath floats into unit A where the work $\Delta W_A < 0$ is emitted, leading to the engine efficiency $\eta_{\rm en}^A = -\Delta W_A/\Delta Q_h$. Via spin 3 the remaining heat $\Delta Q^* = \Delta Q_h - \Delta W_A$ is forwarded to unit B where another amount of work $\Delta W_B < 0$ is released. This leads to $\eta_{\rm en}^B = -\Delta W_B/(\Delta Q_h + \Delta W_A) = -\Delta W_B/(\Delta Q_c + \Delta W_B)$.

For the entire circuit, the self-consistent relation

$$\eta_{\rm en}^{\rm tot} = \eta_{\rm en}^A + \eta_{\rm en}^B - \eta_{\rm en}^A \eta_{\rm en}^B = -(W_A + W_B)/Q_h \qquad \text{and} \qquad \eta_{\rm tot}^{\rm p} = 1/\eta_{\rm tot}^{\rm en}$$

holds by virtue of the Gibbs relation or the continuity condition for the heat flux through the effective bath, respectively, i. e. $\Delta Q_h + \Delta W_A = -(\Delta Q_c + \Delta W_B)$.

Summarizing, this circuit of two unidirectionally working quantum machine units comes pretty close to the description of the ideal Quantum Otto cycle since the circuit efficiencies rapidly approach their Quantum Otto bounds. The critical temperature gradient neither is too different from the ideal one. In spite of all, a simple three- or four- spin machine circuit is preferable due to its higher heat transport capability, related to a lower spin chain resistance.

It must also be remarked that, possibly, the special character of the presented model is only a consequence of the relative phase the gas spins 2 and 4 are driven with, guaranteeing simultaneous resonance to spin 3 and therefore better heat transfer. For other relative phases a significantly different behavior of the circuit might emerge, concerning efficiencies, heat transport and leakage currents.

6. Complex Quantum Machine Circuits

In this chapter generalized quantum machine circuits shall be investigated with regard to efficiency and heat transport behavior. This is purely meant to be an extension of the ideal Quantum Otto cycle discussed in Sec. 3.3, that is, full step control is assumed, and neither leakage currents nor correlations are taken into account. Two or more resonant spins are supposed to equilibrate, approaching an average energy. In practice this is feasible only in a first approximation, as seen in the previous chapters. However, these simplifying assumptions have to be made for lack of a fully quantum mechanical description and because numerical calculations have not been available due to insufficient computing capacities for corresponding high-dimensional systems.

6.1. Efficiencies of Elementary Quantum Machine Networks

6.1.1. Circuit of Three Machine Units

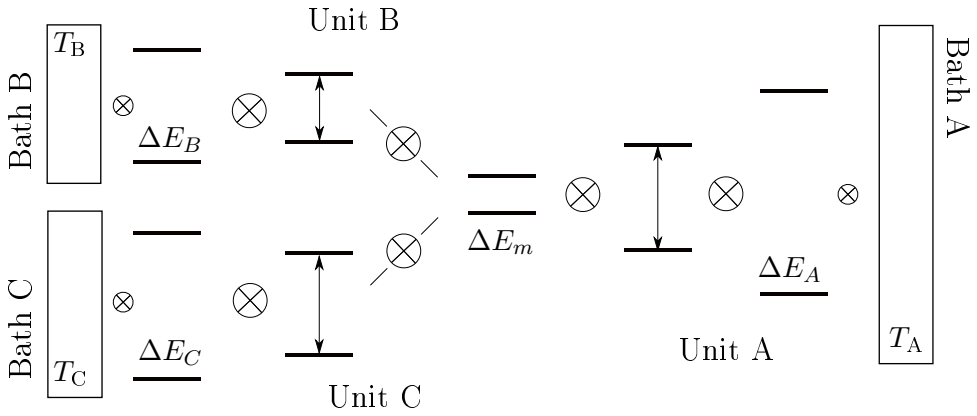

Figure 6.1.: Quantum machine network with one connector spin. Unit A works as heat engine, B and C as heat pumps. Symbols for couplings are same as above.

Consider a model of three quantum machine subunits labeled A, B and C as depicted in Fig. 6.1. Each unit is coupled to an infinite heat bath with temperature $T_i\,(i = A, B, C)$ on one side via a bath spin with local energy gap ΔE_i. All machines are

mutually connected via a connector spin with energy gap ΔE_m and temperature T_m, interpreted again as effective heat bath. The interaction between two neighbored spins is of Heisenberg type, staying in the weak coupling limit (cf. Sec. 2.5.1).

System A shall work as heat engine, the others as heat pumps. Therefore the energy gaps of the bath spins are ordered $\Delta E_A > \Delta E_B, \Delta E_C > \Delta E_m$ and, without loss of generality,

$$\mathrm{e}^{-\Delta E_A/T_A} > \mathrm{e}^{-\Delta E_B/T_B} > \mathrm{e}^{-\Delta E_C/T_C} \tag{6.1}$$

which is also of the order of the respective energy expectation values of the bath spins, $\langle E_{A,B,C} \rangle$. For further simplification all machines are operated in-phase, i. e. all driven spins are simultaneously brought into resonant contact with the connector spin. Provided an ideal Quantum Otto cycle scenario, the latter exhibits the average distribution (cf. Sec. 5.1.1 and Eq. (2.72))

$$\langle E_m \rangle / \Delta E_m = \tanh \frac{\Delta E_m}{2T_m} = \frac{1}{3} \left(\tanh \frac{\Delta E_A}{2T_A} + \tanh \frac{\Delta E_B}{2T_B} + \tanh \frac{\Delta E_C}{2T_C} \right) . \tag{6.2}$$

In the following the shorthand notation $X_i \equiv \tanh \frac{\Delta E_i}{2T_i}$ is used where $i = A, B, C$ refers to one of the subunits, and $i = m$ labels the connector spin.

In order to determine the heat engine efficiency of the entire circuit related to the reservoir of unit A, we first make an ansatz for the joint engine efficiency of units B and C coupled in parallel,

$$\eta_{\mathrm{en}}^{BC} = 1 - \frac{b\Delta E_B + c\Delta E_C}{\Delta E_m} < 0$$

where the coefficients b and c describe the amount of heat transferred into the respective unit. This expression is negative since B and C actually work as heat pumps, however we are looking for a global heat engine efficiency. Together with the local engine efficiency of unit A, $\eta_{\mathrm{en}}^{A} = 1 - \frac{\Delta E_m}{\Delta E_A}$ and (2.12) the engine efficiency of the entire circuit reads

$$\eta_{\mathrm{en}}^{\mathrm{tot}} = \eta_{\mathrm{en}}^{A} + \eta_{\mathrm{en}}^{BC} - \eta_{\mathrm{en}}^{A}\eta_{\mathrm{en}}^{BC} = 1 - \frac{b\Delta E_B + c\Delta E_C}{\Delta E_A} . \tag{6.3}$$

The corresponding heat pump efficiency is the inverse hereof, $\eta_{\mathrm{p}}^{\mathrm{tot}} = 1/\eta_{\mathrm{en}}^{\mathrm{tot}}$.

Furthermore, with Eqns. (3.16) and (3.17) the work done by each unit and the corresponding heat fluxes can be obtained. The heat transport out of unit A through the connector spin per cycle,

$$\Delta Q_{A\to m} = \frac{\Delta E_m}{2}(X_m - X_A)$$

is conserved and splits up into

$$\Delta Q_{A\to m} = -(\Delta Q_{m\to B} + \Delta Q_{m\to C}) = \frac{\Delta E_m}{2}(X_B - X_m) + \frac{\Delta E_m}{2}(X_C - X_m) .$$

Thus, identify

$$b \equiv \frac{X_m - X_B}{X_A - X_m} \qquad c \equiv \frac{X_m - X_C}{X_A - X_m} \qquad b + c = 1 . \tag{6.4}$$

Special cases

Provided that the bath contact spins of the "receptor" units B, C feature the same canonical probability distributions, $\frac{\Delta E_B}{T_B} = \frac{\Delta E_C}{T_C}$. Then $b = c = \frac{1}{2}$, and (6.3) simplifies to

$$\eta_{\text{en}}^{\text{tot}} = 1 - \frac{\Delta E_B + \Delta E_C}{2\Delta E_A} \,.$$

If, on the other hand, $\Delta E_B = \Delta E_C \equiv \Delta E_{BC}$, one obtains (cf. Sec. 2.1.5)

$$\eta_{\text{en}}^{\text{tot}} = 1 - \frac{\Delta E}{\Delta E_A} \,.$$

Comparison to a Swap Scenario

In a possible scenario of a network of quantum machines one might desire selective control on between which subunits heat transport effectively takes place. Hence, instead of assuming heat transfer via contact equilibrium let us now simulate this control in that a cyclic swapping of states between the gas spins in Fig. 6.1 is assumed, governed by some "playing rules" that define the order of swapping. Each time the connector spin spin is in resonant contact with one of the gas spins of units A, B or C, both shall exchange their respective state. In succession the involved gas spin shall run a Quantum Otto cycle, cf. Sec. 3.3. Note that in this case swapping does not require additional work expense because the energy gaps of the spins to be swapped are equally split [41].

With regard to Fig. 6.1, let the connector spin initially feature the same state as the gas spin of unit A, or $X_m = X_A$ in shorthand notation. Then it swaps with the gas spin of unit B, $X_m \leftrightarrow X_B$. This is repeated counter-clockwise until the connector spin returns to its initial state X_A. Skipping some calculations, the engine efficiency related to reservoir A becomes for this "protocol":

$$\eta_{\text{en}}^{\text{swap}} = 1 - \frac{c\Delta E_C + b\Delta E_B}{\Delta E_A}$$

with the coefficients $c = \frac{X_B - X_A}{X_C - X_A}$ and $b = \frac{X_C - X_B}{X_C - X_A}$. It is easy to show that this exceeds the engine efficiency obtained for the case where contact equilibrium was assumed, provided that the order of the local energy splittings is $\Delta E_A > \Delta E_C > \Delta E_B$. Similarly, the same applies to $\Delta E_A > \Delta E_B > \Delta E_C$ for clockwise operation. The converse holds for the heat pump efficiencies related to the bath of unit A, respectively.

This simple scenario points at a much more fundamental conclusion, namely, the best way to transport heat in spin systems can be performed by swapping of states, being rather a quantum mechanical way of control (cf. [45]). Therefore this may be the favorable operation method for quantum machine networks.

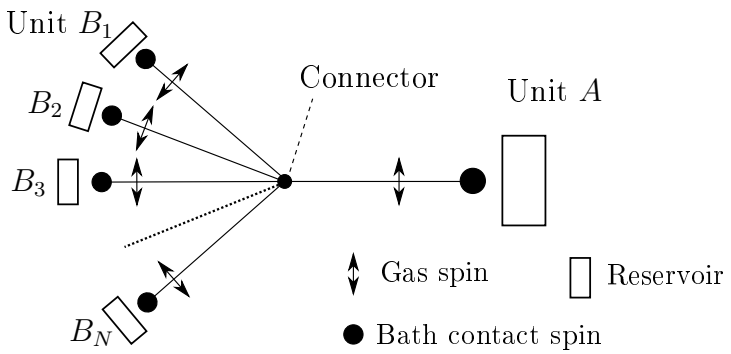

Figure 6.2.: Quantum machine network. The connector spins couples unit A, running as heat engine, to units $B_1, \ldots, B_N$ which are heat pumps.

6.1.2. Circuit of N Machine Units

The three-machine circuit from Sec. 6.1.1 is now extended to N heat pump clients B_j, $j = 1, \ldots, N$ as depicted in Fig. 6.2. The order of local energy gaps of bath and connector spins is chosen as $\Delta E_A > \Delta E_{B_j} > \Delta E_m$ for any j. The average distribution of the connector spin now reads

$$X_m \equiv \tanh \frac{\Delta E_m}{2T_m} = \frac{1}{N+1} \left(\sum_{j=1}^{N} \tanh \frac{\Delta E_{B_j}}{2T_{B_j}} + \tanh \frac{\Delta E_A}{2T_A} \right) . \tag{6.5}$$

Using analog shorthand notations (e. g. $X_{B_j} = \tanh \frac{\Delta E_{B_j}}{2T_{B_j}}$), the heat transported out of the heat engine unit A through the connector spin and the respective work become

$$Q_{A\to m} = \frac{\Delta E_m}{2}(X_A - X_m) \qquad \text{and} \qquad W_A = \frac{1}{2}\left(\Delta E_A - \Delta E_m\right)\left(X_A - X_m\right)$$

while all heat pump clients B_j together perform the work

$$W = -\frac{1}{2} \sum_{j=1}^{N} \Delta E_{B_j}(X_m - X_{B_j}) .$$

The global engine efficiency yields

$$\eta_{\text{en}}^{\text{tot}} = 1 - \frac{\sum_{j=1}^{N} \Delta E_{B_j}(X_m - X_{B_j})}{\Delta E_A(X_m - X_A)} . \tag{6.6}$$

Especially for equal energy splittings $\Delta E_{B_1} = \Delta E_{B_2} = \ldots = \Delta E_{B_N} \equiv \Delta E$ this becomes

$$\eta_{\text{en}}^{\text{tot}} = 1 - \frac{\Delta E}{\Delta E_A} .$$

If all bath spins exhibit the same distributions, $X_{B_1} = X_{B_2} = \ldots = X_{B_N}$, we would obtain

$$\eta_{\text{en}}^{\text{tot}} = 1 - \frac{\sum_{j=1}^{N} \Delta E_{B_j}}{N \Delta E_A} .$$

Finally, for M heat engines $A_1, A_2 \ldots A_M$ and N heat pump clients $B_1, B_2, \ldots, B_N$, Eq. (6.6) is modified to

$$\eta_{\text{en}}^{\text{tot}} = 1 - \frac{\sum_{j=1}^{M} \Delta E_{B_j}(X_{B_j} - X_m)}{\sum_{i=1}^{N} \Delta E_{A_i}(X_{A_i} - X_m)} \tag{6.7}$$

For the first special case, $\Delta E_{A_i} \equiv \Delta E_A$ and $\Delta E_{B_j} \equiv \Delta E_B$, we obtain

$$\eta_{\text{en}}^{\text{tot}} = 1 - \frac{\Delta E_B}{\Delta E_A}$$

For the second special case where all X_{A_i} and all X_{B_j} are equal amongst each other,

$$\eta_{\text{en}}^{\text{tot}} = 1 - \frac{N \sum_{j=1}^{M} \Delta E_{B_j}}{M \sum_{i=1}^{N} \Delta E_{A_i}} .$$

By simply combining all these expressions it should be able to calculate the efficiencies for arbitrary complex quantum machine circuits within the frame of the ideal description of the Quantum Otto cycle. Therefore only some simple elementary cases have been presented here. In practice, however, it remains yet unclear what would happen in actual network scenarios under consideration of correlations and leakage currents and, primarily, an energetic up-shift of the connector spin in analogy to Ch. 5.

6.2. Generalized quantum machine networks

Finally, consider a simple array of four elementary quantum machine circuits as displayed in Fig. 6.3. They are all driven in-phase and coupled to a heat bath on one side and to an edge or node spin of a spin network mesh on the other side. All node spins feature the same local energy splitting ΔE_m. The energies of the bath spins are determined by their local energy gaps ΔE_{A_i} and the respective bath temperatures T_{A_i}. The energy expectation values shall be ordered

$$\langle E_{A_1} \rangle > \langle E_{A_2} \rangle > \langle E_{A_3} \rangle > \langle E_{A_4} \rangle$$

When the gas spins of all units simultaneously are in resonant contact with the respective node spins, the latter will adopt the corresponding bath spin distributions after equilibration, being

$$X_{m_i} \equiv \tanh \frac{\Delta E_m}{2T_{m_i}} = \tanh \frac{\Delta E_{A_i}}{2T_{A_i}}$$

where T_{m_i} are the respective node spin temperatures.

In the following the whole spin mesh is supposed to relax into equilibrium, leading to an overall average distribution. This is completed by heat currents equalizing the differences between the distributions X_{A_i} of the node spins. Indeed such a behavior is found in Heisenberg-coupled spin rings [46].

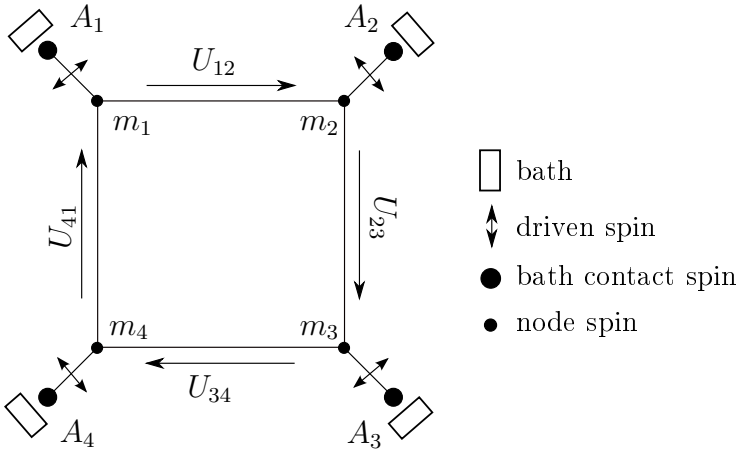

Figure 6.3.: Network mesh of four quantum machines A_i ($i = 1, 2, 3, 4$) connected via node spins m_i (see text). The gas, node and bath contact spins are represented by arrows, small and big dots, respectively.

In analogy to an electric circuit, it is thus manifest to interpret the different distributions X_{A_i} of the node spins as potentials. Then the potential difference $U_{ij} = \frac{\Delta E_m}{2}(X_{A_i} - X_{A_j})$ between the nodes of units A_i and A_j can be considered as a kind of voltage. It is easily verified that along one mesh all U_{ij}-terms add up to zero,

$$\sum_{i,j} U_{ij} = 0\,.$$

This is analog to the Kirchhoff mesh rule for electrical circuits, except that here the voltage only exists at the beginning but not during the whole cycle because equilibrium shall be attained within the mesh at the end of each cycle. Nevertheless, according to Sec. 6.1.1 heat currents emerge due to the potential differences since a heat quantity is effectively transported per period.

At all edges of the mesh the heat current inflows and outflows add up to zero due to energy conservation,

$$\sum_i J_i \equiv \frac{\Delta E_m}{2} \sum_i (X_{A_i} - X_{m_i}) = 0\,,$$

cf. Sec. 4.1. This can be seen in relation to the Kirchhoff node rule, in turn.

Summarizing, under the simplifying assumptions of the ideal Quantum Otto cycle model a circuit of quantum thermodynamic machines can be compared to an electric circuit. Hereof analogs to the Kirchhoff rules arise. These should principally be applicable also for more general suchlike heat pump networks where nodes are not necessarily coupled to infinite heat reservoirs as indicated in Fig. 6.3, but also to neighbored meshes, serving as effective heat baths likewise in Ch. 5.

7. Quantum Machines versus Brownian Motor

In this thesis, only machine models realized with spin chains have been investigated so far. Another class of microscopic systems being able to convert heat into work are Brownian motors. A Brownian motor is generally understood to be based on some particles in contact with one or several heat baths from which thermal fluctuations arise. Consequently, the particles are exposed to non-equilibrium. A further typical ingredient is a spatial ratchet potential which has the function to rectify these fluctuations, resulting in a net current of particles.

If a load force is added against the direction of this current, mechanical work may be extracted. This can be interpreted as an energetic transfer from the motor to the load, or in that the potential energy of the particles raises [22]. A famous example is the ratchet-and-pawl setup by Feynman [47], see also [48]. Further applications are widespread in cell biology and nanotechnology.

A special class of Brownian motors is given by the Sakaguchi model, see e. g. [49] where the Brownian particle moves in a spatially periodic and asymmetric potential and alternately interacts with two thermal baths of different temperatures in space. This ratchet picture in combination with non-equilibrium is allows to break detailed balance, i. e. different probabilities to cross the potential barriers in either direction are needed for directed particle flux. In general, the motion of particles is governed by a Langevin equation

$$\dot{x}(t) = -\frac{1}{\gamma}U'(x,t) - \frac{1}{\gamma}F_{\text{ext}} + \sqrt{2D(x,t)}\,\xi(t) \tag{7.1}$$

relating the particle velocity $\dot{x}$ to the gradient of the spatial potential $U'(x,t)$, the external force F_{ext} and a Gaussian noise $\xi(t)$ following the auto correlation function $\langle \xi(t)\xi(t')\rangle = \delta(t-t')$. The viscous drag coefficient γ and the diffusion coefficient $D(x,t)$ obey the dissipation relation $\gamma D(x,t) = k_{\text{B}}T(x,t)$ where T denotes the absolute temperature and k_{B} the Boltzmann constant [19].

In the same reference the model depicted in the upper part of figure 7.1 is discussed, being similar to the Sakaguchi case. The potential $U(x)$ is time-independent but inhomogeneous in space. A particle moving in x-direction is mainly in contact with a hot reservoir at temperature T_h, only on small segments it is exposed to a cold reservoir at temperature T_c. The particle motion is rectified rightwards as the cooling happens on a descending part of the potential. At the potential barriers the hot reservoir raises the particle's energy by $\Delta E = \Delta W$, whereas the heat ΔQ is transferred to the cold bath. If this work is expended against some load, the hot reservoir has to be recharged with

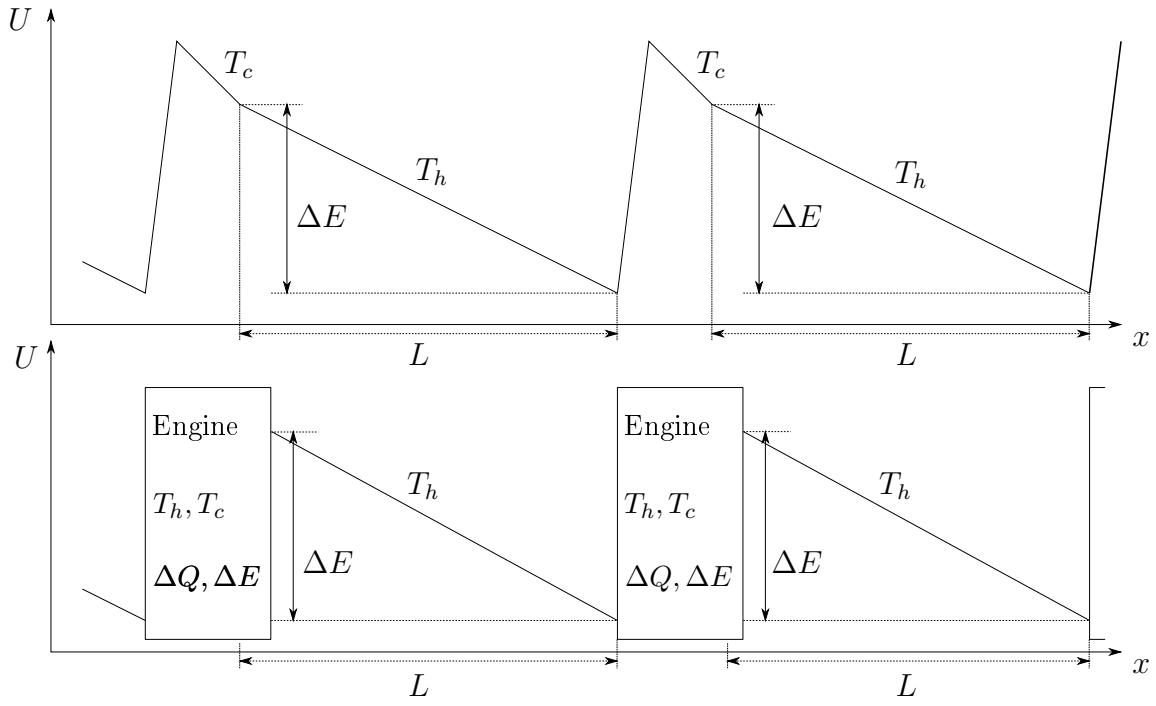

Figure 7.1.: Upper part: generalized ratchet picture of a Brownian motor, lower part: machine chain picture

$\Delta W + \Delta Q$. On the other hand, in the load-free case where all of the work $\Delta E = \Delta W$ is dissipated back into the hot reservoir as the particle moves along the down-slides of length L, only a recharging with ΔQ is necessary. As depicted in the lower part of Fig. 7.1 this scenario can be mapped onto a periodic array of heat engines connected via the said down-slides at temperature T_h. Supposed that the heat engines work reversibly in the load-free case, the heat ΔQ to recharge the engines is

$$\frac{\Delta Q + \Delta E}{T_h} = \frac{\Delta Q}{T_c} \quad \Longrightarrow \Delta Q = \frac{T_c}{T_h - T_c}\Delta E$$

This may be realized by reversibly operating a heat pump between both reservoirs:

$$\frac{\Delta Q}{T_h} = \frac{\Delta Q - E_{\text{in}}}{T_c}$$

yielding a minimum energy input per period of $E_{\text{in}} = (T_c/T_h)\Delta E$. Otherwise the heat ΔQ is simply lost.

With regard to directed heat transport, this model of serially connected heat engines is very similar to the serial quantum machine circuits from Ch. 5. It may be argued that a heat engine combined with a down-slide in the Brownian Motor model corresponds to one pair of a heat engine and a heat pump in the serial circuit model. As depicted in Fig. 7.2 the latter is arranged as a chain between two heat baths. Spatial asymmetry

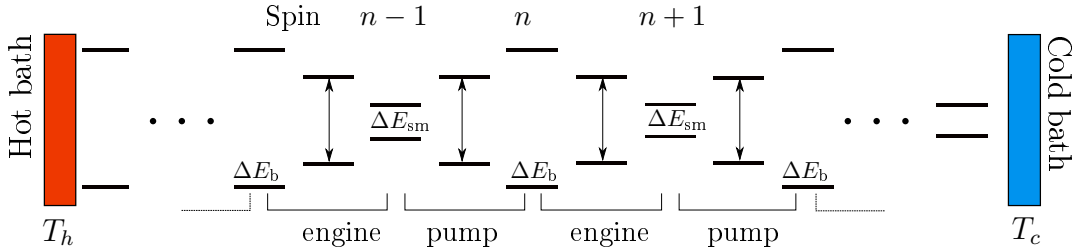

Figure 7.2.: Chain of pairwise arranged quantum heat engines and heat pumps between two thermal reservoirs. $\Delta E_{\mathrm{sm}}, \Delta E_{\mathrm{b}}$ are the local energy gaps of the constantly split spins $n = 1, \ldots, N$.

is arranged for by the constant local energy splittings of spins $n = 1, \ldots, N$, which may only take one of two values, say $\Delta E_{\mathrm{sm(all)}} < \Delta E_{\mathrm{b(ig)}}$. For any gas spin i in between with local energy splitting $\Delta E_i(t)$ the resonance condition $\Delta E_{\mathrm{sm}} \leq \Delta E_i(t) \leq \Delta E_{\mathrm{b}}$ must apply.

While in the ratchet model energy transport happens via a particle moving through the potential landscape and steadily being in contact with the thermal environments, the spins transporting heat in the quantum machine model are spatially fixed, and the whole chain is only locally coupled to infinite heat reservoirs at the end of the chains. In between, the sole environment to exchange energy with is the external driving source which acts as working reservoir and enables the heat current to overcome the potential barriers by modulating the local energy gaps of the gas spins. As discussed in Sec. 3.2.1 a semi-classical driver such as an external magnetic field is inappropriate for this purpose since the work released by the machine units cannot be extracted. A better option is to couple the gas spins to harmonic oscillators, cf. [14].

Given a reversible working reservoir, no excess energy is lost if an amount of work ΔW is applied to one of the heat pumps in Fig. 7.2. The same work $-\Delta W$ rather is released again by the heat engines corresponding to the down-slides in the ratchet model. For reasons of simplicity, this is made plausible here with the model of the ideal Quantum Otto cycle, neglecting any kind of dissipative effects.

The condition of energy conservation for the heat current through the spin n with $\Delta E_n = const$ reads (cf. (3.17) and (5.2))

$$\frac{\Delta E_n}{2}\left(\tanh\frac{\Delta E_{n-1}}{2T_{n-1}} - \tanh\frac{\Delta E_n}{2T_n}\right) = \frac{\Delta E_n}{2}\left(\tanh\frac{\Delta E_n}{2T_n} - \tanh\frac{\Delta E_{n+1}}{2T_{n+1}}\right),$$

leading to the distribution

$$\tanh\frac{\Delta E_n}{2T_n} = \frac{1}{2}\left(\tanh\frac{\Delta E_{n-1}}{2T_{n-1}} + \tanh\frac{\Delta E_{n+1}}{2T_{n+1}}\right).$$

This can finally be reduced to an expression only depending on spins 1 and N which, respectively, exhibit the same temperatures temperatures T_h and T_c as the baths,

$$\tanh\frac{\Delta E_n}{2T_n} = \frac{1}{N-1}\left((N-n)\tanh\frac{\Delta E_1}{2T_h} + (n-1)\tanh\frac{\Delta E_N}{2T_c}\right).$$

where $\Delta E_1 = \Delta E_\mathrm{b}$ and $\Delta E_N = \Delta E_\mathrm{sm}$.

Thus, the canonical distributions of all constantly split spins mark a gradient directed from the hot to the cold bath which is tantamount to global non-equilibrium. If now the gas spin between spins $n-1$ and n works as heat pump, i. e. $\Delta E_{n-1} = \Delta E_\mathrm{sm} < \Delta E_n = \Delta E_\mathrm{b}$ (cf. Fig. 7.2), the work to be applied is

$$\Delta W_{n-1,n} = \frac{1}{2(N-1)} \left(\Delta E_\mathrm{sm} - \Delta E_\mathrm{b}\right) \left(\tanh \frac{\Delta E_1}{2T_h} - \tanh \frac{\Delta E_N}{2T_c}\right) > 0$$

and, consequently, in the heat engine between spins n and $n+1$ the same amount of work $\Delta W_{n,n+1} = -\Delta W_{n-1,n} < 0$ is released. In this most ideal situation the obligatory heat quantity $\Delta\Delta Q = \frac{\Delta E_\mathrm{sm}}{2(N-1)} \tanh \frac{\Delta E_\mathrm{sm}}{2T_c}$ must be paid only once to the cold bath at the end of the spin chain. In contrast, for N potential barriers in the ratchet the heat quantity $N\Delta\Delta Q$ is lost.

Interpreting both model systems as possibilities for directed heat transport, the quantum machine chain would be favored under ideal conditions, the more so as phase-coherent driving may be enabled.

The presence of leakage currents would change the situation, however. Losses within each partial heat pump then do require compensation, to be furnished by the external driving source. Therefore the said advantage of the spin chain model is likely to be reduced for dynamical scenarios. On the other hand, losses might be kept small for a sufficiently large global temperature gradient.

Ref. [19] mentions further that the spatial temperature dependence in the ratchet model (upper part of Fig. 7.1) may be dissolved by applying the transformation $\{T, U, x\} \rightarrow \{\kappa T, \kappa U, \kappa x\}$ with $\kappa = T_h/T_c$ to the segments at temperature T_c, changing their height and length. In the following all potential barriers vanish and all down-slides line up as one straight slope along which the Brownian particle moves unidirectionally, driven by alternating segments at temperature T_h and T_c representing the heat engines in the lower part of Fig. 7.1.

Similarly, for the sole purpose of directed heat transport, the described scenario of a chain of quantum machines and heat pumps may likewise be replaced by a simple homogeneously split spin chain, featuring unidirectional heat transport from the hot to the cold heat reservoir.

It remains an open question if the considered chain of quantum machines represents something like the quantum limit of a Brownian motor, i. e. if one can be mapped onto the other. The similarity of both models nevertheless calls for further research.

8. Summary and Outlook

How small can quantum systems be in order to work as thermodynamic machines? Down to what scales is it possible to downscale modern devices for this purpose, and where does the transition from classical to quantum thermodynamic behavior actually occur?

In this work numerical simulations on several quantum machine models realized with modulated spin chains have been presented and characterized with regard to efficiency as well as heat and work characteristics.

All this has been built on a basic approach given in [16, 15], where it was first shown that a single spin can run a thermodynamic cycle, more precisely a Quantum Otto cycle. For further comparison, an idealized description of such a Quantum Otto cycle [11] was consulted and verified numerically by manipulating the spin-spin coupling strength within the three-spin machine.

With regard to extended quantum machine circuits, it has been found that, in a first order approximation, extended models such as paralleled units also run Quantum Otto cycles, show a similar behavior as the basic three-spin machine model. The same applies to serial circuits including their subunits. Here the connector spins not only arrange for lower heat conductivity but also appear as effective finite heat baths, shielding the subunits from each other and determining their local mode of operation as heat engine or pump. This influence becomes crucial for models with tapered internal temperature gradients since, in this case, the effective bath spins are heated up. This eventually leads to considerable dissipation effects.

The concept of serial and parallel quantum machine networks can be expanded to more complex arrangements. Some examples hereof have been presented with respect to the ideal Quantum Otto cycle. It has been shown that the behavior of heat current in a spin chain can be mapped to that of electrical current in an electric circuit, and analogs to the Kirchhoff rules apply.

Moreover, comparisons with other models of directed heat transport are feasible, which has been shown for the ratchet model for a Brownian motor.

All these quantum machine models share the general problem of being high-dimensional, why analytical quantum mechanical descriptions are hardly available and numerical investigation could only be carried out so far for dynamic models with no more than five spins. For these reasons more detailed comprehension of actual processes in these complex systems is hard to set. Thus, common effects such as leakage currents and dissipation had to be approached via a phenomenological ansatz while correlations could only be invoked on a qualitative level.

Remedy can possibly be found in a promising recent approach to quantum thermodynamic processes with external control [50] which also may be able to yield analytical expressions for the efficiency of a quantum machine at maximum power output. A

comparison to the results obtained so far will be subject of future investigation. The inclusion of quantum effects into the discussed models will be of similar importance. A potential starting point for this purpose is furnished by [43].

Nevertheless, the presented approaches and underlying concepts are able to deliver at least qualitative insight into the complicated dynamics of the treated class of thermodynamic machine models from a theoretical viewpoint.

Anyway, it will finally be left to experiment to realize thermodynamic processes in quantum systems such as spin chains. Not until then will it reveal if the concepts presented here are really applicable in physical sense.

A. Appendix: Note on Numerical Methods

All models treated in the present work have been solved in Mathematica with the help of a four-step Runge-Kutta algorithm and the notepads `Temp-tools` [44] and `QMDef` [51].

As mentioned, closed analytical solutions are impossible to obtain due to the high dimensionality of the Liouville spaces corresponding to the considered spin systems. For reasons of insufficient memory and enormous runtime requirements numerical investigation of these dynamical scenarios had to be limited to five spins up to the present.

In order to solve the master equation for the reduced density matrix $\hat{\varrho}$ of the spin system after [17] (see chapter 2.3) the Liouville super-operator $\hat{\mathcal{L}}$ is calculated for a given number of sampling points using [44], then interpolated over one period $\tau = 2\pi/\omega$ and periodically continued. This handling is possible because $\hat{\mathcal{L}}$ does not depend on the actual state of the system but only on the (known) time-dependent eigenvalues and constant given parameters (temperatures, coupling constants etc.), and provides an enormous advantage in runtime, compared to the calculation of $\hat{\mathcal{L}}$ four times per calculation step. Furthermore, the initial system state $\hat{\varrho}_{int}$ is usually chosen a global thermal state for reasons of simplicity.

The chosen step size is $h = 0.2$ time steps which is small enough to avoid the trace or the diagonal elements of $\hat{\varrho}$ from diverging. At the same time, arriving at the non-equilibrium attractor state of $\hat{\mathcal{L}}$ requires evaluation over a large enough number of time steps. For three- and four-spin models a total time of $T_f = 10,000$ time steps is sufficient, whereas for five-spin models $T_f = 30,000$ is necessary. In general, a too small value of T_f will be indicated by non-compliance of the Gibbs relation for the whole system, $\Delta W + \Delta Q \neq 0$. In addition, the relative numerical error herein only remains negligible ($< 1\%$) for adequately small intervals in terms of the periodic time $\tau = 2\pi/\omega$ in which data points are saved to a file for further evaluation.

Another difficulty arises from the fact that Mathematica, but also other interpreters, usually sort numerical eigenvalues by order. Whenever energy level crossings occur in the observed four-and five-spin systems, the order of energy eigenvalues and eigenvectors is therefore altered. As a consequence, calculating the system state in the system energy eigenbasis leads to a wrong Liouvillian $\hat{\mathcal{L}}$ and to meaningless results. This problem can be circumvented by moving to a product basis, but for the sake of runtime, since then all matrices to be multiplied contain considerably more non-zero entries.

For evaluation, the density matrix entries are interpolated again over the whole range of time evolution. The heat currents follow from (2.78) while the local states of the single spins and spin groups are obtained by the routines `RedStateQubit` and `TraceOutQubit` [51], respectively. The local temperatures are extracted by the function `TempSpin` [44].

The Work ΔW and heat ΔQ result from integrating the ST-curves and heat currents J over one period as discussed in Sec. 3.1, using a simple Newton integration algorithm.

This work has been written in LaTeX. All figures were created in `Inkscape`, diagrams were plotted with `Gnuplot`.

Bibliography

[1] J. Gemmer. A quantum approach to thermodynamics, 2003. Doktorarbeit, Stuttgart.

[2] J. Gemmer, M. Michel, and G. Mahler. *Quantum Thermodynamics*. Springer Verlag Berlin, 2004.

[3] L. Boltzmann. Über die mechanische Bedeutung des zweiten Hauptsatzes der Wärmetheorie. *Wien. Ber.*, 53, 1896.

[4] J. W. Gibbs. Elementary principles in statistical mechanics. *Dover Publications, New York*, 1960.

[5] M. Hartmann. On the microscopic limit for the existence of local temperature, 2005. Doktorarbeit, Stuttgart.

[6] P. Curie. Sur la symétrie dans les phénomènes physiques, symétrie d'un champ électrique et d'un champ magnétique. *J. de Phys., Paris*, 12(3):393, 1894.

[7] J. E. Geusic, E. O. Schulz-DuBios, and H. E. D. Scovil. Quantum equivalent of the carnot cycle. *Phys. Rev.*, 156(2):343–351, 1967.

[8] R. Kosloff and T. Feldmann. Quantum four-stroke heat engine: Thermodynamic observables in a model with intrinsic friction. *Phys. Rev. E*, 68(1):016101, 2003.

[9] D. Segal and A. Nitzan. Molecular heat pump. *Phys. Rev. E*, 73(2):026109, 2006.

[10] J. Palao, R. Kosloff, and J. M. Gordon. Quantum thermodynamic cooling cycle. *Phys. Rev. E*, 64(5):056130, 2001.

[11] T. D. Kieu. Quantum heat engines, the second law and maxwell's demon. *Eur. Phys. J. D*, 39:115–128, 2006.

[12] P. Borowski. Quantenthermodynamische Maschinen und Prozesse, 2002. Diplomarbeit, Stuttgart.

[13] C. Kostoglu. Zum Quanten-Carnotprozess, 2004. Diplomarbeit, Stuttgart.

[14] F. Tonner and G. Mahler. Autonomous quantum thermodynamic machines. *Phys. Rev. E*, 72(6):066118, 2005.

[15] M. J. Henrich, M. Michel, and G. Mahler. Small quantum networks operating as quantum thermodynamic machines. *Europhys. Lett.*, 76:1057, 2006.

[16] M. J. Henrich, M. Michel, and G. Mahler. Driven spin systems as quantum thermodynamic machines: Fundamental limits. Phys. Rev. E, in press, 2007.

[17] K. Saito, S. Takesue, and S. Miyashita. Energy transport in the integrable system in contact with various types of phonon reservoirs. *Phys. Rev. E*, 61:2397, 2000.

[18] H. Wichterich, M. J. Henrich, H.-P. Breuer, J. Gemmer, and M. Michel. Modelling heat transport through completely positive maps. quant-ph/0703048, 2007.

[19] I. Derenyi, M. Bier, and R. D. Astumian. Generalized efficiency and its application to microscopic engines. *Phys. Rev. Lett.*, 83(5):903–906, 1999.

[20] H. B. Callen. *Thermodynamics and an introduction to thermostatistics.* John Wiley, New York, 1985.

[21] J. Gemmer, M. Michel, and G. Mahler. Emergence of thermodynamic behavior within composite quantum systems. *Physica E*, 29:53–65, 2005.

[22] J. M.R. Parrondo. Energetics of Brownian motors: a review. In *Applied Physics A: Materials Science and Processing*, volume 75, page 79. Springer, Berlin, 2002.

[23] F. L. Curzon and B. Ahlborn. Efficiency of a carnot engine at maximum power output. *APS*, 43(1):22–24, 1975.

[24] R. Kubo. *Thermodynamics.* North Holland, Amsterdam, 1968.

[25] S. Bandyopadhyay et al. Thermoeconomic optimization of combined cycle power plants. *Energy Conversion and Management*, 42(3):359, 2001.

[26] H.-P. Breuer and F. Petruccione. *The Theory of Open Quantum Systems.* Oxford University Press, 2002.

[27] G. Mahler and V. A. Weberruß. *Quantum Networks: Dynamics of Open Nanostructures.* Springer Verlag Berlin, 2nd edition, 1998.

[28] A. N. Jordan and M. Büttiker. Entanglement energetics at zero temperature. *Physical Review Letters*, 92(24):247901, 2004.

[29] A. Einstein, B. Podolsky, and N. Rosen. Can quantum-mechanical description of physical considered complete? *Phys. Rev.*, 47(10):777–780, 1935.

[30] M. A. Nielsen and I. L. Chuang. *Quantum Computation and Quantum Information.* Oxford University Press, 2002.

[31] U. Weiss. *Quantum Dissipative Systems.* World scientific, Singapore, 1999.

[32] M. O. Scully and M. S. Zubairy. *Quantum Optics.* Cambridge University Press, 1997.

[33] M. J. Henrich. Deriving a master equation for non-equilibrium steady states. Unpublished, 2006.

[34] M. Michel. Nonequilibrium aspects of quantum thermodynamics, 2006. Doktorarbeit, Stuttgart.

[35] M. J. Henrich, M. Michel, M. Hartmann, G. Mahler, and J. Gemmer. Global and local relaxation of a spin chain under exact schrödinger and master-equation dynamics. *Phys. Rev. E*, 72(2):026104, 2005.

[36] M. Hartmann, G. Mahler, and O. Hess. Existence of temperature on the nanoscale. *Phys. Rev.Lett.*, 93(8):080402, 2004.

[37] M. Hartmann, G. Mahler, and O. Hess. Local versus global thermal states: Correlations and the existence of local temperatures. *Phys. Rev. E*, 70(6):066148, 2004.

[38] M. J. Henrich. Dynamische und thermische Eigenschaften abgeschlossener modularer quantenmechanischer Systeme, 2006. Diplomarbeit, Stuttgart.

[39] M. Michel, J. Gemmer, and G. Mahler. Microscopic quantum mechanical foundation of fourier's law. *Int. J. Mod. Phys. B*, 20:4855, 2006.

[40] M. Michel, M. Hartmann, J. Gemmer, and G. Mahler. Fourier's law confirmed for a class of small quantum systems. *European Physical Journal B*, 34(3):115, 2004.

[41] M. J. Henrich. Private communication.

[42] T. D. Kieu. The second law, maxwell's demon, and work derivable from quantum heat engines. *Phys. Rev. Lett.*, 93(14):140403, 2004.

[43] L. Quiroga, F. J. Rodriguez, M. E. Ramirez, and R. Paris. Nonequilibrium thermal entanglement. *Phys. Rev. A*, 75(3):032308, 2007.

[44] M. J. Henrich et al. `temp-tools 2.0`– utility package for temperature fitting and master equation solving. Mathematica Notepad (unpublished), 2006.

[45] F. Rempp, M. Michel, and G. Mahler. A cyclic cooling algorithm, 2007. quant-ph/0702071.

[46] H. Schmidt and G. Mahler. Control of local relaxation behavior in closed bipartite quantum systems. *Phys. Rev. E*, 72:016117, 2005.

[47] R. P. Feynman, R. B. Leighton, and M. Sands. *Feynman Lectures on Physics*, volume 1. Addison-Wesley, Reading, MA, 1963, 1963.

[48] A. Gomez-Marin and J. M. Sancho. Ratchet, pawl and spring Brownian motor. *Physica D*, 216:214, 2006.

[49] A. Gomez-Marin and J. M. Sancho. Tight coupling in thermal Brownian motors. *Phys. Rev. E*, 74:062102, 2006.

[50] Y. Byrukov, T. Jahnke, and G. Mahler. Quantum thermodynamic processes in a model of controlled relaxation. Unpublished, 2007.

[51] M. Michel et al. `qmdef 1.1`– utility and definition package for quantum mechanical calculations. Notepad for Mathematica (unpublished), 2006.

Danksagungen

Zu guter Letzt möchte ich folgenden Personen meinen Dank aussprechen für die direkte und indirekte Unterstützung beim Erstellen dieser Arbeit:

Prof. Dr. G. Mahler für die hervorragende Betreuung, zahlreiche Diskussionen und Hilfestellungen bei Problemen und eine immer offene Tür,

Prof. Dr. U. Seifert für die Übernahme des Mitberichts,

Prof. Dr. G. Wunner für die Aufnahme am 1. Institut für Theoretische Physik,

meinem Zimmerkollegen Harry Schmidt für das gute Arbeitsklima im Büro, interessante Gespräche und unzählige Tipps und Hilfestellungen unter anderem bezüglich Linux, Mathematica und vor allem Latex,

Mathias Michel und vor allem Markus Henrich für die Starthilfe sowie zahlreiche Diskussionen, hilfreiche Anregungen und Ideen, die immerwährende Motivation und das Korrekturlesen dieser Arbeit

den weiteren derzeitigen und ehemaligen Mitgliedern der AG Mahler und der erweiterten Kaffeerunde für interessante und witzige Gespräche, Unterstützung und gemeinsame Aktivitäten:

Yan Byrukov, Florian Hardt, Thomas Jahnke, Alex Kettler, Florian Rempp, Heiko Schröder, Marcus Stollsteimer, Jens Teifel, Friedemann Tonner, Pedro Vidal (für spannende Schachpartien!), Hendrik Weimer und Mohamed Youssef,

allen anderen Institutsmitgliedern für hervorragenden Service und ein sehr angenehmes Arbeitsklima,

Jürgen Falb, Daniel Guggenmos und meinen übrigen Kommilitonen für viele gemeinsame Aktivitäten und Spaß miteinander während der gesamten Studienzeit,

zu guter letzt meiner Familie, die mich immerwährend nicht nur finanziell unterstützte und des öfteren meine Launen aushalten musste

sowie allen anderen, die hier unerwähnt bleiben.